MASS TRANSFER AT LOW REYNOLDS NUMBER IN LIQUID FLUIDIZED BEDS

by

Khaliqur Rahman

A thesis submitted for the degree of

Doctor of Philosophy

Department of Chemical Engineering and
Chemical Technology
Nuclear Technology Laboratory
Imperial College of Science and Technology
London S.W.7.

ABSTRACT

Mass transfer rate data in a shallow liquid fluidized bed has been obtained in the range $1 < Re_s < 25$, $8 < Re_o < 56$. An ion exchange neutralization reaction was chosen as the most convenient physico-chemical system for this purpose. From the analysis of data, it is inferred that for $Re_s/Re_o < 1/6$ fluidized beds tend to maintain an ordered axial structure in which individual particles are arranged parallel to the main flow. This arrangement effectively shields a portion of the surface of the particles from the main flow with a resulting decrease in mass transfer. For $Re_s/Re_o > 1/6$ this ordered structure is lost due to perturbations in the flow and the bed attains a random structure. In order to account for the physical properties of different solid-liquid systems, the terminal Reynolds number Re_o is introduced as the characteristic property that allows precise representation of data in liquid fluidized beds. For $Re_s/Re_o > 1/6$, the following correlation is obtained:

$$Sh_m = 0.86\, Re_o^{\frac{1}{2}} \left(\frac{Re_s}{Re_o}\right)^q Sc^{1/3}$$

where $q = 0.5\, Re_o^{-0.3}$

To gain a further understanding of fluidized bed mass transfer results, some single particle mass transfer studies were made using the same physico-chemical system. The single particle experiments were carried out by allowing particles to fall at their terminal settling velocity in a reacting solution. The amount of mass transfer was estimated by a spectro-chemical method of analysis. The results are correlated by the equation:

$$Sh = 0.75\ Re_o^{\frac{1}{2}}\ Sc^{1/3}$$

Comparison of single particle and extrapolated fluidized bed results at a voidage of unity indicates that fluidized bed data is about 11% higher than expected from a consideration of single particle study. This increase is thought to be due to some kind of "turbulence" and is possibly generated by the flow distributor of the bed.

To estimate the mass transfer rate in any multiparticle bed, whether fixed, distended or fluidized a semi-theoretical correlation based on Carberry's boundary layer model (9) has been proposed and tested using the fluidized bed data. This generalised correlation is

$$Sh_m = 0.86\ \frac{Re_s^{\frac{1}{2}}}{\varepsilon}\ Sc^{1/3}$$

By a small perturbation of velocity and voidage, both of which may fluctuate in a fluidized bed, it is found that the effects of these two parameters oppose each other and cancel out. This explains why both fixed and fluidized bed data may be represented by a single equation, although their physical characteristics are different.

As an extension to the problem of forced convective diffusion, a case where the diffusion coefficient is not constant has been analysed. This case would arise in an ion exchange solid-liquid system. Due to the complexity of the problem, only an approximate solution has been possible. The solution predicts the correct dependence of mass transfer coefficient on the flow rate, but its dependence on concentration is uncertain.

ACKNOWLEDGEMENTS

It is a pleasant duty to express my gratitude to Dr. M. Streat for his continuous guidance and advice during the course of this work. My sincere thanks to him for all his help.

Grateful thanks are due to Prof. G.N. Walton for his interest in the project and for providing the necessary facilities to carry out the work.

Acknowledgements are also made to Mr. L. Tyley and Mr. R. Wood for designing the temperature controller and to Mr. P.L. Bird and Mr. S. Wahid for the help provided in carrying out the spectro-chemical analysis. The assistance of Mr. G.V. Stubbings in procuring materials is also appreciated.

I would also like to thank the British Council and Bangladesh University of Engineering and Technology for providing the grant and study leave respectively.

Khaliqur Rahman

CONTENTS

NOMENCLATURE

The dimensions are given in terms of mass (M), length (L), time (t) and temperature (T). The numbers in parentheses after description refer to equations in which symbols are used.

A = constant (2.2-1), dimensionless

A = complex term (A.3-23), dimensionless

A = cross sectional area, L^2

a = radius of a unit cell in the free surface model, L

a_1 a_2 = exponents (2.3-10), dimensionless

B, B_0, B_1, B_2, B_3, B_4, B_m = pre exponential coefficients in equation of the type (2.2-1) or (2.2-17), dimensionless

b = thickness of concentration boundary layer, L

C = total concentration, mols/L^3

C_i = molar concentration of species 'i', mols/L^3

C_{iR}, C_{ib} = concentration of species 'i' at points R and b respectively, mols/L^3

C_i^1 = $(C_i - C_{ib})/(C_{iR} - C_{ib})$, dimensionless

C_{ib}^i, C_{ib}^e = bulk inlet and exit concentration of species 'i' of the fluid stream in a fluidized bed, mols/L^3

$\overline{C}_i$ = concentration of species 'i' in the particle phase, mols/L^3

D_{is} = binary diffusivity of the pair i-s, L^2/t

$Đ_{ij}$ = diffusivity of the pair i-j in a multicomponent mixture, L^2/t

D = coupled diffusion coefficient (4.1-3), L^2/t

D_{eff} = effective diffusion coefficient (4.1-16), L^2/t

D^e = effective diffusivity in a multiparticle bed (2.32), L^2/t

d = particle diameter, L

d_Q = ratio of particle diameter in H^+ form to the mixed (H^+, Na^+) form, dimensionless

E = pseudo voidage (2.3-14), dimensionless

E_1, E_2, E_3 = constants (6.1-14), dimensionless

F_T = total drag on a sphere, ML/t^2

G = constant (2.3-10), dimensionless

G_1, G_2, G_3, G_4 = constant (4.2-2) to (4.2-5), dimensionless

g = body force per unit mass, L/t^2

h = bed height, L

j_i = diffusional mass flux with respect to mass average velocity, M/tL^2

J_i^* = diffusional molar flux with respect to molar average velocity, moles/tL^2

$\overline{K}_C$ = overall mass transfer coefficient for constant diffusivity system, L/t

$\overline{K}_V$, $K_V(\theta)$ = overall and local mass transfer coefficient where diffusion coefficient is not constant, L/t

L = volume flow rate, L^3/t

M_i = molecular weight of species i, M/mole

m = exponent of Re and Re_s, dimensionless

N_i = molar flux with respect to stationary coordinates, moles/tL^2

N = exponent (6.1-10), dimensionless

n = exponent of Sc, dimensionless

p = fluid pressure, M/Lt^2

Q = resin loading i.e. ratio of sodium present in the resin to the total capacity of the resin, dimensionless

q = exponent (6.1-4), dimensionless

R = gas constant, ML^2/t^2T mole

R = radius of particle, L

r = radial distance in spherical coordinates, L

S = total surface are of particles, L^2

T = temperature, T

t = time, t

t_s = saturation time, t

t_f = time of fall, t

U = approach velocity, L/t

U_s = superficial velocity, L/t

U_i = interstitial velocity, L/t

v = mass average velocity, L/t

v^* = molar average velocity, L/t

v^1 = v/U, dimensionless

$\overline{v'}$ = time averaged fluctuating velocity, L/t

V_B = volume of particles used in the fluidized bed, L^3

W_{Na} = total amount of Na in a particle, moles

W = $2 - 3\eta + 3\eta^5 - 2\eta^6$ (2.3-6), dimensionless

w_i = mass fraction of species 'i', dimensionless

x_1 = distance perpendicular to flow, L

x_i = mole fraction of species 'i', dimensionless

y_A = C_A/C_C, equivalent fraction of A, dimensionless

z = axial coordinate in cylindrical coordinate, L

z_1 = distance in the direction of flow, L

Z_i = valency of species 'i', dimensionless

α = $D_A/D_B - 1$, dimensionless

α' = intensity of turbulence, dimensionless

β = angle between the direction of flow and the axis of a multiparticle bed, radians

γ = ratio of inert to active spheres, dimensionless

δ = ratio of average channelling length to particle diameter, dimensionless

ε = voidage, dimensionless

η = R/a, dimensionless

θ = angle in spherical coordinates, radians

μ = viscosity, M/Lt

ν = μ/ρ, kinematic viscosity, L^2/t

ρ = fluid density, M/L^3

ρ_s = density of the particle, M/L^3

ρ_i = mass concentration of species 'i', M/L^3

τ = shear stress, M/t^2L

ϕ = angle in spherical coordinates, radians

ψ = stream function, dimension depends on coordinate system

Dimensionless groups

$Re = \frac{dU\rho}{\mu}$, Reynolds number based on approach velocity (used in single particle study)

$Re_s = \frac{dU_s\rho}{\mu}$, Reynolds number based on superficial velocity (used in multiparticle study)

$Re_i = \frac{dU_s\rho}{\mu(1-\varepsilon)}$, Reynolds number based on hydraulic diameter (used in multiparticle study)

$Sc = \frac{\mu}{\rho D_{AS}}, \frac{\mu}{\rho D}$, Schmidt number

$Sh = \frac{\overline{K}_C d}{D_{AS}}, \frac{\overline{K}_C d}{D}$, overall Sherwood number in single particle study

$Sh_m = \frac{\overline{K}_C d}{D_{AS}}, \frac{\overline{K}_C d}{D}$, overall Sherwood number in multiparticle study

$Sh_m^e = \frac{\bar{K}_C d}{D^e}$, effective overall Sherwood number in a multiparticle bed

$Pe = Re.Sc$, Peclet number in single particle study

$Pe_s = Re_s.Sc$, Peclet number in multiparticle study

$Ga = \frac{d^3 \rho(\rho_s - \rho)g}{\mu^2}$, Galileo number

$Fs = \frac{Sh - 2}{Re^{1/2} Sc^{1/3}}$, Frossling number

$j = \frac{Sh}{Re\ Sc^{1/3}}$, j factor in single particle study

$j_m = \frac{Sh_m}{Re\ Sc^{1/3}}$, j factor in multiparticle study

$j'_m = j_m \varepsilon$, interstitial j factor

$Re_o = \frac{d U_o \rho}{\mu}$, terminal settling Reynolds number where u_o is the terminal settling velocity of a single particle

CHAPTER 1

INTRODUCTION

1. INTRODUCTION

Fluidization is an established unit operation and the use of fluidized beds as reactors for a wide range of chemical processes involving mass and/or heat transfer operations is well known. Industrially, gas-solid systems are mostly used and an extensive study of gas-solid fluidization has appeared in the literature during the past two decades and interest in this particular field is still sustained today. Liquid-solid fluidization, on the other hand has not been as widely studied for mass and heat transfer operations, although some of the early fundamental hydrodynamic studies were carried out using liquid-solid systems. The lack of interest in liquid fluidization is possibly because as yet there are too few large-scale applications. Most solid-liquid operations have traditionally been carried out in batch or semi-continuous fixed bed type equipment and there is no reason for departing from well established fixed bed technology unless fluidized beds can be shown to offer real technological and economic advantages.

With the development of new techniques in solid-liquid handling, it has recently been shown that a liquid-solid system can be designed for continuous operation and this has given a fresh impetus to the study of liquid fluidized beds. The incentive has come largely in ion exchange processes, adsorption and hydrometallurgy where a number of continuous plants now exist employing fluidized bed equipment. Examples are the Cloete-Streat contactor (71) and pulsed contactor (74) for ion exchange processes. The principle of operation of these contactors is a periodic reversal of flow, which in conjunction with a suitable plate design allows particles to be transferred from stage to stage counter current to the direction of liquid flow. The important advantages of such multistage liquid fluidized beds are the low resin inventory cost, uniformity in product quality, low pressure drop across the bed ($\sim$ 0.02 to

0.03 m head of water compared with several metres for fixed beds) and that no separate back-wash of the bed is necessary. Also a liquid fluidized bed can be designed to operate with suspended materials in the fluid stream. The Nuclear fuel processing and waste water and sewage treatment industries will find this feature particularly attractive. In Nuclear fuel processing, there is an urgent economic need to upgrade uranium from very low grade ore. This can be achieved by passing an unfiltered leached uranium slurry through a fluidized bed of ion exchange particles suitable for uranium exchange. This technique is likely to save the considerable cost of clarification and filtration. Treatment of waste water and sewage containing suspended particles can also be carried out in equipment of this type. Weber et al. (86) found that reclaiming of waste water containing organic contaminants present in very small concentration, can be advantageously carried out using a fluidized bed of active charcoal. A kinetic study indicated that the rate of uptake of organic material present in waste water was inversely proportional to the square of the particle diameter so that if was desirable to keep the particle size small and hence a fluidized bed was used to avoid the high cost of pumping.

Though fluidized beds offer certain advantages compared to fixed beds, the final choice of operation will depend on the economics. Due to a limitation in the maximum velocity that can be used in a fluidized bed, vessel diameter may be larger than a fixed bed for the same volumetric throughput. On the other hand, the pressure drop in a fixed bed is generally higher than for fluidized beds, often requiring the use of pressure vessels.

A quantitative knowledge of mass transfer rates is a crucial requisite for the overall economic evaluation and design of a fluidized bed reactor in addition to the other considerations mentioned above. With

this in mind, the present project was undertaken to obtain liquid phase mass transfer rates in liquid fluidized beds. It has been mentioned earlier that liquid fluidized beds will be restricted regarding the flow rate. Hence experiments were carried out in the lower range of the Reynolds number ($1 < Re_s < 25$) which is expected to be the range of operation for many solid-liquid fluidized beds and where surprisingly little reliable data is available (see Fig. 6.1-17).

Since one of the important solid-liquid contacting operations would involve ion exchange reactions, it was felt desirable, that some effort be made in understanding the mass transfer results that would be obtained using such systems. This was looked at theoretically by obtaining an approximate solution of the forced convective diffusion equation around a single sphere where mass transfer due to diffusion occurred under an electro-chemical potential gradient. This problem in general is complicated due to the presence of the electric gradient in addition to the concentration gradient. The latter is normally present in most mass transfer studies.

CHAPTER 2

LITERATURE REVIEW

2. LITERATURE REVIEW

2.1. Introduction

The rate of mass transfer between a particulate and continuous phase is the subject of much research and a steady effort to improve knowledge on the topic has been made during the past few decades. The systems studied include solids, liquid drops and gas bubbles as the particulate phase and liquid or gas as the continuous phase. Convective mass or heat transfer may occur by either free or forced convection. In general interaction between these two modes of transfer occurs, but for practical purposes, particularly at moderate flow rates, free convection effects are small. Much of the theoretical work has been confined to forced convective physical mass transfer studies between a single particle and a fluid rather than to multiparticle systems such as fixed or fluidized beds of solids because of the very complex nature of the latter systems. The complications arise as a result of the interactions due to the presence of other particles. Nevertheless, the single particle studies are a useful framework for developing an understanding of the more complicated multiparticle case. Experimental studies are more readily available both for single and multiparticle systems than are theoretical studies.

Various theoretical models and mathematical techniques have been used to obtain solutions to the problem of forced convective mass transfer. All the work surveyed here refers to binary mixtures, where the diffusing component is present in small amount so that the assumption of constant density, diffusivity and negligible effect of flux allowing uncoupling of the basic equations are valid. Also no chemical reaction is allowed. The equations that describe steady state forced convective diffusion are:

$$\nabla \cdot v = 0 \qquad (2.1\text{-}1)$$

$$v \cdot \nabla v = -\frac{1}{\rho} \nabla p + \frac{\mu}{\rho} \nabla^2 v \qquad (2.1\text{-}2)$$

$$v \cdot \nabla C_A = D_{AS} \nabla^2 C_A \qquad (2.1\text{-}3)$$

with the appropriate boundary conditions. Here v is the velocity, p is the pressure, ρ and μ the density and viscosity of the fluid, C_A is the concentration of the species 'A' and D_{AS} is the diffusivity of the pair 'A' and 'S' where 'S' is the solvent.

For ease of presentation, single and multiparticle systems will be reviewed separately. This survey will mostly deal with solid particles, but a few relevant liquid droplet studies will also be mentioned and in general no distinction will be made between mass and heat transfer study and the Nusselt and Sherwood number will be used interchangeably.

2.2. Forced convective mass transfer from a single solid sphere

Equations (2.1-1) to (2.1-3) which describe forced convective diffusion, under the restrictions mentioned, are a set of non linear partial differential equations and in general contain three space coordinates. Before attempting to solve the diffusion equation, the equation of motion must be solved. For flow past spheres, the flow may be considered two dimensional axisymmetric, thus reducing the space coordinate by one. However, it has not yet been possible to integrate the full equation of motion analytically even for a single sphere placed in an infinite flowing medium. As a result, approximations have been made to obtain analytic solutions for certain ranges of the Reynolds number. Consequently analytic solutions for the convective diffusion equation are at best only possible for the limiting cases.

Experimentally, however, a wide range of results have appeared in the literature. Based on theoretical and dimensional analysis, workers in this field have generally correlated experimental data by an expression of the form:

$$Sh = A + B_1 Re^m Sc^n \qquad (2.2\text{-}1)$$

where Sh, Re and Sc are the dimensionless groups known as the Sherwood, Reynolds and the Schmidt numbers (see Notation) and A, B_1, m and n are numbers that are usually taken as constants. Experimentally it is difficult to eliminate free convection effects entirely, particularly at low flow rates. Therefore, free convection effects are also taken into account when correlating data by the above equation. It is often thought that the contribution to total transfer due to pure molecular diffusion, free convection and forced convection are simply additive. When free convection effects may be neglected, the constant A is assumed to take a value of 2.0, i.e. the Sherwood number corresponding to the stagnant medium case. The constants of the above equations are obtained from the analysis of experimental data and theoretical considerations.

Though the aim is to restrict the review to low particle Reynolds number (Re up to 100), very often work will be cited that covers a much higher range (Re about 10^3). This is because very few experimental studies are confined to a narrow range of the Reynolds number and also because there has been little experimental work at low Reynolds number below Re about 50. Also as mentioned earlier, analytic solutions are possible only for some limiting cases, these being either very low Reynolds number or boundary layer flow. When there is no flow equation (2.1-3) reduces to

$$\nabla^2 C_A = 0 \qquad (2.2\text{-}2)$$

Using the boundary conditions

$$r = R, \quad C_A = C_{AR} \quad \text{and} \quad r = b, \quad C_A = C_{AB} \tag{2.2-3}$$

the solution for the Sherwood number is

$$Sh = \frac{2}{1 - R/b} \tag{2.2-4}$$

where $Sh = \dfrac{\overline{K}_C 2R}{D_{AS}}$ and $\overline{K}_C$ is the mass transfer coefficient defined by the equation,

$$\overline{K}_C(C_{AR} - C_{Ab}) = - D_{AS} \left.\frac{dC_A}{dr}\right|_{r=R} \tag{2.2-5}$$

Equation (2.2-5) is the expression for the diffusional mass transfer which in dilute solution is effectively the total rate of mass transfer. When $b \to \infty$, $Sh \to 2$ in equation (2.2-4), the well known result in an infinite medium. For any practical situation natural convection will be present and hence the above result applies for a sphere of infinitesimally small radius. As a consequence, experimental verification is difficult, but there is little to doubt this result.

For very slow motion, inertial terms in equation (2.1-2) may be neglected. The equation then reduces to

$$\nabla p = \mu \nabla^2 v \tag{2.2-6}$$

The solution to the above equation under the boundary conditions

$$r = R, \quad v = 0 \quad \text{and} \quad r = \infty, \quad v = U \tag{2.2-7}$$

is available in any standard text and is known as the Stokes' solution. The important result is

$$\psi = - \tfrac{1}{2} U r^2 \sin^2\theta \left(1 - \frac{3}{2}\frac{R}{r} + \frac{1}{2}\frac{R^3}{r^3}\right) \tag{2.2-8}$$

where U is the undisturbed stream velocity or the approach velocity and ψ is the stream function defined such that

$$v_r = -\frac{1}{r^2 \sin\theta} \frac{\partial \psi}{\partial \theta}$$

and (2.2-9)

$$v_\theta = \frac{1}{r \sin\theta} \frac{\partial \psi}{\partial r}$$

Here v_r and v_θ are the velocity components in r and θ directions in spherical coordinates.

Stokes' solution is valid when $Re \to 0$ and provides a good description of the flow field in the neighbourhood of a particle for $Re < 1$. Various workers have attempted to extend the Stokes' solution to a higher Reynolds number range by a perturbation method. Both regular and singular perturbation procedures have been considered. A perturbation method has also been used to obtain a solution to the diffusion equation and it seems proper to outline very briefly the general nature of this procedure.

The principle of the regular perturbation technique is to assume that the perturbed quantity is small so that the original equations can be simplified to a new set of approximate equations. The approximate equations are obtained by substituting an assumed solution in a power series form and then collecting terms of equal order of the perturbed quantity. In some cases straightforward perturbation may yield a satisfactory result but when the series do not converge at every point, one resorts to the singular perturbation technique. At low Reynolds number, stretched variables are applied into results obtained from the regular perturbation method. A good summary of this technique in low Reynolds number field is given by Taylor (76).

Consider the diffusion equation in dimensionless form which may be written as

$$v^1 . \nabla C_A^1 = \frac{2}{Pe} \nabla^2 C_A^1 \qquad (2.2\text{-}10)$$

where $v^1 = v/U$, $C_A^1 = (C_A - C_{Ab})/(C_{AR} - C_{Ab})$ and $Pe = 2RU/D_{AS}$. For creeping flow, $Re \to 0$ and from the Stokes' solution it can be seen that the dimensionless velocity field is dependent on spatial coordinates alone. It, therefore, follows that the Sherwood number which in fact is a dimensionless concentration gradient at the surface of the particle is a function of the Peclet number alone. However the exact form of the function depends on the Peclet number itself. An order of magnitude analysis shows that if the Peclet number is large then the concentration change occurs within a very small region close to the sphere. Under these conditions, diffusion in the angular direction θ, can be neglected and the whole analysis is considerably simplified. This is the usual thin boundary layer assumption for the concentration field. The criterion for this approximation to be valid is given by the equation

$$\frac{2}{Pe} \left(\frac{R}{b}\right)^3 = O(1) \quad \text{i.e.} \quad Pe >> 1 \qquad (2.2\text{-}11)$$

where b is the thickness of the concentration boundary layer. When the Peclet number is small, the diffusion layer becomes thick and diffusion in the angular direction must be taken into account. Thus depending on the Peclet number we have two asymptotic solutions, one for $Pe \to \infty$ and the other for $Pe \to 0$.

For large Peclet number and low Reynolds number analytic solutions have been obtained by Levich (50) and Friedlander (18,19). Levich's (50) solution involves a change of coordinate from $C_A(r,\theta)$ to $C_A(\psi,\theta)$ and then by a suitable transformation he reduced the partial differential equation into an ordinary differential equation. Using the Stokes' stream

function he obtained an expression for the overall Sherwood number as

$$Sh = .997\ Pe^{1/3} \qquad (2.2\text{-}12)$$

Friedlander (18) obtained a solution by an integral method. He assumed a concentration profile which satisfied as many boundary conditions as possible and substituted the assumed profile in the integrated form of the original diffusion equation. With sufficient terms in his assumed profile and a Stokes' stream function he obtained essentially the same result as Levich (50). The weakness of this analysis is the arbitrary nature of the assumed concentration profile since different functions could satisfy the same boundary conditions and hence the uniqueness of the solution is not guaranteed. Levich (50) pointed out that the integral method may lead to a substantial error in the concentration distribution. However, the total rate of mass transfer may agree quite well, because very near the surface, the integral method would yield a reasonably accurate value of the concentration gradient. It may be pointed out that Friedlander (18) used the wrong sign in two of his equations, but fortunately the errors cancelled out.

It is worth noting that the thin boundary layer approximation is not valid near the rear of the sphere where the diffusion layer grows sufficiently to invalidate the boundary layer analysis. Sih and Newman (70) by the singular perturbation method showed that six distinct regions of mass transfer exist around a sphere and one of these regions is the thin boundary layer region. In order to obtain mass transfer rates from the entire sphere, it is necessary to form a composite solution for the regions close to the sphere. However, for any practical purpose, the boundary layer solution is sufficiently good since the boundary layer region exists over most of the sphere surface.

For low Peclet numbers, the boundary layer assumption is not valid and so the entire diffusion equation must be solved. Kronig and Bruijsten (45) obtained a solution for the low Peclet number case by the use of the regular perturbation method. The solution, however, was not completely satisfactory. The concentration field vanished everywhere at infinity except in the direction of flow. Acrivos and Taylor (1) overcame the difficulty of satisfying the boundary condition at infinity by the use of the singular perturbation method. The authors obtained the following expression for the overall Sherwood number in the range $0 \leqslant Pe \leqslant 1$ as

$$Sh = 2 + \tfrac{1}{2}Pe + \tfrac{1}{4}Pe^2 \ln Pe + O(Pe^2) \qquad (2.2\text{-}13)$$

These authors (1) also obtained an expression for the Sherwood number for large Peclet number and for slightly higher Reynolds number using pertubation correction of the Stokes' solution obtained by Proudman and Pearson (76). The expression is

$$Sh = .991\ Pe^{1/3}\ (C_D/C_{DS})^{1/3} \qquad (2.2\text{-}14)$$

where C_D and C_{DS} are drag coefficients at the Re considered and $Re \to 0$ respectively. From this equation, the authors (1) pointed out that the effect of increasing Re on Sh is considerably less sensitive to an increase in the Reynolds number than the drag coefficient.

Yuge (90) considered the same problem of forced convective transfer for creeping flow using a coordinate perturbation procedure, rather than parameter perturbation as used by the workers previously mentioned. He used the spherical angle as the perturbed quantity and expressed the dimensionless coordinate in terms of a series of even power of θ with the coefficients that are a function of the radial coordinate alone. The first approximation was obtained by neglecting the angular diffusion term

from the diffusion equation and the assumed series substituted in the diffusion equation. Equating coefficients of equal power in θ an infinite set of ordinary differential equations were obtained and integrated numerically for values of the Peclet number of 0.3, 1, 3 and 10. Fortunately it turned out that the coefficients converged very rapidly and only the first three were required to obtain a solution. The term neglected in the first approximation could be corrected by a second approximation. He found that for the Peclet number less than 0.3 the average value of the Sherwood number was indistinguishable from the value of the stagnant medium case. Though Yuge (90) obtained results for the small Peclet number range his method should be valid for the entire Peclet number range for he makes no assumption of the magnitude of the Peclet number. Although this type of expansion cannot be proven to be mathematically rigorous, the method seems logical since in the limiting case as $Re \to 0$, the concentration distribution will be that for a sphere in a stationary medium. Yuge's (90) result disagrees by about 15% at $Pe = 1$ with the Acrivos and Taylor (1) solution. The latter authors' perturbation procedure is quite rigorous but it cannot predict the value of the Peclet number where the solution will breakdown and possibly their solution becomes poorer for $Pe > 0.3$.

Some experimental confirmations of the theory are available for the very low Reynolds number region. Rowe et al. (67) report experimental data obtained by Aksel'rud for benzoic acid spheres that were moved in a circle in a stagnant tank of oil for which the data could be correlated as

$$Sh = 1.1\, Pe^{1/3} \qquad (2.2\text{-}15)$$

in the range $0 < Re < 2.5$ and $Sc \sim 3 \times 10^6$. Calderbank and Korchinsk (8) also observed the rate of heat transfer at low Reynolds number for mercury drops falling in aqueous glycerol solution. Though experiments

were carried out using drops, these authors found that the drag coefficients for mercury drops deviated from solid sphere behaviour at $Re > 200$ when drop oscillation started. Hence this study can be used to compare solid sphere results for $Re < 200$. The authors carried out experiments by feeding hot mercury drops, formed by means of nozzles to a vacuum jacketed constant temperature glass column through which the continuous phase was recirculated. The transfer coefficient was determined by a heat balance on the drop and the results plotted as $Sh/Sc^{.3}$ vs Re on logarithmic coordinates. However, if one uses an exponent of $1/3$ instead of 0.3 for the Schmidt number, the low Reynolds number result could be correlated using an equation of the type (2.2-12) with a coefficient of 1.05 to within $\pm 15\%$ for $0.5 < Re < 10$. The Schmidt number for these runs was about 3×10^3. Thus it may be concluded that the high Peclet number low Reynolds number theoretical studies are in good agreement with experiments. Very few reliable low Peclet number experiments are known.

At large Reynolds number the velocity components appearing in the diffusion equation will be a function of the Reynolds number and thus the Sherwood number will no longer be a unique function of the Peclet number. At sufficiently high Reynolds number, where the flow may be described by the laminar boundary layer theory, the velocity components vary as $Re^{3/2}$ and the solution for the Sherwood number varies with $Re^{\frac{1}{2}}$ instead of $Re^{1/3}$. Various workers have tried to obtain solutions for the diffusion equation at high Reynolds number.

Frossling (20) was one of the earliest to obtain a solution from a single sphere for laminar boundary layer flow. Frossling (20) in an identical manner to the series solution for two dimensional laminar flow, expressed the potential velocity, the contour of the body, the stream function and the concentration in a series form. Equating coefficients

of equal power of the independent variable along which expansion was made, a series of ordinary differential equations were obtained which he solved numerically. He found that the first few equations were sufficient to obtain a solution. Frossling (20) was unable to eliminate the Schmidt number from his equations, thus the coefficients were functions of the Schmidt number. For the particular case of $Sc = 2.532$ which corresponds to the sublimation of naphthalene in air he obtained an expression for the local Sherwood number as follows:

$$Sh(\theta) = 1.366\ (1 - .1837\theta^2 + \ldots)\ Re^{1/2}\ Sc^{1/3} \qquad (2.2\text{-}16)$$

The above theory, however, does not predict the velocity profile in the wake and hence overall transfer rates cannot be obtained by this method and the analysis is valid only upto the flow separation point.

Lochiel and Calderbank (52) obtained a solution using a quartic velocity profile obtained from an integral solution of the momentum equation. They obtained an expression for the overall Sherwood number similar in form to equation (2.2-1) except for the constant A as follows:

$$Sh = B\ Re^{1/2}\ Sc^{1/3} \qquad (2.2\text{-}17)$$

From the theoretical analysis, the authors found that upto the flow separation point which was at about 108°, the value of the coefficient B was 0.7. Since the flow in the wake was not amenable to analysis, the authors on the basis of experimental results assumed that the wake contributed about 20% in magnitude of the frontal transfer and suggested a value of B as 0.84 for the entire sphere. Garner and Kee (27) and Grafton (32) presented a method for the prediction of mass transfer in the wake region. Garner and Kee (27) obtained a solution for wake flow assuming a quartic velocity distribution in the boundary layer and zero skin friction in the wake. The main objection to this work is the

assumption of constant pressure which implies a constant velocity at the outer edge of the boundary layer, though the velocity alters quite rapidly close to the rear stagnation point and separation point. Their result is similar in form to equation (2.2-17) with the value of $B = 0.94$ and recommended between $250 < Re < 900$. Grafton (32) tried to account for the variation of the velocity at the edge of the boundary layer in terms of the velocity within the wake and the angle between the surface and contour of circulation. The disadvantage here is that a trace of the flow pattern within the vortex is required. The author predicts a value of 0.9 for the coefficient B of equation (2.2-17) for a Reynolds number about 500 and suggests that the coefficient is slightly dependent on the Reynolds number.

Experimental verification of the theory at large Reynolds number is not complete since the theory is only approximate. Most authors correlate data using an equation similar to equation (2.2-1) and is usually expressed as:

$$Sh = 2 + B_1 Re^{1/2} Sc^{1/3} \qquad (2.2\text{-}18)$$

The constant 2 and the value of the exponents in the above equation follow from theoretical considerations. In general the value of coefficient B_1 depends on the Reynolds number and various authors report this value to lie between about 0.55 and 0.95. Frossling (21) suggested a value of 0.552 for the coefficient B_1 in the range $2 < Re < 1300$ for the mass transfer studies from suspended solid naphthalene spheres and drops of aniline, nitrobenzene and water in air stream. This work has been criticized by Rowe et al. (67) since Frossling (21) obtained the value of diffusion coefficient by measuring the mass transfer rate at zero air velocity and equating the Sherwood number to the theoretical value of 2, which in actual case was probably influenced by natural con-

vection. Ranz and Marshall (63) suggest $B_1 = 0.6$ for $2 < Re < 200$ from evaporation of water drops in air and Linton and Sutherland (51) quote $B_1 = 0.582$ for $490 < Re < 7580$ but without the constant 2 in equation (2.2-18).

Garner and coworkers (26-28) carried out an extensive study of the dissolution of solid spheres. The maximum Re was about 10^3. Since the Grashof number, which is a measure of natural convection, was about 10^4 in their study, their (27) results were influenced by this effect even at Re about 750. In general their data was in good agreement with the theoretical solution of Garner and Kee (27) where the coefficient B in equation (2.2-17) is suggested as 0.94. An important point to notice in the studies of Garner and coworkers (26-28) is that they use an average velocity in the experimental correlations rather than the approach velocity in defining the Reynolds number. In theoretical work the latter is used. The approach velocity is the undisturbed stream velocity and could be taken as the centreline velocity for a uniform stream, but for other profiles it could be taken as the average velocity over the cross sectional area of the particle. Hence in most of these authors' experiments where a nearly parabolic profile existed, the value of the coefficient B or B_1 would decrease by about $\sqrt{2}$ and would be about 0.66 instead of 0.94 if an approach velocity is used to define the Reynolds number. Garner and Suckling (28), however, tried to use an approach velocity but were not successful in correlating two sets of data, one for parabolic flow and the other for evenly distributed flow. This failure has been attributed (51) to the appreciable turbulence that was possibly present in their work. Rowe et al. (67) criticized the work of Garner and Kee (27) since the value of the diffusion coefficient used by these authors was rather low and this factor alone could effect results by a factor of 2.

Rowe, Claxton and Lewis (67) carried out an extensive investigation on both heat and mass transfer from single spheres in water and air streams for $20 < Re < 10^3$. They achieved a uniform velocity in their experiments. Using $A = 2$, $n = 1/3$ and $m = 0.4$ to 0.6 in equation (2.2-1), they found from a least square analysis that the minimum error variance occurred for $m = 0.48$, but for the most remote value of $m = 0.6$, the error variance was too small to be significant. However, they thought that m increased slightly with Re, but for any practical purpose it could be considered constant for two to three orders of magnitude change in Re. They finally suggested the same equation as (2.2-18) with the value of $B_1 = 0.79$ and 0.69 in water and air respectively or a single value of $B_1 = 0.72$ with an error of 10% for both water and air.

A recent study for $400 < Re < 1250$ is due to Gibert, Couderc and Angelino (15) who used an electro-chemical technique employing oxidation and reduction of potassium ferricyanide. By statistical analysis of a large amount of data they suggested an equation similar to (2.2-17) with $B = 0.882$ but the exponent of Re as 0.452. However,as suggested by Rowe et al. (67) an equally acceptable correlation could be obtained with the exponent as 0.5 and a constant about 0.75 since the error variance is insignificant over two to three orders of magnitude change in Re.

For a low Reynolds number between 5 and 100 few results are known. Baird and Hamielec (4) obtained a solution for a Reynolds number range of 10 to 100 using the Kawaguti (reference given in the authors' paper) velocity profile. For $Re > 40$ there is a region of reverse flow in which the velocity gradient is negative resulting in an imaginary term in the solution. The authors overcame this difficulty by suggesting that the reverse region could be treated separately as a

foward flow region. In this region it is assumed that fresh liquid at the initial concentration impinges on the rear stagnation point. They realised that this was not a satisfactory explanation since the vortex region would contain very little fresh fluid. The predicted overall Sherwood numbers were in agreement with the values predicted by the empirical equation (2.2-18) with a value of the constant B_1 about 0.57 for Reynolds number above 40. At Reynolds number less than 20, the theory begins to deviate from the experimental condition because the Kawaguti velocity profile does not reduce to the Stokes' solution as Reynolds number becomes very small.

In the range $5 < Re < 150$ Peltzman and Pfeffer (59) experimentally studied the local and overall transfer rates from cast benzoic acid and betanaphthanol spheres dissolving in water. They found that the overall Sherwood number could be correlated by equation (2.2-18) with the value of B_1 as .87 and .47 for benzoic acid and betanaphthanol systems respectively. They were also able to correlate the data by an equation similar to equation (2.2-12) used in very low Reynolds number work but with different coefficients. The authors observed that at a Reynolds number greater than 25, flow separation occurred and so their data can not be considered as a confirmation of the very low Reynolds number theory though reasonable correlation was obtained with $Pe^{1/3}$. The reason for the increased mass transfer rates from benzoic acid spheres compared to betanaphthanol system was believed to be due to grain dropping of the cast benzoic acid spheres which they used. The authors report that they used an average velocity based on Reynolds number but Chen (10) one of Pfeffer's students compares his data with that of Peltzman and Pfeffer (59) and from this it appears that the latter in fact used an approach velocity for the parabolic velocity profile which existed in their experiment. Chen (10) reported seven experimental points for the dissolution

of benzoic acid spheres in water using the same technique and apparatus as Peltzman and Pfeffer (59) and covering a Reynolds number between 8.4 and 56. He suggested no correlation, but for five points lying between $25 < Re < 56$ a correlation similar to equation (2.2-17) could be suggested with the value of B as .85 with about 4% deviation. It may be mentioned that the author used an approach velocity to define the Reynolds number.

Some relevant liquid drop data are available in this range of Reynolds number. Calderbank and Korchinsks' (8) work with mercury drops for $20 < Re < 200$ may be correlated using equation (2.2-17) with the constant B equal to .75 to within ±10%. Recently Clinton and Whatley (12) have reported mass transfer results from water drops and thoria sol droplets fluidized in 2-Ethyl-1-hexanol. A surfactant was added in the continuous phase so that the drop behaved as if it were a rigid sphere with no induced circulation. The Reynolds number was calculated using the centreline velocity for the parabolic profile which existed in their experiments and was between 0.4 and 14. For a very large number of runs (about 10^3 determinations for water drops only) they correlated their data using an equation similar to (2.2-18) with B_1 equal to 0.82 and the constant as 5 instead of 2. There is some scatter between the water drop data which possibly covered an Re upto about 5 and the thoria sol data. Unfortunately the data is not tabulated to check if the very low Reynolds number data could be fitted with $Pe^{1/3}$ correlation which is valid for the high Schmidt number case (Sc = 35,700) and also to see if a better correlation could be proposed. It appears that the data could be better represented without the constant 5, in the range $5 < Re < 14$.

Recently, numerical solutions have been presented (3,39,49) for the entire laminar range. The solution obtained by Leclair and Hamielec

(49) is suspect, since their result indicates that the maximum transfer occurs about six degrees away from the front stagnation point. The solution obtained by Al-Taha (3) shows that for $Re > 100$ and high Schmidt number ($Sc > 300$) equation (2.2-17) could be used with the coefficient B equal to 0.6 but without the constant 2. For $Re < 100$ if equation (2.2-17) is used, the constant B would take higher values than 0.6 and would depend on the range of the Reynolds number and the Schmidt number. Ihme et al. (39) showed that for $Re > 10$ and large Schmidt number the coefficient B would take a larger value than 0.6 (e.g. for $Sc \approx 10^3$ the constant would be about 0.85). The solutions of Al-Taha (3) and Ihme et al. (39) are shown in Fig. 6.1-12.

2.3. Forced convective mass transfer in multiparticle assembly

Considerable disagreement exists among the various workers who have studied the mass and heat transfer problem in multiparticle systems. Even, the apparently simple task of finding the minimum value of the Sherwood number for a particle in an assembly of particles has given rise to wide disagreement.

In general a multiparticle bed may consist of active and inert particles and can be viewed schematically as shown in Fig. 2.3-1.

Fig. 2.3-1: Schematic representation of a multiparticle bed.

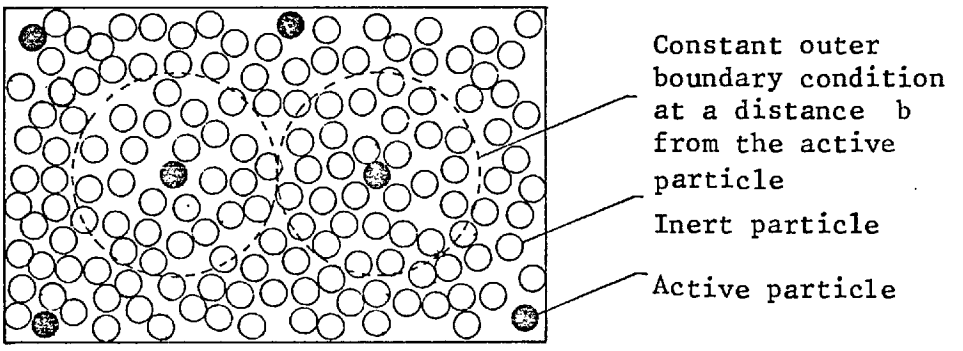

It is easy to see that equation (2.2-4) cannot be used to predict the Sherwood number even for zero flow since the surrounding medium is not homogeneous. However if an effective value of diffusivity can be attributed to the medium, then equation (2.2-4) may be used to calculate an effective value of the Sherwood number. If b is the thickness over which the concentration change occurs, γ the ratio of inert to active spheres and ε the voidage of the bed, then $R/b = (\frac{1-\varepsilon}{\gamma})^{1/3}$ and from equation (2.2-4)

$$Sh_m^e = \frac{2}{1 - (\frac{1-\varepsilon}{\gamma})^{1/3}} \qquad (2.3\text{-}1)$$

Here, the superscript 'e' denotes an effective value and the subscript 'm' is used to remind us that this is a multiparticle assembly. For $\gamma >> 1$ Miyauchi (55) suggests the following relation for the effective diffusivity D^e:

$$D^e = D_{AS}\, \varepsilon/1.5 \qquad (2.3\text{-}2)$$

Then

$$Sh_m = Sh_m^e\, \varepsilon/1.5 \qquad (2.3\text{-}3)$$

when $\gamma \to \infty$, the medium is infinite and $Sh_m^e \to 2$ and for the general case $Sh_m \leqslant 2$. When $\gamma = 1$ i.e. all the spheres are active, the medium may be finite or infinite and

$$Sh_m = \frac{2}{1 - (1-\varepsilon)^{1/3}} \qquad (2.3\text{-}4)$$

Here a molecular value of the diffusivity is used since b necessarily shrinks in between the spaces of active spheres.

Cornish (13) has objected to this concept of the limiting value of the Sherwood number for the case when $\gamma = 1$. Based on the analogous solution available in the field of electrostatics for the capacitance between two spheres at the same surface potential, he concluded that if

the number of spheres was increased, then the progressive value of the Sherwood number would decrease and ultimately approach zero. He explained this due to a non availability of an effective sink in a multiparticle bed. .Cornish (13) indicated that this possibility of zero Sherwood number in a multiparticle bed could possibly explain the very low values of the Sherwood number found in some works for low flow rates. Zabrodksy (91,92) has opposed Cornish's view and suggested that the observed low values of the Sherwood number at low flow rates in multiparticle beds was due to effects resulting from non uniformity in flow distribution and that equation (2.3-4) could be used to determine the true limiting value of the Sherwood number. He showed (92) that even micro non uniformities of flow distribution could reduce the value of the Sherwood number by several orders of magnitude. His micro non uniformity model was criticized by Rowe (65) but nevertheless it is true that at very low Reynolds number dispersion may become important.

Cornish (13), however, suggested that the surroundings could act as a sink when flowing and it seems that the answer to the above controversy lies here. If the fluid is flowing, however small the flow rate may be, it is possible to conceive a steady state. For very small flow rates the effect of convection on the concentration gradient may be neglected and as a first approximation equation (2.3-4) may be used to evaluate the Sherwood number. However, if the surrounding medium is stationary, it cannot act as an effective sink and the Sherwood number would be less than 2 and for an infinite number of spheres the Sherwood number would tend to zero. It is difficult to check this viewpoint since experimental determination of the Sherwood number at such low flow rates is very difficult. Miyauchi et al. (56) report a value of the Sherwood number between 2 and 10 for Re_s between 0.1 and 1 for a maximum of eight active spheres. Unfortunately this is not representative for a large number of

spheres. The data reported by Wilson and Geankoplis (88) shows a value between 7 and 14 for $10^{-3} < Re_s < 10^{-2}$. Below Re_s about 10^{-3} the Sherwood number is less than 5, but at such low flow rates, the data ought to be corrected for axial dispersion and natural convection which the authors did not take into account since these effects are difficult to predict. However, these results possibly suggest that equation (2.3-4) may be used at low flow rates at least as a rough approximation.

In a practical situation, where the effect of convection cannot be neglected, any theoretical study is quite involved due to the complex hydrodynamic field that exists around a sphere in a multiparticle system. Obviously, the first step is to establish the flow field for creeping flow. Considerable advances have been made and the monograph by Happel and Brenner (35) is a useful source of reference for this.

Voskanyan, Golovin and Tolmachev (84) obtained an analytic solution to the problem of convective diffusion for creeping flow past a cubic array of spheres using the velocity field obtained by Hasimoto (36) for the above system. Hasimoto restricted his attention to dilute suspensions and obtained a solution by a point force approximation method where each sphere is replaced by a point force retarding the motion of the fluid. For a cubic array he obtained the total drag F_T acting on a sphere as

$$F_T = \frac{6\pi\mu RU}{1 - 1.7601\ (1-\varepsilon)^{1/3}} \qquad (2.3\text{-}5)$$

It is easy to see that for $\varepsilon \simeq 0.82$, the drag tends to infinity and hence the solution is valid only for very high voidage range.

Voskanyan et al. (84) showed that for a sufficiently widely spaced lattice and large Peclet number, the problem could be reduced to that considered by Levich (50) except for the fact that the concentration of

the stream flowing past the K-th sphere in the region outside the diffusion boundary layer could be considered equal to the concentration which would be produced by all the diffusion wakes at the K-th node of the lattice. The criterion for the solution to be valid is that the period of the lattice must be much greater than $R.Pe_s^{1/3}$ where $Pe_s = Re_s.Sc$ showing the extremely dilute concentration of spheres. This range is of little practical interest, though this is the most rigorous solution available to date in multiparticle systems.

Pfeffer and Happel (60) and Pfeffer (61) presented solutions for creeping flow using a cell model proposed by Happel (34) for a voidage between 0.4 and 1.0. The model is based on the assumption that a three dimensional assembly of spheres can be considered to be a number of identical unit cells consisting of a particle surrounded by a spherical fluid envelope. The fluid contained in each cell contains the same amount of fluid as the relative amount of fluid to particle in the entire assemblage. The outside surface of each cell is assumed frictionless and hence this model is also known as the free surface model. Thus the entire disturbance, due to each particle is confined to the cell of fluid with which it is associated. For mass or heat transport the concentration or temperature of the forward moving fluid is assumed to be that of the cell boundary. Schematically this is shown below in Fig. 2.3-2.

Fig. 2.3-2: Schematic representation of a unit cell.

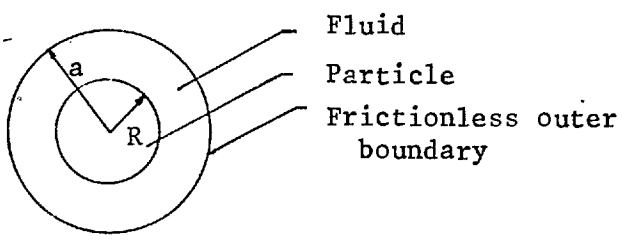

The appropriate solution (34,35) for the stream function is given as

$$\psi = -\frac{U_s \sin^2\theta}{2W}\left[(2 + 3\eta^5)r^2 + \frac{R^3}{r} - (3 + 2\eta^5)\,Rr - \frac{\eta^5 r^4}{R^2}\right] \tag{2.3-6}$$

where $\eta = R/a$ and $W = 2 - 3\eta + 3\eta^5 - 2\eta^6$.

Pfeffer and Happel (60) obtained a solution to the convective mass or heat transfer problem by the Yuge coordinate perturbation method (90) mentioned earlier. Plots of j_m factor against Re_s show that the j_m factor is not independent of the Schmidt number at low Reynolds number. At very low Reynolds number a straight line with a slope of -1 is obtained and as the Reynolds number increases the slope deviates from unity finally merging into a straight line of slope -2/3 for a Peclet number of about 70. Thus for large Peclet number ($Pe_s > 70$) the following equation is obtained

$$Sh_m = B_2(\varepsilon)\, Pe_s^{1/3} \tag{2.3-7}$$

where B_2 is a function of bed voidage and decreases with decreasing voidage. For a single sphere they predict essentially the same result as obtained by Yuge (90). Pfeffer (61) in continuation of this work used the thin boundary layer approximation for the high Peclet number low Reynolds number case and proceeded in an analogous manner to the Levich (50) solution for a single sphere. He obtained the following result

$$Sh_m = 1.26\left[\frac{1 - (1-\varepsilon)^{5/3}}{W}\right]^{1/3} Pe_s^{1/3} \tag{2.3-8}$$

which reduces to equation (2.2-12) for $\varepsilon \to 1$. The agreement with the experimental data available for $Re_s < 100$ may be considered reasonable. Yaron and Gal-Or (89) also obtained essentially the same result using an integral method of solution. The reason why the free surface

model using the creeping flow velocity distribution applies at higher Reynolds number is explained by the fact that in a particular assemblage flow separation occurs at a higher Reynolds number. This hypothesis is also supported by the work of Leclair and Hamielec (48) who numerically solved the entire equation of motion through particle assemblages for Re_s upto 10^3 using a cell model similar to that mentioned above except for the outer boundary condition. These authors (48) assume a zero vorticity instead of zero shear stress at the outer cell boundary. Happel and Brenner (35) have raised a minor objection to this boundary condition, but there is little difference in the result. Leclair and Hamielec (48) found that as porosity decreased the flow separation angle (measured from the rear stagnation point) and the size of the ring decreased with decreasing porosity for the same Reynolds number. For example at a voidage of 0.4 and Reynolds number about 100 separation would possibly just start. Local mass transfer measurements by Peltzman and Pfeffer (59) from an active particle placed in an assembly of inert particles also indicates that the separation ring moves back towards the rear stagnation point with decrease in voidage. Leclair and Hamielec (49) in another paper solved the heat or mass transport problem for large Peclet number for the intermediate range of Reynolds number. An examination of their result indicates that for a Reynolds number of upto 100 the j_m factors are possibly the same as obtained by Pfeffer (61). From a least square analysis they found that the following relationship correlated their theoretical results

$$j_m \varepsilon^{.854} = 1.485\ Re_s^{-.632} \qquad (2.3\text{-}9)$$

Since the mass and heat transfer results are difficult to obtain experimentally, it is probably best to check the cell models against experimental data available on flow through packed and fluidized beds. For example

the difference between the theoretical and experimental values of drag coefficients as reported by Leclair and Hamielec (48) is 15.5, 4.1, -13, -36 and 54% for Re_s 1, 10, 20, 50 and 100 respectively. Disagreement with fluidized beds is much greater. Values of relative velocity predicted by Happel (34) for creeping flow are 25-100% below experimental data. Leclair and Hamielec (48) suggest that this discrepancy is due to the oversimplified assumption of a spherical outer shell.

Carberry (9) proposed a solution based on the concept of diffusion within a developing boundary layer which is repeatedly destroyed and developed as the fluid passes through an assembly of particles. This was an extension of the work of Mixon and Carberry (54) who considered the case of diffusion within a boundary layer of arbitrary velocity distribution of the form :

$$\frac{v}{U} = \frac{(Gx_1)^{a_1}}{\left(\frac{\nu z_1}{U}\right)^{a_2}} \qquad (2.3\text{-}10)$$

where a_1 and a_2 are arbitrary constants and x_1 and z_1 are the distance perpendicular to flow and distance in the direction of flow. For $a_1 = 1$ and $a_2 = 0.5$, the form of the velocity distribution is similar to the laminar boundary layer theory on a flat plate which is given as

$$\frac{v}{U} = \frac{x_1}{\sqrt{\frac{12\nu z_1}{U}}} \qquad (2.3\text{-}11)$$

In fact equation (2.3-11) is the first linear term of various power series development that describe laminar boundary flow on a flat plate. Carberry (9) considered that a multiparticle system could be viewed as a series of discrete surfaces of length z_1 separated at points by

void cells and the flow over the surfaces may be described by equation (2.3-11). Assuming that $U = 2U_i = 2U_s/\varepsilon$ and the linear length z_1 is equal to one particle diameter, he obtained an expression for the mass transfer coefficient. He made the latter assumption from mixing data which suggests that more or less perfect mixing occurred every particle diameter. The expression for the Sherwood number takes the form:

$$Sh_m = 1.15 \frac{Re_s^{1/2}}{\varepsilon^{1/2}} Sc^{1/3} \qquad (2.3\text{-}12)$$

without considering convection normal to the surface, and

$$Sh_m = .974 \frac{Re_s^{1/2}}{\varepsilon^{1/2}} Sc^{1/3} \qquad (2.3\text{-}13)$$

considering convection normal to the surface. This model agrees well with a wide variety of experimental data, mostly for fixed beds over the range $0.5 < Re < 10^3$ and may be considered satisfactory bearing in mind the approximate nature of the theory and the diversity of the source of data.

Kusik and Happel (47) employed a free surface model and a boundary layer theory to predict the rate of mass transfer in a multiparticle system. They assumed that the presence of vortices behind particles had the effect of lowering the area available for liquid flow. Therefore, the volume of the vortex behind each sphere was approximated and subtracted from the total volume of the unit cell and they obtained an expression for the effective voidage E as

$$E = \varepsilon - .75\ (1-\varepsilon)(\varepsilon-0.2) \qquad (2.3\text{-}14)$$

Solving the integral velocity and concentration equation they obtained the following expression:

$$Sh_m = .93 \frac{Re_s^{1/2}}{E^{1/2}} Sc^{1/3} \qquad (2.3\text{-}15)$$

The maximum Reynolds number recommended for the above equation is about 300 which is the limit of stable vortices. Moderate agreement was found with experimental data.

Kataoka, Yoshida and Ueyama (43) have recently proposed a semi theoretical correlation for packed beds based on the classical hydraulic radius model where a packed bed is assumed as a series of inclined tubes. The authors viewed mass transfer in packed beds analogous to that between a pipe surface and a stream of fluid where the tube radius for this model is $\varepsilon d/3(1-\varepsilon)$ and the path length $d/\cos\beta$ where β is the angle between flow direction and axis of bed and is usually taken as 45°. The authors showed that the entrance length required for a fully developed profile was at least an order in magnitude smaller than the path length. For a parabolic profile and high Peclet number ($Pe_s > 500$) they obtained the solution

$$Sh_m = 1.85 \frac{(1-\varepsilon)^{1/3}}{\varepsilon^{2/3}} Pe_s^{1/3} \qquad (2.3\text{-}16)$$

The authors found that their solution was quite similar to that of Pfeffer (61) and in fact represented data better at low Re_s. Hydraulic radius model is not suitable at high voidage due to a $(1-\varepsilon)$ term in the equation. Very recently Hughmark (38) used this type of model to correlate momentum, mass and heat transfer data where the author suggested that for expanded beds the ratio of fluid path length to bed height should be modified empirically between $\sqrt{2}$ and 1.0.

Kuni and Suzuki (46) put forward a channelling model in packed beds for low Peclet number ($Pe_s < 10$). In this model the bed structure is assumed as a stagnant zone where concentration of the fluid is in equili-

brium with the solids and a channelling zone through which the fluid is in plug flow and that mass transfer occurs in the channel. The area of the channel is taken equal to half the surface of the solids and the channel length is determined by the residence time distribution of the fluid. The authors showed that for no stagnant zones and $Pe_s < 15$, the following expression could be written

$$Sh_m = \frac{Pe_s}{6(1-\varepsilon)\delta} \qquad (2.3\text{-}17)$$

where δ denotes the ratio of average channelling length to diameter of particle and is unity for the ideal case and increases with non ideality thus decreasing the value of the Sherwood number. This model predicts the correct order of magnitude for the Sherwood number obtained in gas fluidized beds though physically this is not a very realistic model.

The theoretical models that have found most acceptance are the free surface model of Pfeffer (61) and the boundary layer model of Carberry (9). For a voidage of about 0.4 the difference between the models for $10 < Re_s < 500$ is probably within the above uncertainties and this explains why the data of McCune and Wilhelm (53), Gaffney and Drew (22) and Thodos and Hobson (78) fit both the models. For $Re_s < 50$ reliable data is scarce. Since the various models are not conclusive it becomes necessary to rely more on the experimental results which might aid in better understanding and formulation of more realistic models.

A large amount of experimental work is available on the mass and heat transfer problem from particles in a particulate bed. Barker (5) in 1965 listed 486 references for heat transfer in fixed and fluidized beds. Gelperin and Einstein (30) recently suggested a particle to fluid heat transfer correlation as

$$Sh_m = 0.4 \left(\frac{Re_s}{\varepsilon}\right)^{2/3} Sc^{1/3} \qquad (2.3\text{-}18)$$

for $\frac{Re_s}{\epsilon} > 200$. This correlation is based on existing heat transfer data and may deviate 100 to 200%. Unfortunately, the overwhelming part of the work carried out was with gas fluidized beds and very few reliable results are known for $Re_s < 50$ in liquid fluidized beds.

A number of authors (77, 59, 29, 41) have made some useful studies of local and overall transfer rate from single particles placed in an assembly of particles.

Thoenes and Kramers (77) investigated the mass transfer rates from benzoic acid and porous spheres soaked with liquids in various packings of inert spheres for a voidage between 0.26 and 0.48 in water and gaseous streams. They found that in general the results were quite complex which they attributed to different flow conditions that could exist for different voidage but for same Re_s. For a rough average of 438 runs they proposed that for $40 < Re_i < 4000$:

$$Sh_m = 1.0 \; Re_i^{1/2} \; Sc^{1/3} \qquad (2.3\text{-}19)$$

where $Re_i = \frac{dU\rho}{\mu(1-\epsilon)}$. The authors found that it was difficult to correlate both liquid and gas runs by a single equation. This is due to different order of the thickness of the concentration boundary layer for the two systems particularly at low flow rates.

Peltzman and Pfeffer (59) found that presence of an inert sphere in front of the active sphere caused the separation ring to move towards the rear stagnation point and with sufficiently large number of particles it is possible that separation does not occur until flow is substantially increased. They found that an axial and equilateral triangular arrangement reduced the mass transfer rate due to an effective "area blockage". However an open triangular and hexagonal arrangement gave an overall mass transfer higher than for a single particle, simulating the behaviour of a large array of particles. In all studies it was observed that axial

proximity of other spheres had a larger effect than radial proximity. Due to the complex form of the relationship among various groups for different arrangements, the authors could not propose any generalised correlation.

Gillespie, Crandall and Carberry (29) studied the local and average heat transfer coefficients from an internally heated copper sphere situated in a randomly packed bed of inert spheres using air as the continuous medium. By examining local heat transfer coefficients, they found that over certain regions the Sherwood number was dependent on the square root of the Reynolds number, so that in these regions the velocity profile could be assumed to be described by boundary layer theory. The effect of repacking was to alter the local transfer coefficient, but had little effect on the average value. Their work also showed entrance and wall effects. For the bulk of the experiments they proposed the following correlation at the centre of the bed:

$$Sh_m = 0.63\ Re_s^{0.65} \qquad (2.3\text{-}20)$$

Near the wall, the coefficient increased to about 0.75.

Jolls and Hanratty (41) studied the mechanism of flow and mass transfer around a single particle in a packed bed ($\varepsilon = 0.41$) using the electrochemical reduction of ferricyanide at a high current density on a nickel cathode embedded in the test sphere. From a knowledge of mass transfer to an electrode of small size, they could calculate the velocity gradient and hence the shear stress. With the exception of the extreme rearward portion of the spheres, the effect of Reynolds number on the local mass transfer rate and local shear stress suggests that flow can be described by a three dimensional boundary layer which is in broad agreement with the investigation of Gillespie et al. (29). Jolls and Hanratty, however, found that the exponent of Reynolds number was some-

what greater than 0.5. This indicates that in the rear of the sphere mass transfer rate had a greater dependence on flow than predicted by boundary layer theory. A previous investigation by these authors (40) showed that the laminar-turbulent transition occurred in the range Re_s between 100-150 with large flow fluctuations. However, their measured mass transfer showed no dramatic changes in the average rates. They found that a single correlation was difficult to obtain due to the statistical variation of the environment, but for a large number of runs for which the bed was repacked before each experiment they suggest the following correlations:

$$Sh_m = 1.59\ Re_s^{0.56}\ Sc^{1/3} \quad \text{for} \quad Re_s > 140 \tag{2.3-21}$$

$$Sh_m = 1.44\ Re_s^{0.58}\ Sc^{1/3} \quad \text{for} \quad 35 < Re_s < 140 \tag{2.3-22}$$

$$Sh_m = 1.64\ Re_s^{0.6}\ Sc^{1/3} \quad \text{for} \quad Re_s < 35 \tag{2.3-23}$$

The authors stated that for $Re_s < 35$, there were wide variations and that this result is of questionable significance. In another study, Hanratty et al. (42) reported mass transfer data in a packed bed in cubic array ($\varepsilon = 0.26$) using the same electrochemical technique and suggested

$$Sh_m = 2.39\ Re_s^{0.56}\ Sc^{1/3} \tag{2.3-24}$$

which is possibly valid for $30 < Re_s < 10^3$. These results are shown in Fig. 6.1-18.

The experimental work mentioned so far does not include a study of the effect of voidage. Theons and Kramers (77) varied voidage in a limited range $0.26 < \varepsilon < .48$ but their correlation cannot be extended to a higher voidage range due to the appearance of a $(1-\varepsilon)$ term. Rowe, Claxton and Lewis (68) made overall heat and mass transfer measurements for a voidage between 0.365 and 0.632. Following the approach of

their single particle study (67) they correlated data as

$$Sh_m = \frac{2}{1 - (1-\varepsilon)^{1/3}} + B_3 Re_s^m Sc^{1/3} \qquad (2.3\text{-}25)$$

where the first term is the value of the Sherwood number for the stagnant case as given by equation (2.3-4). The value of m is given by $\frac{2-3m}{3m-1} = 4.65\ Re_s^{-0.28}$ and $B_3 = 0.61/\varepsilon$ in air and $0.7/\varepsilon$ in water. The value of m is about 0.5 for the usual range of interest and hence $Sh_m \propto \varepsilon^{-1}$ instead of $\varepsilon^{-1/2}$ as predicted by the boundary layer model. The authors checked their data with a few fluidized bed runs and found reasonable agreement. However, in their experiments they used single benzoic acid spheres and inert table tennis balls and the authors do not mention whether segregation occurred due to the density difference.

Chu, Kalil and Wetteroth (11) obtained mass transfer data for the evaporation of naphthalene in an air fluidized bed and obtained the following correlations:

$$j_m = 5.7\ Re_i^{-0.78} \quad \text{for} \quad 1 < Re_i < 30 \qquad (2.3\text{-}26)$$

$$j_m = 1.77\ Re_i^{-0.44} \quad \text{for} \quad 30 < Re_i < 10^4 \qquad (2.3\text{-}27)$$

This work has quite often been quoted in the literature, though the experimental scatter is large (see Fig. 6.1-7). Also the use of Re_i is not suitable for beds having a high voidage and these authors possibly carried out experiments for $\varepsilon > 0.9$. Evans and Gerald (17) measured mass transfer rates from benzoic acid granules to fixed and fluidized beds for Re_s between 1 and 100. The authors calculated surface area from pressure drop data and this could have introduced a large error in their result since they reported difficulty in obtaining reliable pressure drop data.

Thodos and coworkers (78-83) have reported several studies on the mass and heat transfer rates in fixed and fluidized beds. In almost all the work, except for few fixed bed experiments, gas was used as the continuous medium. Initially, the workers neglected the effect of longitudinal mixing, but later Thodos and Petrovic (81) corrected for this. The latter authors correlated both packed and fluidized bed runs by the following equation:

$$j'_m = j_m \epsilon = 0.589\ Re_s^{-0.427} \qquad (2.3\text{-}28)$$

for $20 < Re_s < 2000$. Thodos and Wilkins (82) and Thodos and Yoon (83) have experimentally determined the actual driving force in gas fluidized beds using travelling sampling probes and found that for all practical purposes, longitudinal dispersion could be neglected for the flow range they considered. The latter authors suggested the correlation for $100 < Re_s < 450$ as

$$j'_m = j_m \epsilon = 0.947\ Re_s^{-0.5} \qquad (2.3\text{-}29)$$

Beek (6) discussed the form of the correlation that would describe mass transfer in both fixed and fluidized beds. As in practice one description of mass transfer over the whole range of voidage would be preferred, the author suggested the following correlation in a multiparticle bed:

$$Sh_m \epsilon = B_4\ Re_s^m\ Sc^{1/3} \qquad (2.3\text{-}30)$$

where B_4 is only slightly dependent on voidage and hence can be assumed constant and m has a value about 0.5 At low Re_s the author referred to the work of Snowdon and Turner (72) since this is one of the few reliable experimental studies in liquid fluidized beds. These authors (72) studied mass transfer in a shallow liquid fluidized

bed of ion exchange particles using the H^+/Na^+-Chloride, H^+/Na^+-Acetate and $H^+/\frac{1}{2}Cu^{++}$-Chloride systems. The mass transfer coefficient was evaluated assuming plug flow, this being checked by varying the bed height. They expressed both fixed and fluidized bed results by the following equation:

$$Sh_m = \frac{0.81}{\varepsilon} Re_s^{1/2} Sc^{1/3} \qquad (2.3\text{-}31)$$

Beek (6) suggests that the above correlation is valid for $5 < Re_s < 50$ and in a higher range $20 < Re_s < 2000$, equation (2.3-28) could be used (see Fig. 6.1-17).

Quite recently Couderc and Angelino (14) have published results for liquid fluidized beds for $100 < Re < 300$ by following the dissolution of benzoic acid particles. They expressed results as $Sh_m \cdot Sc^{-1/3}$ against ε on logarithmic coordinates with Re_s as a parameter and obtained a series of lines with slopes of -1.98, -2.04, -2.17 and -2.21 for a Re_s of 150, 175, 200 and 225 respectively (see Fig. 6.1-8). They therefore assumed a mean value of the slope as -2 and suggested the following correlation with an average deviation of 4.5% and a maximum of 20% as

$$Sh_m = \frac{0.054}{\varepsilon^2} Re_s Sc^{1/3} \qquad (2.3\text{-}32)$$

This correlation is satisfactory as far as the authors' data is concerned but is unlikely to be valid over a wider range since the slopes mentioned above vary in a systematic way with Re_s. The authors also studied the effect of bed dilution by coating benzoic acid particles with paint so that all the particles had similar characteristics and then found a 10% reduction in the mass transfer coefficient. This is in contradiction to the observation of Wilson and Geankoplis (88) who found no such effects.

One interesting study is due to Mullin and Treleaven (57) who measured mass transfer rates from benzoic acid spheres for voidages upto unity and Re_s between 50 and 700. They obtained single particle results in good agreement with the results of Garner and Kee (27) using an average velocity based Reynolds number. Their method of correlation is rational since a flat velocity profile existed in the test section. For the multiparticle case, they found no observable difference in mass transfer whether or not a particle was fixed and the results could be expressed in a similar form to single particle results except that the coefficient increased with voidage. Mullin and Treleaven (57) assumed that the increase in mass transfer rate in the multiparticle bed was due to increased turbulence in the fluid stream generated by a fluctuating velocity gradient and wake flow of neighbouring particles. By a tortuous argument, they suggested a form of correlation similar to equation (2.3-27) which is empirically successful. From their work it may be seen that the mass transfer rate is more than doubled at a voidage of 0.5 when compared to a single particle for the same flow rate and an increase of this magnitude seems improbable when attributed to turbulence alone. Though turbulence may be a factor, the increase in mass transfer rate is primarily due to an increased velocity gradient of the fluid as it passes through the voids in a particulate bed.

2.4. Summary of forced convective mass transfer studies from solid spheres in single and multiparticle assembly

Mass transfer rates for single particles can be predicted from the theory for the limiting case of creeping flow and boundary layer flow. However, for the latter case the theoretical predictions are not exact, because of the difficulty in describing the flow in the wake. Experimental results are usually correlated by most workers using the equation

(2.2-18):

$$Sh = 2 + B_1 Re^{1/2} Sc^{1/3}$$

where the coefficient B_1 has been reported between 0.55 and 0.95. In the above equation, some workers use the constant 2 to account for the effect of molecular diffusion without regard to the fact that both convection and diffusion are responsible for convective mass transfer in the fluid phase and that molecular diffusion occurs only at the solid-fluid interface when the rate of transfer is small. Thus the effect of convection is to modify the concentration gradient and thus the straightforward addition of conduction and convection terms is not meaningful. Others believe that the Sherwood number should be 2 when $Re \to 0$ without regard for the Reynolds number range for which the data was obtained. For example, it is pointless to use equations similar to (2.2-18) when correlating high Reynolds number data. Indeed $Sh \to 2$ when $Re \to 0$ as may be seen from equation (2.2-13). If equation (2.2-18) is used in correlating data, the constant term should be obtained from regression of data and since this equation would contain more than one unknown it would be more appropriate to choose an equation of the form (2.2-17). Recently Watts (85) has obtained a perturbation solution for the entire Peclet number range assuming flow to be potential. He also believes that the constant term is not necessarily 2.

Theoretical solutions indicate that for boundary layer flow the coefficient B in equation (2.2-17) is about 0.6 and if the same equation is used for low Reynolds number B should be slightly higher. However, a correlation of this type covering a wide range of Reynolds number in the low range is not very accurate and hence this type of correlation should be used over a restricted range of the Reynolds number with different values of B. Experimental data supports this view and the

value of B for $10 < Re_s < 100$ seems to be between 0.75 and 0.85.

Disagreement abounds in the literature amongst various experimental workers. A number of workers use the average velocity instead of the approach velocity in their interpretation and these may vary by a factor of 2 for a parabolic velocity profile. Liquid-solid systems tend to show a higher mass transfer rate than gas-solid systems for the same flow rate due to a generally higher Schmidt number in the former. This reflects an inherent difference between these two systems particularly at low flow rates. In some cases the value of the diffusion coefficients were not known accurately. Also the use of cast organic acid spheres could have caused some grain dropping and this would explain the somewhat higher results that have been observed using such particles. Surprisingly, not all workers made simple direct measurements. For example, mass loss was often determined by photographing the diminishing particles instead of direct weighing. Almost all workers using solid spheres used fixed spheres and the effect of sphere support is not known. Other effects, such as free convection and turbulence which are difficult to account for or to eliminate were often present to a varying degree.

The situation in multiparticle systems is not clear. Even the limiting value of the Sherwood number in a bed of particles remains unanswered. Some authors believe that the limiting value of the Sherwood number in a bed of active particles is less than 2 and tends to zero for an infinite number of particles. It appears that this concept is probably true only at zero flow rate, but for very small flow rates, equation (2.3-4) may be used as a first approximation.

Various models have been suggested to predict theoretically the heat and mass transfer rates in a multiparticle assembly. The most widely used models are the cell model of Pfeffer (61) and the boundary layer

model of Carberry (9) although the difference between the predicted results using these two models in the range $10 < Re_s < 100$ is possibly within the limits of the precision of some of the experimental data. However, some basic differences between the two models can be easily seen.

The complex term in equation (2.3-8) for the cell model is roughly equal to $1/\epsilon$ (88) and the equation may be written as

$$Sh_m \simeq \frac{1.26}{\epsilon} Re_s^{1/3} Sc^{1/3} \qquad (2.4\text{-}1)$$

For a fluidized bed, using the Richardson-Zaki correlation (64) $Re_s/Re_o = \epsilon^N$, equation (2.4-1) can be written as

$$Sh_m = 1.26\, Re_o^{1/N} Re_s^{1/3-1/N} Sc^{1/3} \qquad (2.4\text{-}2)$$

where Re_o is the terminal settling Reynolds number. Similarly equation (2.3-13) can be written as

$$Sh_m = 0.974\, Re_o^{1/2N} Re_s^{1/2-1/2N} Sc^{1/3} \qquad (2.4\text{-}3)$$

For $N = 3$, which would be a representative value in the range of Re_o of interest, the cell model predicts a constant value of the Sherwood number at all values of Re_s whereas the boundary layer model predicts $Sh_m \propto Re_s^{1/3}$. Experimentally this dependence of Sh_m on Re_s has been found to be between these two limits. The cell model employed by Pfeffer (61) and the hydraulic radius model of Kataoka et al. (43) agree quite closely at low voidage (within 7% at $\epsilon = 0.4$) but large deviations occur as the voidage is increased (about 25% at $\epsilon = 0.8$). The channelling model of Kuni et al. (46), though satisfactory in explaining some very low Reynolds number results, is in clear disagreement with the other models. Since the channelling model is not very realistic in a physical sense any agreement must be considered fortuitious.

Relatively little data is available in the range $Re_s < 50$ especially for liquid fluidized beds. Detailed studies of a single particle in an assembly of particles suggests that flow around particles may be approximated to boundary layer flow.

The most important source of error in multiparticle work is the determination of surface area, especially for small particles of irregular shape that are frequently used. Direct or indirect determinations using pressure drop data are usually subject to significant errors. Free convection and dispersion effects may also have been present in some of the experiments. Also difficulties are experienced in determining the concentration and temperature at the surface of particles. In general fluidized bed data tends to show more scatter than fixed bed results and this is due to the uncertainty of voidage determinations. Finally turbulence is an effect which is difficult to take into account.

CHAPTER 3

CHOICE OF THE EXPERIMENTAL SYSTEM

3. CHOICE OF THE EXPERIMENTAL SYSTEM

The object of this work was to obtain reliable convective mass transfer data in liquid fluidized beds in the flow Reynolds number range ($Re_s \sim 20$). The following types of study are possible in a multiparticle system:

1. Local and/or overall studies around a single particle in a multiparticle assembly.

2. An integral analysis of the entire multiparticle system.

The first of these studies is more fundamental, since this would yield detailed and overall knowledge of the multiparticle system, but experimentation is difficult. The latter is of direct interest for design and is slightly easier to perform experimentally. Unfortunately, precise data in such studies is often obscured by effects such as axial and radial dispersion which have a pronounced effect on the rate phenomena and are difficult to account for. In view of the more practical relevance, overall mass transfer data has been obtained in a liquid fluidized bed using a shallow bed to eliminate liquid mixing effects. Although many different solid-liquid systems could be used for this purpose, an ion exchange system is chosen here because it possesses several excellent physical characteristics. The important advantages are:

1. The ion exchange particles are spherical and particle size changes only slightly during the mass transfer process and therefore the total surface area is accurately known.

2. Reliable measurements can be made at low concentrations of the exchanging ions resulting in negligible natural convection and negligible mass flux effects on the mass transfer coefficient. It may be mentioned here, that the interference of the above mentioned factors was possibly

responsible for the uncertainties in some of the fixed and fluidized bed work mentioned previously.

Although ion exchange systems are suitable from the physical point of view, the interpretation of data is considerably more difficult and this may offset some of the important advantages already mentioned. This is because the driving force for the diffusional flux consists of two terms, one due to a concentration gradient and the other due to an electric potential gradient arising as a result of the unequal mobility of the ions. For the experimental work, it will be seen that a neutralization type reaction constitutes a very suitable physico-chemical system. In particular the following ion exchange reaction was chosen:

$$R^{-}H^{+} + Na^{+}OH^{-} \rightarrow R^{-}Na^{+} + H_2O$$

where R^{-} is the negatively charged solid matrix.

CHAPTER 4

THEORETICAL

4. THEORETICAL

4.1. Mass transfer from a single solid sphere by forced convection involving ion exchange reactions

A detailed description of diffusion in ion exchange systems is given in Appendix A.1 and A.2. Equation (A.2-4) shows how the diffusional fluxes for a binary ion exchange system involving counter-ions 'A' and 'B' and co-ion 'C' in the solvent 'S' may be expressed in terms of only the concentration gradient of one of the species. To obtain an expression for the diffusional flux of a particular species it is convenient to consider specific ion exchange reactions. Here two specific cases are considered.

1. This case arises in a neutralization type of ion exchange reaction. In such cases the counter-ion diffusing out of the ion exchange particle phase is instantly consumed at the exchanger-liquid interface so that only one counter-ion is present in the liquid phase. Then one may write

$$J_B^* = 0, \qquad C_B = 0, \tag{4.1-1}$$

where 'B' is the counter-ion that is being consumed. The condition that $C_B = 0$ implies that component 'B' disappears to form some other component and in this case must produce 'A', 'C' or the solvent obeying the constraints (A.2-2) and (A.2-3) since the analysis has been restricted to the above four components only. Using equation (4.1-1) and equation (A.2-4) the diffusion flux for component 'A' may be written as

$$J_A^* = - \frac{(Z_A + Z_C)\, D_{AS}\, D_{CS}}{Z_C (D_{AS} + D_{CS})} \nabla C_A$$

$$= - D \nabla C_A \tag{4.1-2}$$

where $$D = \frac{(Z_A + Z_C)\, D_{AS}\, D_{CS}}{Z_C(D_{AS} + D_{CS})} \qquad (4.1\text{-}3)$$

Equation (4.1-2) shows that the diffusional flux of component 'A' is a product of its concentration gradient and the constant term D comprising the effective binary diffusion coefficients of the ions 'A' and 'C' in the solvent 'S'. This equation is similar to Ficks law of diffusion. Constant D may be thought of as a coupled diffusion coefficient and can be calculated from effective binary diffusion coefficient data. The problem of convective diffusion is then analogous to other solid-liquid systems which are characterised by constant diffusivity e.g. the benzoic acid-water system as discussed in Chapter 2.

2. In this case all the ions are present in the solution phase and this represents a more general case of binary ion exchange. Here it is assumed that the co-ion current is zero after co-ion shift occurs (37a). This is the usual quasi stationary steady state assumption. Thus for this assumption

$$J_C^* = 0, \qquad Z_C \neq 0 \qquad (4.1\text{-}4)$$

Using equations (4.1-4), (A.2-3) and (A.2-4) the expression for the diffusional flux of species 'A' may be written as

$$J_A^* = -\left[\frac{D_{AS}D_{BS}\left\{Z_C C_C (Z_B+Z_C) - Z_A C_A (Z_B - Z_A)\right\}}{D_{BS}Z_C C_C (Z_B+Z_C) + Z_A C_A (Z_A D_{AS} - Z_B D_{BS})}\right] \nabla C_A \qquad (4.1\text{-}5)$$

Again, the diffusional flux of a species can be represented by the product of its concentration gradient and another term, but this time the second term is not constant but depends in a complicated way on concentration.

Since equation (4.1-5) contains both C_A and C_C it will be useful to obtain a relationship between these quantities. From equations

(A.2-1,2,3) and (4.1-4) an additional relationship between C_C and C_A may be written as

$$\frac{dC_C}{dC_A} = - \frac{Z_A Z_C \left(\frac{D_{AS}}{D_{BS}} - 1 \right)}{(Z_B Z_C + Z_C^2) + \left(Z_A^2 \frac{D_{AS}}{D_{BS}} - Z_A Z_B \right) \frac{C_A}{C_C}} \qquad (4.1\text{-}6)$$

Integration of equation (4.1-6) between the bulk of the fluid and any point in the concentration boundary layer gives the desired result.

Consider the specific case for $Z_A = Z_B = Z_C$. The diffusional flux can be written from equation (4.1-5) as follows:

$$J_A^* = - \frac{2D_{AS}}{\alpha \frac{C_A}{C_C} + 2} \nabla C_A \qquad (4.1\text{-}7)$$

where $$\alpha = \frac{D_{AS}}{D_{BS}} - 1$$

Also equation (4.1-6) can be integrated to obtain

$$\frac{C_C}{C_{Cb}} = \left[\frac{\alpha \frac{C_{Ab}}{C_{Cb}} + 1}{\alpha \frac{C_A}{C_C} + 1} \right]^{\frac{1}{2}} \qquad (4.1\text{-}8)$$

where C_{Ab} and C_{Cb} denote the bulk concentration of species 'A' and 'C' respectively.

The steady state continuity equation for ions 'A' may be written as (7a):

$$v . \nabla \rho_A = - \nabla . j_A \qquad (4.1\text{-}9)$$

In dilute solution $v \simeq v^*$ and $j_A \simeq M_A J_A^*$. Using equation (4.1-7), the continuity equation in spherical coordinates may be written as

$$v_r \frac{\partial C_A}{\partial r} + v_\theta \frac{\partial C_A}{\partial \theta} = \frac{1}{r^2} \frac{\partial}{\partial r} \left(\frac{2D_{AS}}{\alpha C_A / C_C + 2} r^2 \frac{\partial C_A}{\partial r} \right) \qquad (4.1\text{-}10) \text{ and } (A.3\text{-}1)$$

where r and θ are radial and angular coordinates and v_r and v_θ the corresponding velocity components. The boundary conditions are

$$r = R, \quad C_A = C_{AR} \qquad (4.1\text{-}11) \text{ and } (A.3\text{-}3)$$

$$r = R+b, \quad C_A = C_{Ab}$$

where R is the radius of the sphere and b the thickness of the concentration boundary layer. In writing equation (4.1-10) it is assumed that the concentration boundary layer is thin which will be true if the Peclet number of the system is high.

Equation (4.1-10) is non linear and contains two dependent variables C_A and C_C linked by a quadratic relationship (see equation 4.1-8). An exact solution seems difficult and hence an approximate solution will be attempted. The method of solution is based on an integral method of analysis due to Friedlander (18) and has been mentioned in Chapter 2. The detailed solution is given in Appendix A.3.

In this method, equation (4.1-10) is partially integrated across the concentration boundary layer and an assumed concentration profile is substituted into the resulting equation. This assumed concentration profile should satisfy as many boundary conditions as possible so that the assumed and the actual profile will match fairly closely. Since there are two concentration terms, i.e. C_A and C_C, it has been found convenient to work with a new variable, called the equivalent fraction and defined as follows:

$$y_A = \frac{C_A}{C_C} \qquad (4.1\text{-}12) \text{ and } (A.3\text{-}11)$$

To obtain an expression for the mass transfer coefficient a local mass transfer coefficient $K_v(\theta)$ has been defined:

$$J_A^*\Big|_{x=0} = K_v(\theta)\, C_{Cb}(y_{AR} - y_{Ab}) \qquad \text{(4.1-13) and (A.3-29)}$$

where the subcript v in $K_v(\theta)$ is used to denote the fact that the diffusion coefficient of the system is not constant and $x = r-R$. This definition of the mass transfer coefficient was originally suggested by Snowdon and Turner (73) who also pointed out that although $C_{Cb}(y_{Ab}-y_{AR})$ was not the true driving force, since $C_{Cb} \neq C_{Ci}$, it was a convenient measure of it. The mass transfer coefficient averaged over the whole surface of the particle is designated $\overline{K}_v$ and the overall mass transfer coefficient is given by the expression as follows:

$$\overline{K}_v = 1.31 \frac{D_{AS}^{2/3}}{d^{2/3}} F \left[\int_0^{\pi} \sqrt{-\psi_R''} \sin\theta \, d\theta \right]^{2/3} \qquad \text{(4.1-14) and (A.3-31)}$$

where ψ_R'' is the second derivative of the stream function at the surface of the sphere and F is a complicated function of y_{Ab}, y_{AR} and α and is given by equation (A.3-32). The quantity F has the following limits:

$$y_{AR} \to y_{Ab} \to 0, \quad F \to \left(\frac{1}{12}\right)^{1/3} \qquad \text{(4.1-15) and (A.3-33)}$$

$$y_{AR} \to y_{Ab} \to 1, \quad F \to \frac{1}{(24)^{1/3}} \frac{(\alpha+2)^{1/3}}{(1+\alpha)}$$

Equation (4.1-14) can be written in a modified form as follows:

Let $F_1^{2/3} = F$

and $D_{eff} = D_{AS} F_1$ (4.1-16)

Then equation (4.1-14) can be written as

$$\bar{K}_v = 1.31 \frac{D_{eff}^{2/3}}{d^{2/3}} \left[\int_0^{\pi} \sqrt{-\psi_R''} \sin\theta \, d\theta \right]^{2/3} \qquad (4.1\text{-}17)$$

This expression of the mass transfer coefficient where $\bar{K}_v \propto D_{eff}^{2/3}$ is similar to cases for which the diffusion coefficient is constant. The diffusion coefficient D_{eff} given by equation (4.1-16) can be thought of as the effective diffusion coefficient of the system and may be used in the dimensionless correlations.

4.2. A model for forced convective mass transfer in a multiparticle assembly

The various theoretical models for multiparticle systems have been discussed in Chapter 2. It is clear from this review that any exact description of momentum, mass and heat transfer in multiparticle systems is very difficult and at best only modest agreement between theory and experiment has been found. The success of any theoretical model depends on how closely it represents the actual physical situation. Most of the models were primarily suggested for fixed beds and despite the fact that voidage was recognised as an important variable, none of the models predict the dependence of the mass transfer coefficient on voidage sufficiently well.

Various studies, particularly the experimental work of Jolls and Hanratty (41), Gillespie et al. (29) and the theoretical work of Leclair et al. (48) suggest that the flow in a multiparticle system is possibly dictated by boundary layer theory even at low flow rates. This explains why the overall Sherwood number varies roughly with the square root of the Reynolds at low flow rates in multiparticle systems. An examination of local mass and heat transfer values reported by the authors (41, 29) shows

that several boundary layer zones separated by regions of complex flow pattern exist around a single particle in an array of other particles. In a fixed bed the number of such zones may be two or three. The flow in these zones is dictated by laminar boundary layer theory since the Sherwood number-Reynolds number relationship in these regions is very close to a square root dependence. However, the local Sherwood number in these regions does not show a smooth variation as it does for a single sphere. Outside these laminar boundary layer regions, the experimental studies shed little light except to indicate the complexity of the flow pattern. There is however no work available at higher voidage which would show, how these boundary layer regions depend on the voidage. It may be argued that the number of individual zones showing laminar boundary layer characteristics would decrease as voidage increases. However, these individual regions would occupy a larger portion of the surface of the sphere, i.e. the length of such zones would be greater at higher voidage than at lower voidage. Thus the length of the boundary layer regions are in some way related to the voidage and this explains why the boundary layer model of Carberry (9) has not been able to determine the dependence of voidage on transfer rates, although it has been successful in explaining fixed bed results which were mostly carried out at a voidage of about 0.4.

A modification to the boundary layer model proposed by Carberry (9) is now proposed. In a multiparticle assembly, Carberry suggested that the point velocity relative to the average interstitial velocity could be described as follows:

$$\frac{v}{U_i} = \frac{.815\ x_1}{\sqrt{\frac{\nu z_1}{U_i}}} \qquad (4.2\text{-}1)$$

where x_1 is the distance perpendicular to flow, z_1 is the distance in

the direction of flow, U_i is the interstitial velocity = U_s/ε where U_s is the superficial velocity and ν is the kinematic viscosity. From boundary layer theory for flat plates and assuming that the velocity at the boundary layer edge is twice the interstitial velocity the author obtained the constant of the above equation.

In view of the approximations that have been made in applying planar boundary layer theory to a spherical particle in an assembly of other spheres and the fact that such systems do not show a simple flow pattern, it seems that a more rational approach would be to determine the approximate form of the functional dependence of various groups and to determine the constant from experimental data, which hopefully would compensate for some of the weaknesses of the model. With this in mind it is here postulated that instead of equation (4.2-1), the velocity relative to the average interstitial velocity is represented by

$$\frac{v}{U_i} = \frac{G_1 x_1}{\sqrt{\frac{\nu z_1}{U_i}}} \qquad (4.2\text{-}2)$$

where G_1 is a constant. Using the solution given by the author (9), the mass transfer coefficient $\overline{K}_c$ is given as

$$\overline{K}_c = \frac{G_2 D_{AS}^{2/3}}{(z_1/U_i)^{\frac{1}{2}}\ \nu^{1/6}} \qquad (4.2\text{-}3)$$

where D_{AS} is the binary diffusion coefficient taken as constant between the diffusing species 'A' and solvent 'S' and $\overline{K}_c$ is the mass transfer coefficient for this constant diffusivity system defined in terms of a concentration driving force.

Carberry (9) assumed that the length over which the boundary layer development occurred is equal to one particle diameter. He based this

on the mixing data available for gas and liquid fluidized beds. It has been mentioned earlier that the length of boundary layer regions is expected to depend on voidage in some way. This dependence is proposed by the simple relationship

$$z_1 \propto \varepsilon d$$
$$= G_3 \varepsilon d \qquad (4.2\text{-}4)$$

Using the above expression for z in equation (4.2-3)

$$\overline{K}_c = \frac{G_4 D_{AS}^{2/3}}{(\varepsilon d/U_i)^{\frac{1}{2}} \nu^{1/6}}$$

and from $U_i = U_s/\varepsilon$ the above equation can be written as

$$Sh_m = G_4 \frac{Re_s^{1/2}}{\varepsilon} Sc^{1/3} \qquad (4.2\text{-}5)$$

where $Re = \frac{dU_s\rho}{\mu}$, $Sc = \frac{\mu}{\rho D_{AS}}$ and $Sh_m = \frac{\overline{K}_c d}{D_{AS}}$.

The constant G_4 may now be determined experimentally and should be constant for a wide range of solid-liquid system. Also, since equation (4.2-5) is proposed for the entire range of voidage, it should be possible to determine the constant G_4 from single particle work.

4.3. Theory of experiment: Evaluation of mass transfer coefficient from experimental data in a shallow liquid fluidized bed

The mass transfer coefficient in a multiparticle system can be obtained by a differential macroscopic (87) mass balance. The rigorous derivation of the macroscopic field equations is difficult and recently several workers have devoted their attention to this subject (87). In a two phase fluidized bed, the variables vary both in space and time

and the average field equations can be obtained in several ways. Panton (58) obtained the average equations for a two phase system by first averaging the variables with respect to a local volume which is large compared to the solid particles and yet small compared to the dimensions of the containing vessel. Anderson and Jackson (2) do the local averaging in a region containing many particles since this smooths out fluctuations in space and time and hence the region is larger than that considered by Panton (58). At the present time there is still some controversy amongst workers about the averaged equations and in particular about the averaged equation of motion. It is to be noted that any averaging, whether with respect to time, area or volume will involve some sacrifice of detailed information and this is usually compensated for by some kind of empiricism. For example, consider a single phase fluid in turbulent flow. The averaging is done with respect to time and as a result some new terms known as the 'Reynolds Stresses' appear in the equation of motion for which an empirical data correlation is used. Similarly, if a solute is introduced to a solvent flowing in a tube at some point in the stream and it is desired to determine the concentration of the solute as a function of time and position, then the usual approach is to average the continuity equation for the solute over the area of the tube. The result would be an average continuity equation in the axial direction where in this equation the diffusion flux is replaced by a longitudinal dispersion flux.

The macroscopic mass balance equation for a component in a fluidized bed in the most general case may be quite complex and difficult to solve. This is chiefly due to the effect of longitudinal dispersion, which is empirical in form and the dependence of the solid-fluid interface boundary condition on bed height. However, in a shallow liquid fluidized bed, the following reasonable assumptions may be made and this yields a

relatively simple equation. It may be assumed that:

1. The liquid in the bed is in true plug flow i.e. there is no liquid mixing.

2. The solid is perfectly mixed and hence the equilibrium solid-liquid interface composition is the same everywhere in the bed.

3. The solution is dilute, so that the flux across the solid-liquid interface is effectively a diffusional flow, i.e. no bulk flow through the interface. Hence the flux across the interface can be described in terms of a mass transfer coefficient which requires no further correction due to mass flux effects.

4. The flow is one dimensional.

In view of assumptions 1 and 4, the fluidized bed can be treated by the method suggested by Bird et al. (76). A fluidized bed is a system in which the solid and liquid phases are continuous and exist side by side with the fluid flowing in the axial direction having a flat velocity profile and allowing transfer of mass between the two phases. Admittedly, this is a bold assumption, but the final equation is the same when proper averaging is done (87).

Fig. 4.3-1: Schematic representation of a fluidized bed.

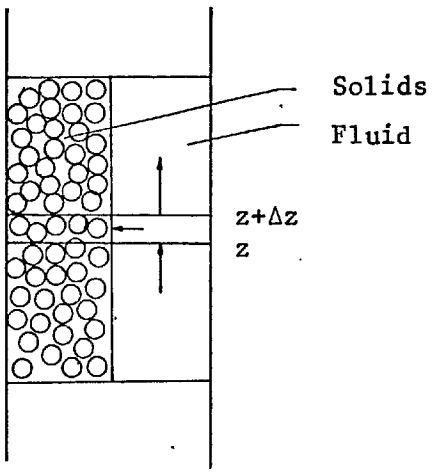

With the other assumptions mentioned above, a mass balance equation for a volume element for a component 'A' in the fluid phase can now be written. Since the mass transfer between the two phases can be written in terms of a mass transfer coefficient it will be convenient to consider whether or not the diffusivity of the component is constant. Here, the two cases are considered separately.

1. For constant diffusivity, the mass transfer coefficient is a constant throughout the fluidized bed at a given flow rate. A mass balance equation for this case, may be written for component 'A' as follows:

$$-\varepsilon \frac{\partial C_{Ab}}{\partial t} - \frac{3(1-\varepsilon)}{R} \overline{K}_c \, (C_{Ab}-C_{AR}) = U_s \frac{\partial C_{Ab}}{\partial z} \qquad (4.3\text{-}1)$$

It may be noted here that the transfer of component 'A' from the fluid to the solid phase is considered and thus the driving force is written $(C_{Ab} - C_{AR})$ instead of $(C_{AR} - C_{Ab})$. Also the mass transfer coefficient is given the subscript 'c' to denote that the diffusivity of the system is constant and hence the mass transfer coefficient depends only on the fluid mechanics. Here ε is the voidage, t is the time, z is the axial coordinate and U_s the superficial velocity. Because of assumption 2, the solid-fluid equilibrium interface concentration C_{AR} may be taken as constant. For the following boundary conditions

$$\left.\begin{aligned} z &= 0, \quad C_A = C_{Ab}^{i} \\ z &= h, \quad C_A = C_{Ab}^{e} \\ t &= t_s, \quad z = h, \quad C_A = C_{Ab}^{i} \end{aligned}\right\} \qquad (4.3\text{-}2)$$

where C_{Ab}^{i} and C_{Ab}^{e} are the inlet and outlet bulk concentration of 'A', h is the bed height and t_s is the saturation time i.e. time when the par-

ticles are completely loaded with species 'A' equation (4.1-1) has been integrated (62) to obtain the following expression for the mass transfer coefficient:

$$\bar{K}_c = \frac{\left(\frac{U_s}{\varepsilon} t_s - h\right) \ln\left(\frac{C^e_{Ab} - C_{AR}}{C^i_{Ab} - C_{AR}}\right)}{\frac{3(1-\varepsilon)}{R\varepsilon} h (t - t_s)} \qquad (4.3\text{-}3)$$

For most systems of interest the variation of C_{Ab} with respect to time compared to space would be negligible when the first term in equation (4.1-1) may be dropped. The equation then reduces to a very simple ordinary differential equation. The expression for the mass transfer coefficient then is

$$\bar{K}_c = \frac{L}{S} \ln \frac{C^i_{Ab} - C_{AR}}{C^e_{Ab} - C_{AR}} \qquad (4.3\text{-}4)$$

where $L = U_s.A$ is the volume flow rate, A the cross sectional area of the tube and $S = \frac{3(1-\varepsilon)hA}{R}$ is the total surface area of the particles in the bed. Equation (4.3-4) may also be obtained as a limiting case of equation (4.3-3).

The chemical system chosen for the experimental work has been discussed earlier. The system chosen is

$$R^-H^+ + Na^+OH^- \rightarrow R^-Na^+ + H_2O$$

which shows that an ion exchange particle in H^+ is treated with an NaOH solution. The H^+ ions diffusing out of the particle phase will be immediately neutralized forming the solvent provided that the OH^- concentration in the solution exceeds 10^{-7}M. This also means that Na^+ concentration at the liquid-particle interface is zero. Since the fluid phase has effectively one counter ion, i.e. the Na^+ ions, equation (4-1-2) indicates that this system may be characterized by a diffusion

coefficient which is constant. This system also has the advantage that the effluent concentration in a fluidized bed should remain constant for a given flow since the diffusion coefficient and the driving force remains constant so that the total rate of mass transfer is constant. A neutralization ion exchange reaction thus offers a definite advantage to other ion exchange reactions. If component 'A' is the Na^+ ion, then $C_{NaR} = 0$ and equation (4.1-4) takes the simple form

$$\overline{K}_c = \frac{L}{S} \ln \frac{C^i_{Nab}}{C^e_{Nab}} \qquad (4.3\text{-}5)$$

Equation (4.3-5) has been used to evaluate the mass transfer coefficient in this study. The expression for the concentration profile may be written as

$$\frac{C_{Nab}}{C^i_{Nab}} = \left(\frac{C^e_{Nab}}{C^i_{Nab}} \right)^{z/h} \qquad (4.3\text{-}6)$$

where C_{Nab} is the bulk concentration of Na^+ ions at a bed height z.

2. In this case the diffusional flux may be of the form given by equation (4.1-5) in which case the flux is not represented by a constant diffusion coefficient. An example may be

$$R^-H^+ + Na^+Cl^- \rightleftarrows R^-Na^+ + H^+Cl^-$$

Such cases have been studied by Snowdon and Turner (73). Following their method a mass balance can be written in terms of the equivalent fraction as

$$-\varepsilon C_{Cb} \frac{\partial y_{Ab}}{\partial t} - \frac{3(1-\varepsilon)}{R} \overline{K}_v C_{Cb} (y_{Ab} - y_{AR}) = U_s C_{Cb} \frac{\partial y_{Ab}}{\partial z} \qquad (4.3\text{-}7)$$

For most practical cases of interest $\varepsilon \frac{\partial y_A}{\partial t} << U_s \frac{\partial y_{Ab}}{\partial z}$ and the mass balance equation takes the simple form

$$U_s \frac{\partial y_{Ab}}{\partial z} = - \frac{3(1-\varepsilon)}{R} \bar{K}_v (y_{Ab} - y_{AR}) \qquad (4.3\text{-}8)$$

The boundary conditions are

$$\begin{aligned} z &= 0, \quad y_{Ab} = y^i_{Ab} \\ z &= h, \quad y_{Ab} = y^e_{Ab} \end{aligned} \qquad (4.3\text{-}9)$$

Here $\bar{K}_v$ is the mass transfer coefficient for the case where the diffusion coefficient is not constant. Single particle mass transfer study indicates that $\bar{K}_v$ depends on y_{Ab} and y_{AR} and hence integration of equation (4.3-8) is difficult. Snowdon and Turner (73) assumed that $\bar{K}_v$ could be taken as constant in equation (4.3-8) but when a comparison with single particle mass transfer is to be made an average value of y_{Ab} should be used. Their study indicates that this approach is reasonable. Integration of equation (4.3-8) with the above boundary conditions gives

$$\bar{K}_v = \frac{L}{S} \ln \frac{y^i_{Ab} - y_{AR}}{y^e_{Ab} - y_{AR}} \qquad (4.3\text{-}10)$$

This equation is analogous to equation (4.3-4) where concentrations are used instead of equivalent fraction.

CHAPTER 5

EXPERIMENTAL

5. EXPERIMENTAL

5.1. Experimental criteria

For an accurate determination of the mass transfer coefficient in a fluidized bed using equation (4.3-5) an experiment must be designed which fulfils the assumptions made in obtaining this equation and in addition provides an accurate measurement of the variables. The important assumption is plug flow of liquid in the bed. This is most closely achieved by employing a shallow bed of particles since mixing of liquid would be small in such bed. Also the velocity profile of the fluid in a fluidized bed has been shown theoretically to be almost flat by Taganov and Romankov (75). These authors considered the average equations of motion of the phases in a fluidized bed and presented approximate solutions of the flow profiles of the two phases. Graphically the solutions for the average velocities are shown in Fig. 5.1-1.

Fig. 5.1-1: Velocity profile of the phase in a fluidized bed

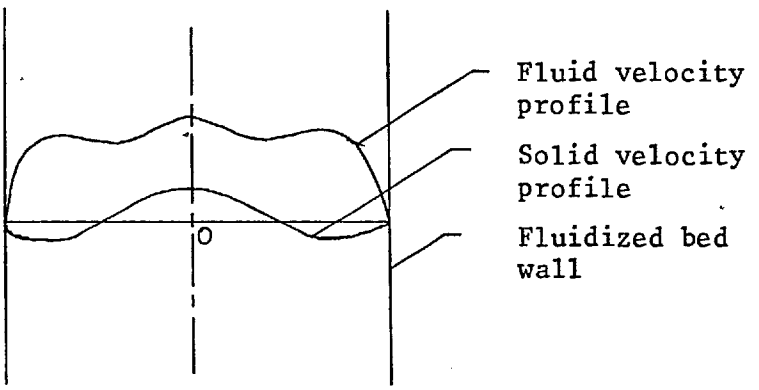

The average fluid velocity profile may be considered roughly flat and the velocity of the solid phases corresponds to a circulating flow indicating perfect mixing of the solids. The averaged equations considered by these

authors (75) contain fluctuating components which are difficult to assess and various approximations have been employed to obtain the solution. However, this can give a rough description of the fluid mechanics of a fluidized bed. Beek (6) points out that if the exchange between the two phases is fast, no departure from real plug flow can be detected, though this does not necessarily mean that actual plug flow is achieved. The neutralization reaction used in the present experiments satisfies this condition adequately. Perfect mixing of the solids is not an important consideration, since the solid-liquid equilibrium concentration of Na^+ ions is essentially zero whether or not the solids are mobile.

Equation (4.3-5) shows that the quantities to be measured are flow rate, the total surface area available for mass transfer and the inlet and outlet concentration of the Na^+ ions in the stream. An analysis of error will indicate the quantities that require most careful measurement.

$$\text{If} \quad Q = f(g_1, g_2, g_3 \ldots) \tag{5.1-1}$$

then the differential change in Q corresponds to a differential change in each of the g's i.e.,

$$dQ = \left(\frac{\partial f}{\partial g_1}\right) dg_1 + \left(\frac{\partial f}{\partial g_2}\right) dg_2 + \left(\frac{\partial f}{\partial g_3}\right) dg_3 + \ldots \tag{5.1-2}$$

If the differentials dg_1, dg_2, dg_3 etc. are replaced by small finite increments Δg_1, Δg_2, Δg_3 etc. then ΔQ may be given to a reasonable approximation by the expression,

$$\Delta Q = \frac{\partial f}{\partial g_1} \Delta g_1 + \frac{\partial f}{\partial g_2} \Delta g_2 + \frac{\partial f}{\partial g_3} \Delta g_3 + \ldots \tag{5.1-3}$$

where ΔQ and Δg's may be considered as the deviation of Q and g's from the mean value.

Hence for a population N

$$\frac{\Sigma\Delta Q^2}{N} = \frac{1}{N}\sum\left(\frac{\partial f}{\partial g_1}\Delta g_1 + \frac{\partial f}{\partial g_2}\Delta g_2 + \frac{\partial f}{\partial g_3}\Delta g_3 + \ldots\right)^2 \qquad (5.1\text{-}4)$$

Now by definition $\sigma_Q = \sqrt{\frac{\Sigma\Delta Q^2}{N}}$ is the standard deviation of Q. When errors in the g's are independent $\Sigma(\Delta g_1 . \Delta g_2 . \Delta g_3 \ldots)$ becomes zero and equation (5.1-4) may be written as

$$\sigma_Q = \pm\sqrt{\left(\frac{\partial f}{\partial g_1}\right)^2 \sigma^2_{g_1} + \left(\frac{\partial f}{\partial g_2}\right)^2 \sigma^2_{g_2} + \left(\frac{\partial f}{\partial g_3}\right)^2 \sigma^2_{g_3} + \ldots} \qquad (5.1\text{-}5)$$

The relative error in Q defined as $\eta_Q = \sigma_Q/Q$ then can be written as

$$\eta_Q = \pm\frac{1}{Q}\sqrt{\left(\frac{\partial f}{\partial g_1}\right)^2 \sigma^2_{g_1} + \left(\frac{\partial f}{\partial g_2}\right)^2 \sigma^2_{g_2} + \left(\frac{\partial f}{\partial g_3}\right)^2 \sigma^2_{g_3} + \ldots} \qquad (5.1\text{-}6)$$

The subscripts of σ and η indicate the quantities for which the standard deviation and the relative error are evaluated. From equation (4.3-5) the relative error in mass transfer coefficient can be written with the help of equation (5.1-6) as

$$\eta_{K_c} = \pm\sqrt{\eta_L^2 + \eta_S^2 + \frac{1}{\left(\ln\frac{C^i_{Na}}{C^e_{Na}}\right)^2}\left(\eta^2_{C^i_{Na}} + \eta^2_{C^e_{Na}}\right)} \qquad (5.1\text{-}7)$$

It is easy to see from the above equation that the error in the mass transfer coefficient depends naturally on the errors in the flow rate L, the surface area S, the inlet and exit concentrations C^i_{Na} and C^e_{Na} respectively but additionally on the ratio C^i_{Na}/C^e_{Na}. If $C^i_{Na}/C^e_{Na} < e$ then this ratio has an adverse effect on the error in the mass transfer coefficient, ~~and vice versa~~. In the present experiments C^i_{Na}/C^e_{Na} is

near unity and hence it is essential that $\eta_{C^i_{Na}}$ and $\eta_{C^e_{Na}}$ be very small to have a reliable estimate of the mass transfer coefficient. For example, taking a typical set of values

$$L = 20 \pm .2 \ \text{cm}^3/\text{sec} \qquad \eta_L = .01$$

$$S = 400 \pm 10 \ \text{cm}^2 \qquad \eta_S = .025$$

$$C^i_{Na}/C^e_{Na} = 1.1$$

for $\eta_{C^i_{Na}} \simeq \eta_{C^e_{Na}} = .01$, using equation (5.1-7)

$$\eta_{\overline{K}_c} = \pm \sqrt{(.01)^2 + (.025)^2 + 2 \times .0118} \simeq \pm .15$$

and for $\eta_{C^i_{Na}} \simeq \eta_{C^e_{Na}} \simeq .001$

$$\eta_{\overline{K}_c} = \pm \sqrt{(.01)^2 + (.025)^2 + 2 \times .000118} = \pm .031$$

Thus, if a relative error of not more than 5% is to be tolerated in the measured value of the mass transfer coefficient, then the concentration of the fluid stream must be measured to within 0.1% provided of course that the error in other quantities do not greatly exceed those cited in the example.

The concentration range for the NaOH solution chosen for the work is between 10^{-3} to 10^{-4} (N). A low concentration ($\sim 10^{-2}$ (N) or less) of the solution is needed to maintain a liquid film controlled mass transfer mechanism. Additional advantages of solution concentration are that the Nernst Planck equation (A.1-12), is valid in this dilute range and there is negligible effect of mass flux on the velocity profile and a relatively long time to particle saturation thus allowing a series of

experiments to be carried out easily.

The next step in the design of the experiment is to select a technique for the analysis of the solution. It was hoped to develop a continuous analysis of the effluent stream since a batch method would be very tedious. Consideration of the various standard techniques, viz. titration, pH determination, photometric, radioactive and conductivity method indicates that the most suitable method of analysis would be the last one. However, the continuous measurement of concentration by a conductivity method to within 0.1% in a flow system poses many difficult problems, since the conductivity of an NaOH solution changes by about 1.71% per degree change in temperature. This would require that the temperature of the fluid stream be maintained constant at a desired value to within about $\pm 0.02^{o}C$ and a high sensitivity conductivity bridge preferably of the autobalance type be used for the measurement.

5.2. General description of the design of the experiment

The design of a flow loop capable of maintaining temperature to within $\pm .02^{o}C$ is not easy. Indeed, a considerable amount of time and effort was devoted to achieving this and finally a relatively simple design was found to work. Most conductivity data is normally available at 25^{o} and $30^{o}C$ and so it was felt that the flow loop should be designed for this range of temperature.

The general apparatus layout is shown in simplified form in Fig. 5.2-1. Distilled water from a laboratory reservoir is pumped by a stainless steel reciprocating pump [1] through a mixed bed deionizer [2] to polythene storage tanks [6] and solution tank [7]. Carbonate free concentrated NaOH solution is transferred under a nitrogen atmosphere to

Fig. 5.2-1 : Simplified flow diagram of the fluidized bed equipment.

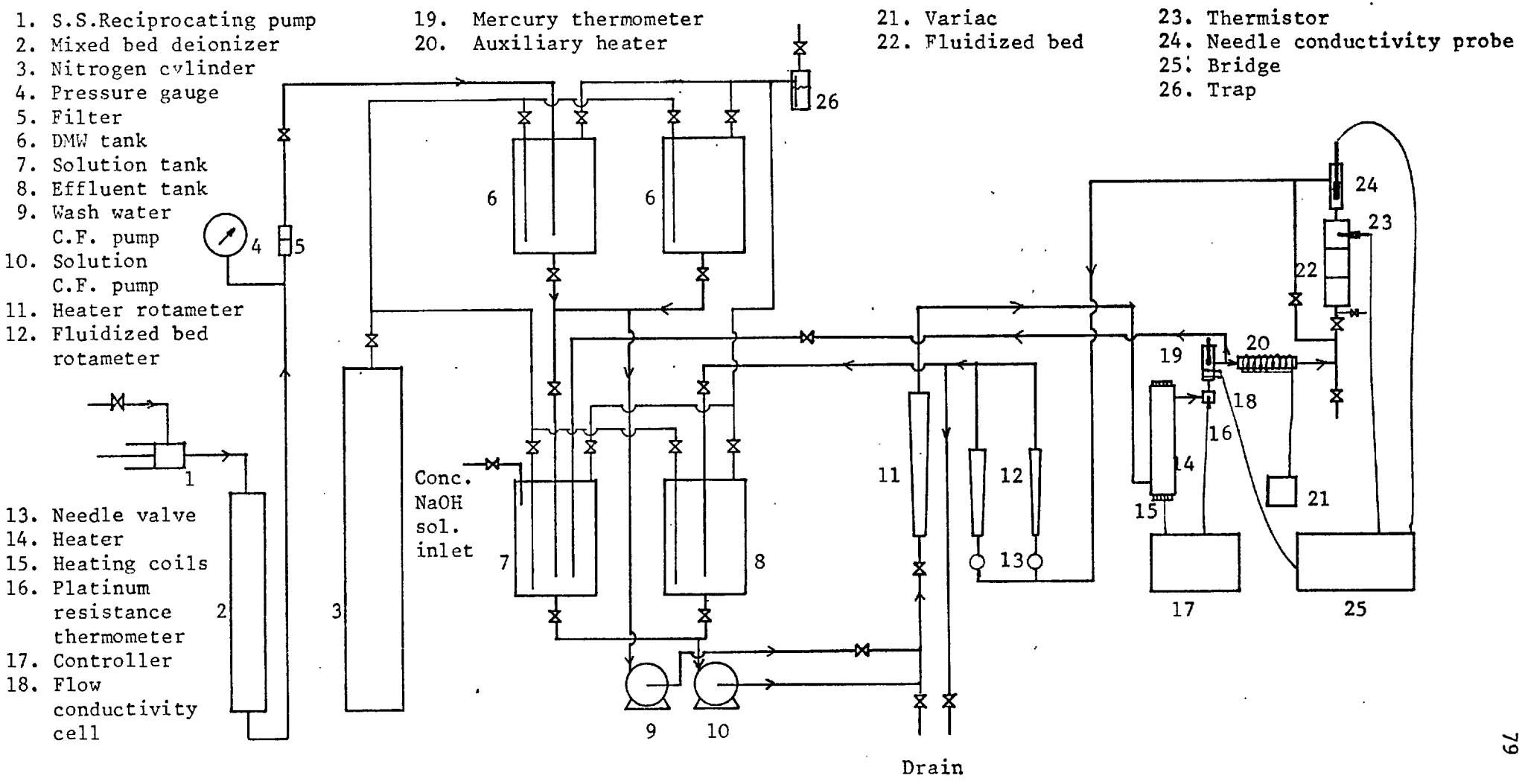

the solution tank [7] to prepare about 45ℓ 10^{-3} to 10^{-4} (N) NaOH solution. Feed solution is then pumped by the stainless steel pump [10] through the rotameter [11] and recirculated back to the feed solution tank through the heater [14] which is controlled by the phase angle controller [17] designed to the required sensitivity, a flow conductivity cell [18] and a thermometer [19]. After about 15 to 20 minutes, when the temperature of the fluid at the heater outlet shows a predetermined value, the flow at that point is divided into two streams. One flows through the fluidized bed [22] via a small heater [20], a needle conductivity cell [24], flow monitoring stainless steel rotameters [12] fitted with fine stainless steel needle valves [13] to either effluent tank [8] or the drain. The other stream is recirculated as before. Temperature sensing devices [16,19,23] are located at suitable points. The flow line is of PVC tubing.

5.2.1. Temperature control: It is not very practicable to maintain the entire flow loop at a constant temperature to within ±.02°C. It will suffice if the temperature of the fluid at the point where the conductivity is to be measured is maintained at the desired temperature level to within ±.02°C. The recirculating loop mentioned above forms the crucial part of the temperature control unit. In the main, it consists of an all glass construction shell and tube type heater [14] through which the fluid circulates. The heater is 18" × 3" and has twelve 1/8" dia glass tubes located axially. In each tube is placed a coiled nicrome resistance heating element [15] with a heat resistant fibre sleeve on each heating coil to ensure a smooth fitting with the glass tube. The resistance elements are suitably connected to give a maximum heat output of about 750 watts and the voltage across the heating elements is controlled by the phase angle controller [17]. The fluid flows through the shell side of the heater and the temperature at the outlet is

sensed by a platinum resistance thermometer [16] which is fed back to the temperature controller. The controller in turn controls the applied voltage across the heating elements.

Initially, the temperature controller is set to a desired value and the flow recirculated through the heat exchanger and back to the feed solution tank until steady state exit temperature of the fluid at about $0.1^{\circ}C$ above 25° or $30^{\circ}C$ depending on the temperature at which the experimental run is to be carried out. A mercury in glass thermometer [19] graduated to $0.1^{\circ}C$ located at the exit of the exchanger, is used for the visual indication of the temperature. In addition a flow conductivity cell [18] is provided at the exchanger outlet. A steady conductivity reading ensures that both temperature and concentration of the fluid is uniform.

After a steady state condition is achieved, the flow is divided into two streams and one of them is directed to the fluidized bed and the other recirculated as before. The flow rate of these two streams may be varied but their sum kept constant by adjusting of valves. This allows a constant flow rate through the heater which can be checked by the rotameter [11], but allows the flow through the fluidized bed to be varied. In the present experiments a maximum flow of about 3.4 ℓ/min was possible, this being the maximum capacity of the rotameters [12] used for flow control in the fluidized bed. The flow rate through the heater was about 4 ℓ/min for all experiments. A constant flow through the heater avoids any abrupt transients in the system when the flow in the fluidized bed is altered. Also, the location of the platinum resistance thermometer [16] just at the exit of the heater reduces the sensing lag and minimises the correction of the temperature of the fluid.

As the stream passes through the fluidized bed the temperature drops below that attained at the outlet of the heater. This drop in temperature

will depend on the flow rate, the length of the flow line and the temperature of the environment. To attain the desired temperature at the point where effluent conductivity is measured, some further heating of the stream may be required. For this a small auxiliary heater [20] about 5 watt in capacity is installed in the feed line to the inlet of the fluidized bed and heavily lagged. The auxiliary heater [20] consists of a glass tube forming part of the feed line with a resistance wire wound around it. The applied voltage across this heater is manually controlled by a variac [21]. The temperature of the effluent stream is measured by a calibrated thermistor above the fluidized bed at a point close to the conductivity probe. The thermistor is calibrated to within $0.01^{o}C$ against a mercury in glass thermometer graduated at $.01^{o}C$ intervals. The resistance of the thermistor is measured using the same bridge used for conductivity measurement. The controller and the auxiliary heater are adjusted so that the fluid temperature above the bed is 25 or $30^{o}C$ at which all but one set of runs was carried out. With the present equipment it is possible to achieve a control of temperature to within $\pm.02^{o}C$ or better. The only drawback is that every time the flow in the fluidized bed is varied, the auxiliary heater setting requires adjustment and this may require several minutes before a new steady state condition is reached. The temperature controller is set such that the thermistor reading corresponds to a value of $25^{o}C$ or $30^{o}C$ for a maximum flow rate through the bed with zero auxiliary heater output. The fluidized bed is surrounded on all sides by a curtain of polythene sheet to maintain a roughly constant condition of the immediate environment.

5.2.2. Construction of the fluidized bed: The fluidized bed is made of multiple push-fit sections of perspex to facilitate easy dismantling and fitting of the column. The middle sections are manufactured from a 3 in.

Fig. 5.2-2 : Sectional view of push-fit parts.

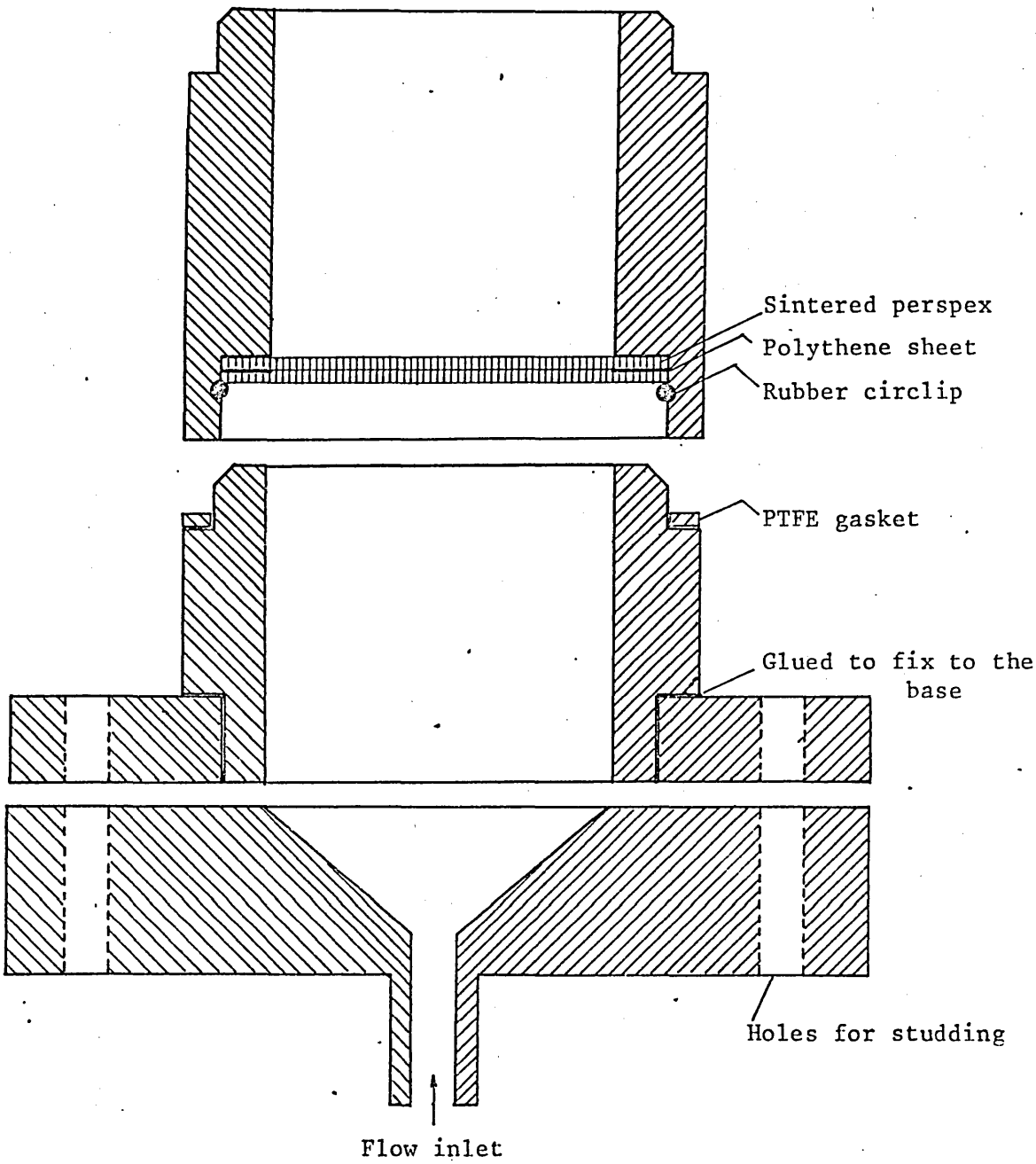

dia perspex rod and the two end sections from 6 in. square perspex block which are drilled to give an inside bed diameter of 2 in. The distributor is made of an 1/8" thick sintered polythene disc (5 μm porosity). The pressure drop through the sinter is much higher than the bed ensuring uniform fluidization. It was found that two such discs fitted with a narrow ring of polythene sheet between them gave the best result as indicated by visual observation. The polythene ring is placed such that the sintered discs have a 2 in. dia uncovered area at the centre. The sintered discs rest on a step cut in the column and are held in place by a thick flexible rubber sleeve made into a circle which in turn rests in a groove cut in the wall of the column and is similar in design to a circlip. This flexible rubber piece and the polythene ring avoid any leakage through the side of the distributor. The column is shown in figure 5.2-2. To help in obtaining a flat velocity profile the test section is preceded by a 6 in. long fixed bed column of glass particles of mixed size range and to reduce end effects the test section is followed by a 3 in. long similar fixed bed. The fixed beds are supported on single polythene sinters. Suitable arrangements have been provided in various sections for the introduction of temperature and conductivity probes. The various sections are held together by means of brass studding bolted from the two ends with PTFE gaskets placed between the sections to prevent leakage.

5.2.3. Precautions: Since NaOH solution is used, it is important that the solution does not come into contact with air so as to avoid the absorption of atmospheric CO_2 thereby altering the equilibria of the system and conductivity of the solution. For this reason the storage and solution vessels are kept under a nitrogen atmosphere by slowly bubbling nitrogen from a nitrogen cylinder [3], this being indicated by the nitrogen bubbles escaping in the trap [26]. No degassing of solu-

tion was necessary. To prevent any blocking of the distributor plate, which will cause an uneven flow, the deionized water supply line is provided with a filter [5] having a porosity much finer than the porosity of the bed support.

5.2.4. Measurement of the conductivity of the solution: The conductivity of the effluent was determined by a needle conductivity probe and measured by a Wayne Kerr autobalance bridge [25] having a sensitivity of 0.1%. The needle probe [24] is 1 in. long and 1/8 in. dia and is placed in a "T" junction. It was observed that if the probe was disturbed the cell constant changed slightly. However, this was avoided by rigid fixing. The conductivity of the feed solution was determined using the flow conductivity cell [18] or by the needle probe [24]. If the latter is used the flow path must be altered such that the feed solution passes through the needle probe [24] and then through the bed in down flow and then to the drain. Every time an experiment was carried out, the cell constant of the needle probe was checked against the flow cell [18] since the cell constant of the latter remained constant. Concentration data can then be obtained from calibration curves.

5.2.5. Determination of particle diameter, surface and voidage: The ion exchange resin particles used in the experiments were commercially available cation beads (Zeo-Karb 225) having a DVB crosslinking of 8 and 20%. It is desirable to obtain a narrow size range to avoid segregation of particles during fluidization and to determine the mean diameter of particles accurately. Dry sieving of resin particles must be avoided since on subsequent wetting the particles tend to crack. Wet sieving was therefore used and repeated sieving was necessary to obtain a closely graded sample. The average diameter of the resin beads was determined by measuring a few hundred beads from each sample using a cali-

brated microscope. It is necessary that the diameter be known when the particles are fully swollen since even partial drying may result in shrinkage. For example, the difference between the diameter of a fully swollen and an air dried resin in the H^+ form may be as high as 15%. The particles were located on a glass plate of suitable design and submerged in water for examination under a microscope. A typical size distribution is shown in Fig. A.6-1. Since the average diameter of the entire population was not known, a "t" test was made. The average diameter of the entire population was determined to better than 2% for a 95% confidence limit.

It is also known that the diameter of the particles changes as the resin is converted from hydrogen to sodium form. The change in diameter with loading is shown in Fig. A.6-2. It may be seen from the figure that the maximum change is less than 3% for the 8% crosslinked and 1.5% for the 20% crosslinked resin. In mass transfer calculations an average diameter between the two limits was used. However, at no time during a run were the particles completely converted from one form to another.

The precise determination of the surface area of the particles making up a shallow bed is difficult. A displacement technique is not suitable since the weight of fully swollen particles is required in this method and this is not easily obtained. The surface area can be determined if the settled volume of particles and the voidage are known. Since a small volume of resin particles were used, this method is also difficult. Measurement in a narrow cylinder gives an accurate settled bed height, but not an accurate voidage, since the wall effect would be high. A large diameter column is more satisfactory, but this requires precise bed height measurement. Further, the bed voidage is not usually known though reasonable estimation is possible. In the present case a more

direct but much more laborious method has been employed. In this method the resin particles were carefully removed from the bed after carrying out the mass transfer experiments and transferred to several sintered glass-bottomed tubes and centrifuged till a constant weight of the samples was recorded. Then the resin particles were transferred to a large petri dish and left for several hours and weighed. Several thousand beads were then counted from the total population and weighed. From this weight and the weight of the total population, the total number of beads and hence the total volume when fully swollen was calculated.

Bed voidage was determined from a knowledge of the absolute resin volume and the expanded bed height. Bed height was determined at a given flow using a cathetometer. The constancy of the flow was checked by direct measurement at least twice during a run.

5.2.6. Determination of viscosity and diffusivity data: The viscosity of the solution is taken as that of water, since at 10^{-3} to 10^{-4} (N) concentration of NaOH the difference in viscosity is negligible. The ionic diffusivities were calculated using the Nernst-Einstein relation: $D_{is} = \frac{RTu}{F}$ where u is the mobility of the ion solvent pair, T the temperature and R the gas constant and F the Faraday constant. The mobility data has been obtained from reference (16). The Nernst-Einstein equation is valid for the limiting case of zero concentration and hence appropriate correction was made to obtain corrected values of diffusion coefficient. However, any correction in the range of concentration 10^{-3} to 10^{-4} (N) is small as may be seen from the Schmidt numbers in tables listed in Appendix A.5.

5.3. Measurement of axial concentration in the fluidized bed

The axial concentration in the bed was determined in order to check the assumption of plug flow of liquid in the bed. This was done by withdrawing samples of solution by means of hypodermic needles. To achieve this, several small holes were drilled into the wall of the fluidized bed and closed by small silicone rubber bungs. Care was taken not to project the bungs into the interior of the fluidized bed and the holes were sealed by a soft resin so that a smooth surface was maintained within the bed by wiping away the surplus resin with tissue paper soaked in carbon tetrachloride. Thin hypodermic needles were then pushed into the bungs so that the end of the needles nearly crossed the thickness of the wall. The other push fit units were then assembled and the run started. After steady state was achieved, a needle was pushed right into the bulk of the stream and a sample was withdrawn into the syringe. It was necessary for the sample to be withdrawn very slowly so that disturbance of the bed was as small as possible. After each sample was collected in the syringe, the needle was withdrawn to the original position and the syringe removed for the analysis of the solution. In this way several samples were collected from different axial positions. The position of the probes was determined by carefully locating the projected needle in the bed by a cathotometer. The samples were analysed for Na^+ content by an EEL flame photometer in view of the lack of a suitable constant temperature bath. The maximum full scale reading with this instrument as quoted by the manufacturer is 5 ppm Na^+ and hence dilution of the samples was necessary for the analysis.

5.4. Single particle mass transfer experiments

In order to obtain a better understanding of the multiparticle mass transfer results some single particle experiments were carried out using the same physico-chemical system. The experiments were carried out by allowing single resin particles to fall in a tall column filled with dilute NaOH solution. A schematic diagram of the equipment is shown in Fig. 5.4-1. The equipment consists of a 2 in. dia 5 feet long glass column [1] fitted with a suitable valve arrangement for washing and collecting of the particle and feed solution and deionized water tank with associated pumps and tubings. The most important unit in this equipment is the two way valve [2] with a sweep elbow type passage in the stopper. This valve, designated valve 1, separates the solution column from the wash unit. It serves to feed the solution to the column, is the exit end of the washing section [4] and initial collection chamber for the particle. The other two way valve [3] with a tee type passage in the stopper, designated as valve 2, is used to feed deionized water into the washing section.

The column is fitted with an easily removable end [5], and is filled with dilute NaOH solution of known concentration through valve 1. After filling the outlet end is removed and a rubber bung placed at the column end to avoid any contact of the solution with the atmosphere. Deionized water is then introduced into the washing section through valve 2 and expelled through valve 1, and bottom of the fritted end column, so that the entire wash unit including the passage of the stopper of valve 1 is thoroughly washed and contains deionized water only. A needle conductivity probe [6] is located just below the valve 1 to detect any possible contamination of the deionized water with feed solution from the solution column.

Fig. 5.4-1 : Flow diagram for single particle mass transfer study.

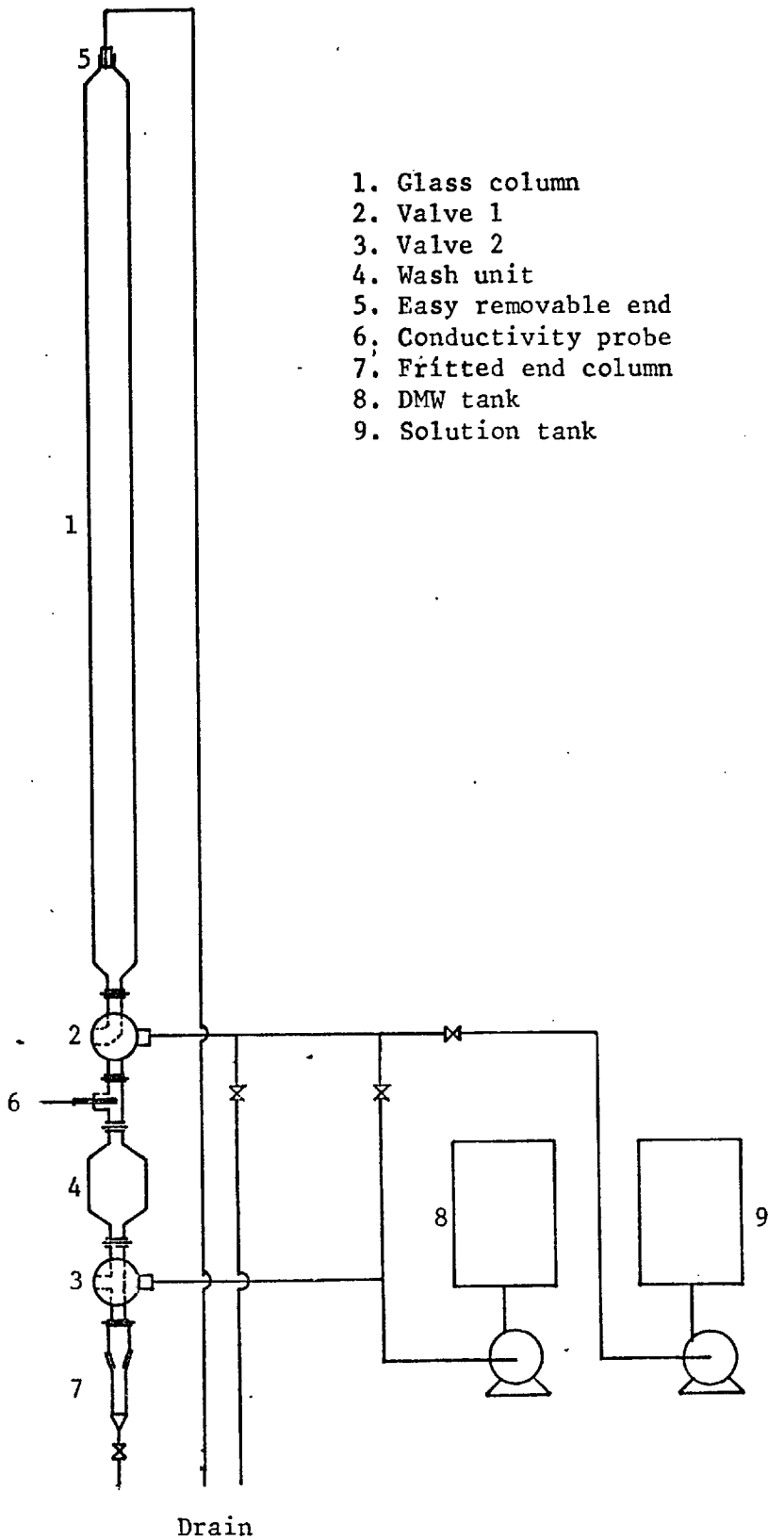

A resin particle is converted to H^+ form by passing a large excess of acid and thoroughly washed with water is then selected and its diameter measured with a calibrated microscope. The particle is then taken on the thin tapered end of a glass rod; the adhering moisture in the particle is sufficient for sticking. The rubber bung at the top end of the solution column is removed and the glass rod with the particle is just dipped into the solution of the column. The dipping of the rod is done very carefully, the object being to drop the particle into the solution. Almost immediately the particle reaches its terminal velocity and falls steadily in the column. When the particle is almost at the bottom end, valve 1 is adjusted so that the particle drops into the passage of the stopper of the valve which is filled with deionized water and the stopper immediately rotated so that the particle falls into a pool of deionized water and finally settles in the fritted end glass column. The particle is now given another thorough wash before the fritted end column is separated for the removal of the particle for analysis. The temperature of the solution and the time of fall of the particle in the glass column is noted.

The mass transfer coefficient can be calculated from a mass balance on the particle. A mass balance gives

$$\frac{d}{dt} (v_R \overline{C}_{Na}) = 4\pi R^2 \overline{K}_c (C_{Nab} - C_{NaR}) \qquad (5.4\text{-}1)$$

where v_R is the volume of the particle, $\overline{C}_{Na}$ the solid phase concentration of Na. Since C_{Nab}, the bulk solution concentration is constant and $C_{NaR} = 0$

$$v_R \int_0^{\overline{C}_{Na}} d\,\overline{C}_{Na} = 4\pi R^2\, \overline{K}_c\, C_{Nab} \int_0^{t_f} dt$$

or, $$W_{Na} = 4\pi R^2 \bar{K}_c C_{Nab} t_f \qquad (5.4\text{-}2)$$

where W_{Na} is the total amount of Na in the particle and t_f, the time of fall of the particle in the column. Thus, the total amount of Na^+ transferred to the particle must be estimated in order to determine the mass transfer coefficient.

The estimation of the amount of sodium in a small resin bead is difficult. The amount of sodium in a bead is about 10^{-7} to 10^{-8} gm. Wet chemical methods are not attractive because of the low concentration and also because a suitable solvent cannot be found to dissolve the particle easily. Radioactivation analysis is attractive, but the preparation of standards is not easy. For these reasons, a spectro chemical method was used. A straightforward standard technique was employed for this, the details of which are given in Appendix 4.

CHAPTER 6

RESULTS AND DISCUSSIONS

6. RESULTS AND DISCUSSIONS

6.1. Fluidized bed

The following relationship is assumed valid in a multiparticle bed

$$Sh_m = \phi_1(Re_s, \varepsilon, Sc) \qquad (6.1\text{-}1)$$

In the above equation the voidage ε is included as an approximate method of accounting for the effect of other neighbouring particles on mass and heat transfer. Voidage alone, does not describe the entire structure of a particulate assembly. For example, it is possible for an assembly of particles to have the same voidage and yet a completely different arrangement of particles. However, if the structure of the bed is the same over the entire range of voidage then the above equation would be a good representation for a multiparticle assembly.

For a fluidized bed, a further relationship is valid, assuming negligible wall effects (64),

$$\varepsilon = \phi_2(Re_s, Re_o) \qquad (6.1\text{-}2)$$

where Re_o is the terminal settling Reynolds number. Equation (6.1-1) may then be written as

$$Sh_m = \phi_3(Re_s, Re_o, Sc) \qquad (6.1\text{-}3)$$

The terminal Reynolds number Re_o is a characteristic property of a fluid-particle system and is a precise parameter in correlating mass and heat transfer results in a fluidized bed. It is noteworthy that Re_o characterises bed expansion (see equation (6.1-2)) and it has been successfully used to correlate mixing data in liquid fluidized beds.

Again, on the basis of single particle work, one may assume that,

$$Sh_m = B_m Re_s^q Sc^{1/3} \qquad (6.1\text{-}4)$$

Equation (6.1-4) is similar in form to equation (2.2-17). Examination of equation (6.1-3) indicates that the coefficient B_m and exponent q may depend on Re_o. It is further assumed that equation (6.1-4) holds good for the entire range of voidage including a value of unity corresponding to a single particle in an infinite medium. Thus,

$$Sh_m \Big|_{\varepsilon \to 1} = B_m \, Re_s^q \Big|_{\varepsilon \to 1} \, Sc^{1/3}$$

or
$$Sh_o = B_m \, Re_o^q \, Sc^{1/3} \tag{6.1-5}$$

Now $Sh_m \Big|_{\varepsilon \to 1} \to Sh_o$, where Sh_o is the value of the Sherwood number at unit voidage and hence corresponds to the case of single particle falling at the terminal Reynolds number so that similarly $Re_s \Big|_{\varepsilon \to 1} \to Re_o$. For a single particle settling at the terminal Reynolds number one can write from equation (2.2-17),

$$Sh_o = B_o \, Re_o^{1/2} \, Sc^{1/3} \tag{6.1-6}$$

where the coefficient B_o is expected to be a constant over a limited range of Re_o. Equating (6.1-5) and (6.1-6),

$$B_m = B_o \, Re_o^{\frac{1}{2}-q} \tag{6.1-7}$$

and using this relationship in equation (6.1-4),

$$Sh_m = B_o \, Re_o^{1/2} \left(\frac{Re_s}{Re_o} \right)^q Sc^{1/3} \tag{6.1-8}$$

The conventional j_m factor can be written as

$$j_m = \frac{Sh_m}{Re_s \, Sc^{1/3}} = B_o \, Re_o^{\frac{1}{2}-q} \, Re_s^{q-1} \tag{6.1-9}$$

Thus, the important quantity to be determined is q since at least some

idea of B_o may be obtained from a single particle study. However, it would be better to determine the value of B_o from fluidized bed data and compare this with the value obtained from single particle studies, since a number of assumptions have to be made to obtain the value of B_o from fluidized bed data.

The j_m factors against Re_s plots for a range of Re_o are shown in Figs. 6.1-1 to 6.1-6 and the data is tabulated in Appendix A.5. Visual examination of the data in these Figures indicates that the experimental data in the higher range of Re_s' can be readily correlated by a single straight line on logarithmic coordinates. Extrapolation of the correlating lines to low values of Re_s shows that the experimental data falls well below and suggests a lowering of mass transfer. From the Figures it may be seen that this deviation occurs for data lying below about $Re_s/Re_o < 1/6$ or at a voidage below about 0.55 though this choice is somewhat arbitrary. The correlating lines (shown as the solid lines) in the Figures include only those data for which the open symbols are shown and usually these points lie above $Re_s/Re_o > 1/6$ and the closed symbols lying below this value are not included in correlating experimental data. From the slope of these curves, which is (1-q), q can be obtained. The values of q are plotted against Re_o (open symbols) in Fig. 6.1-9 using logarithmic coordinates and tabulated in Table A.5-8. A correlation, $q = 0.5\ Re_o^{-0.3}$, can be written as a convenient equation, the least square fit being $q = 0.495\ Re_o^{-0.307}$. It may be seen from Fig. 6.1-9 that when the entire data including the low Re_s range is used to obtain the values of q no suitable correlation between q and Re_o can be obtained. These points are shown as closed symbols in Fig. 6.1-9.

The deviation of the data at low voidage may also be seen in the work of Chu et al. (11) and Conderc et al. (14) shown in Fig. 6.1-7 and 6.1-8.

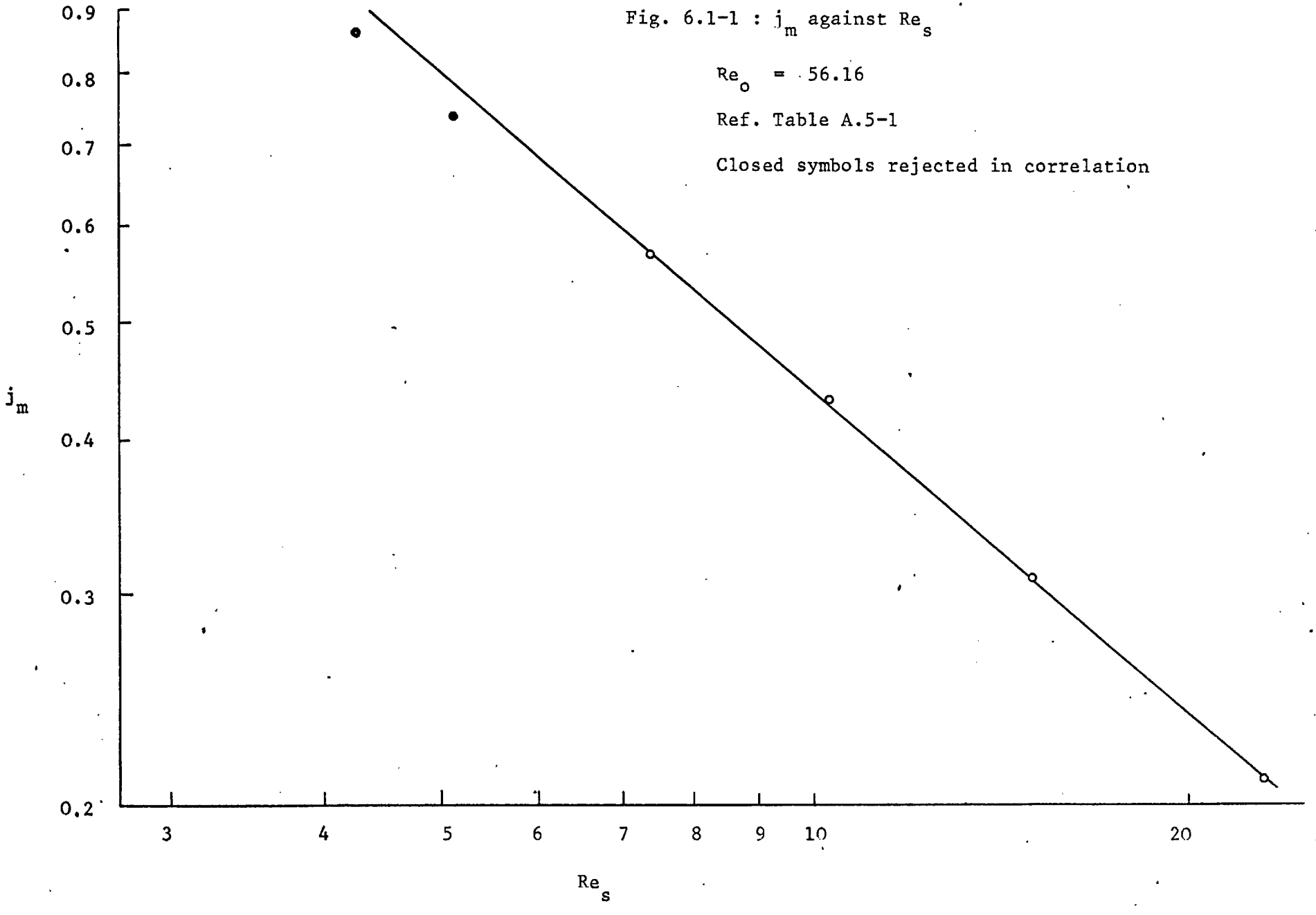

Fig. 6.1-1 : j_m against Re_s

Re_o = 56.16

Ref. Table A.5-1

Closed symbols rejected in correlation

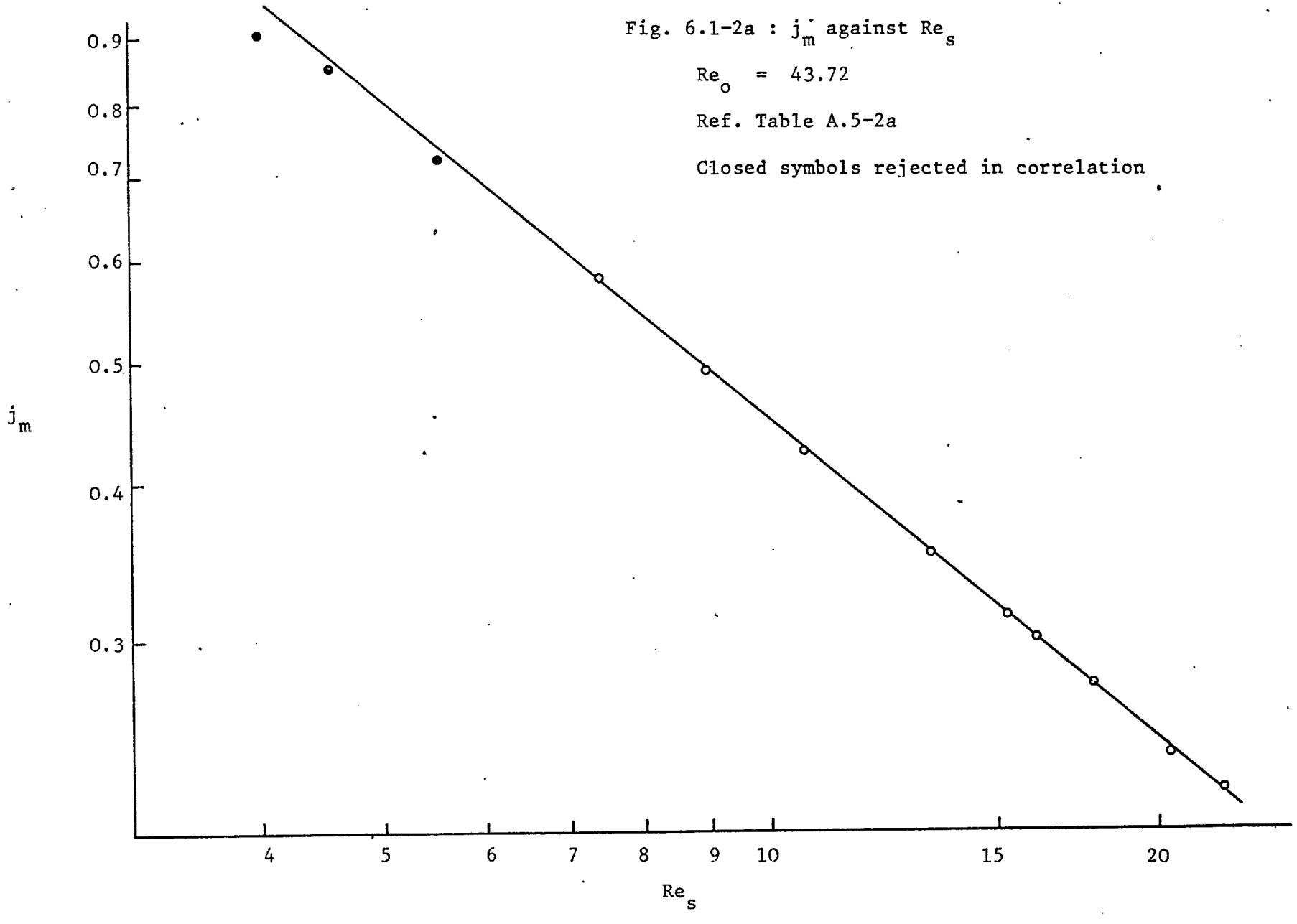

Fig. 6.1-2a : j_m against Re_s

Re_o = 43.72

Ref. Table A.5-2a

Closed symbols rejected in correlation

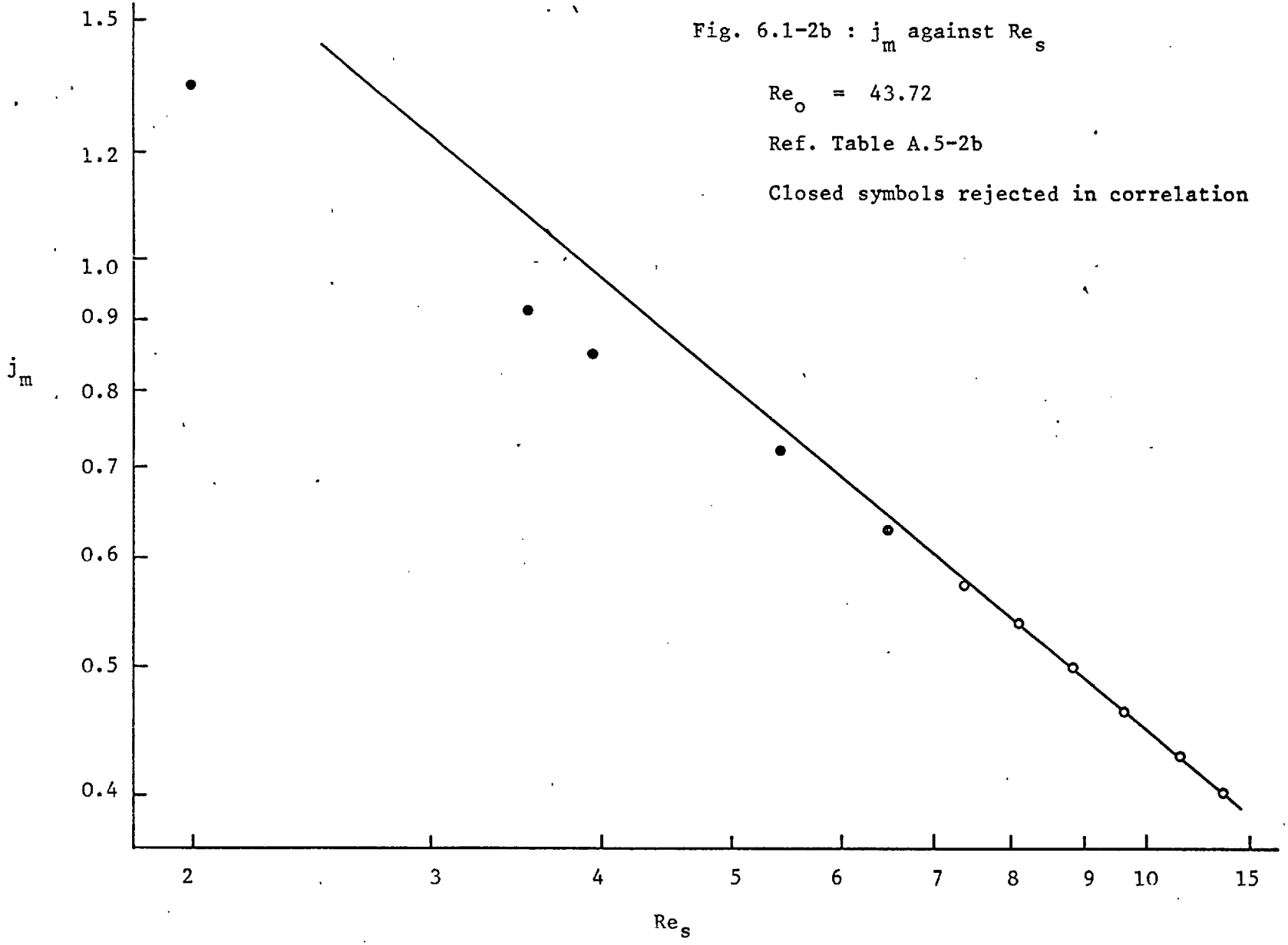

Fig. 6.1-2b : j_m against Re_s

Re_o = 43.72

Ref. Table A.5-2b

Closed symbols rejected in correlation

Fig. 6.1-3 : j_m against Re_s

Re_o = 29.98

Ref. Table A.5-3

Closed symbols rejected in correlation

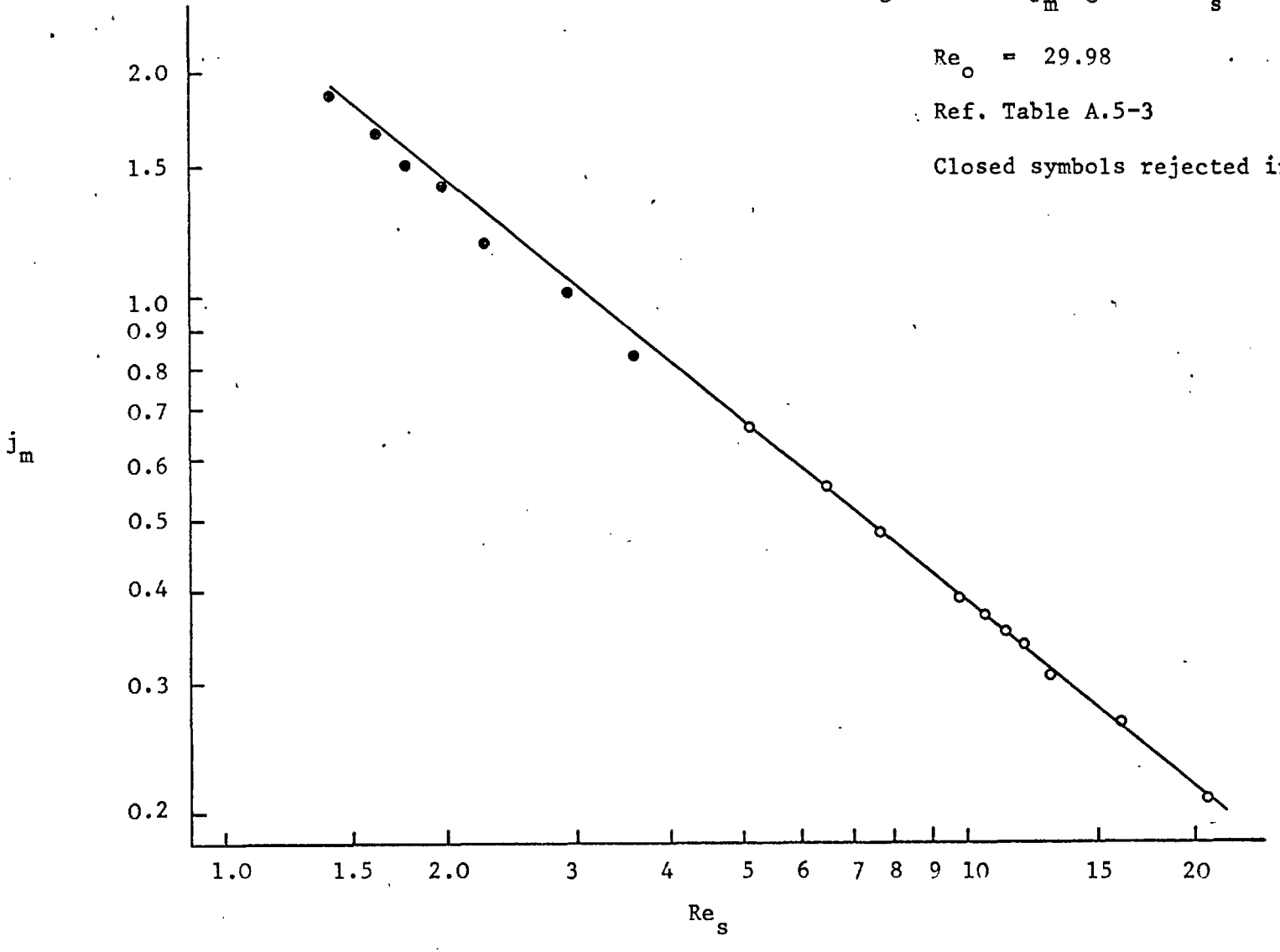

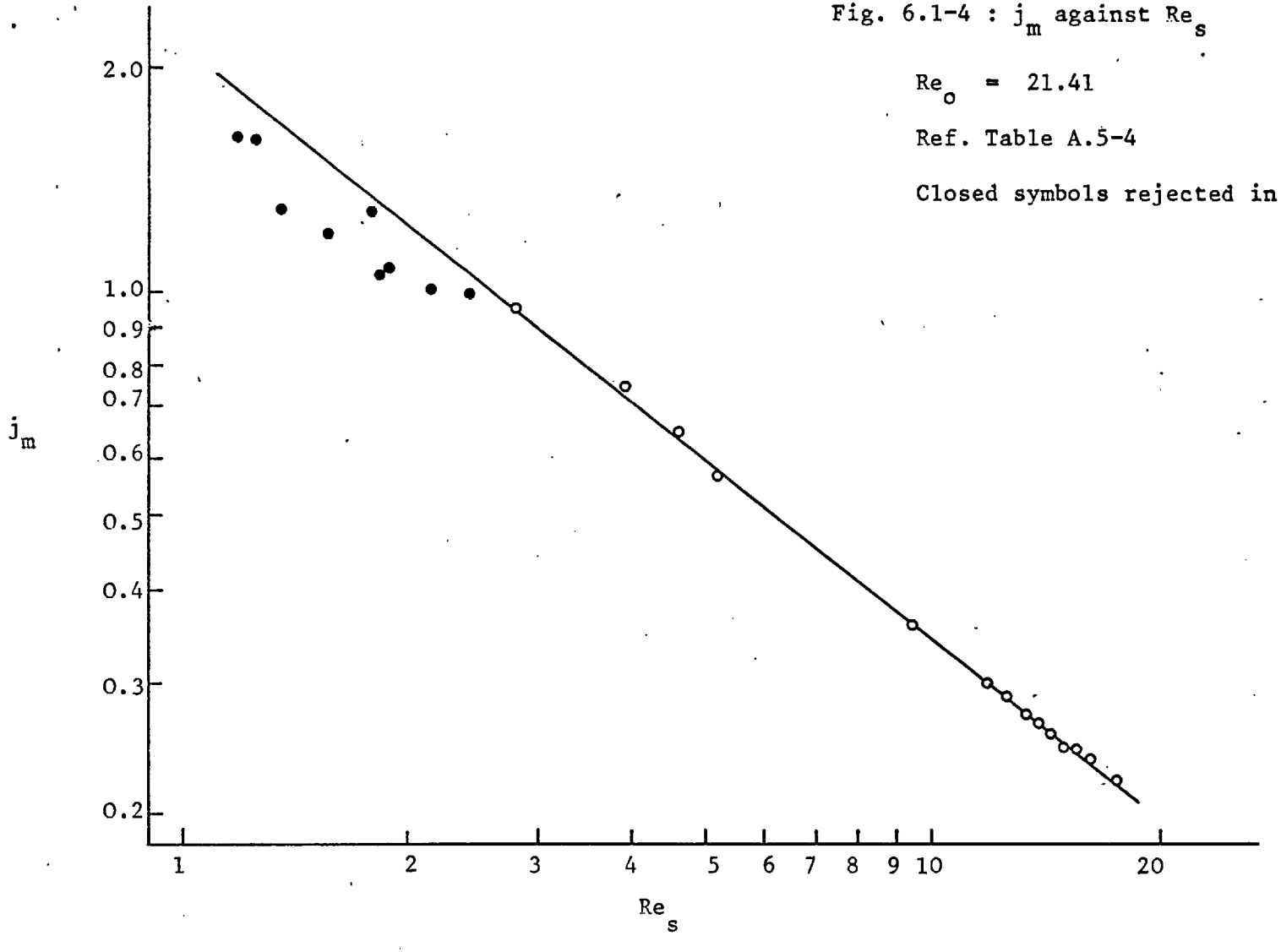

Fig. 6.1-4 : j_m against Re_s

Re_o = 21.41

Ref. Table A.5-4

Closed symbols rejected in correlation

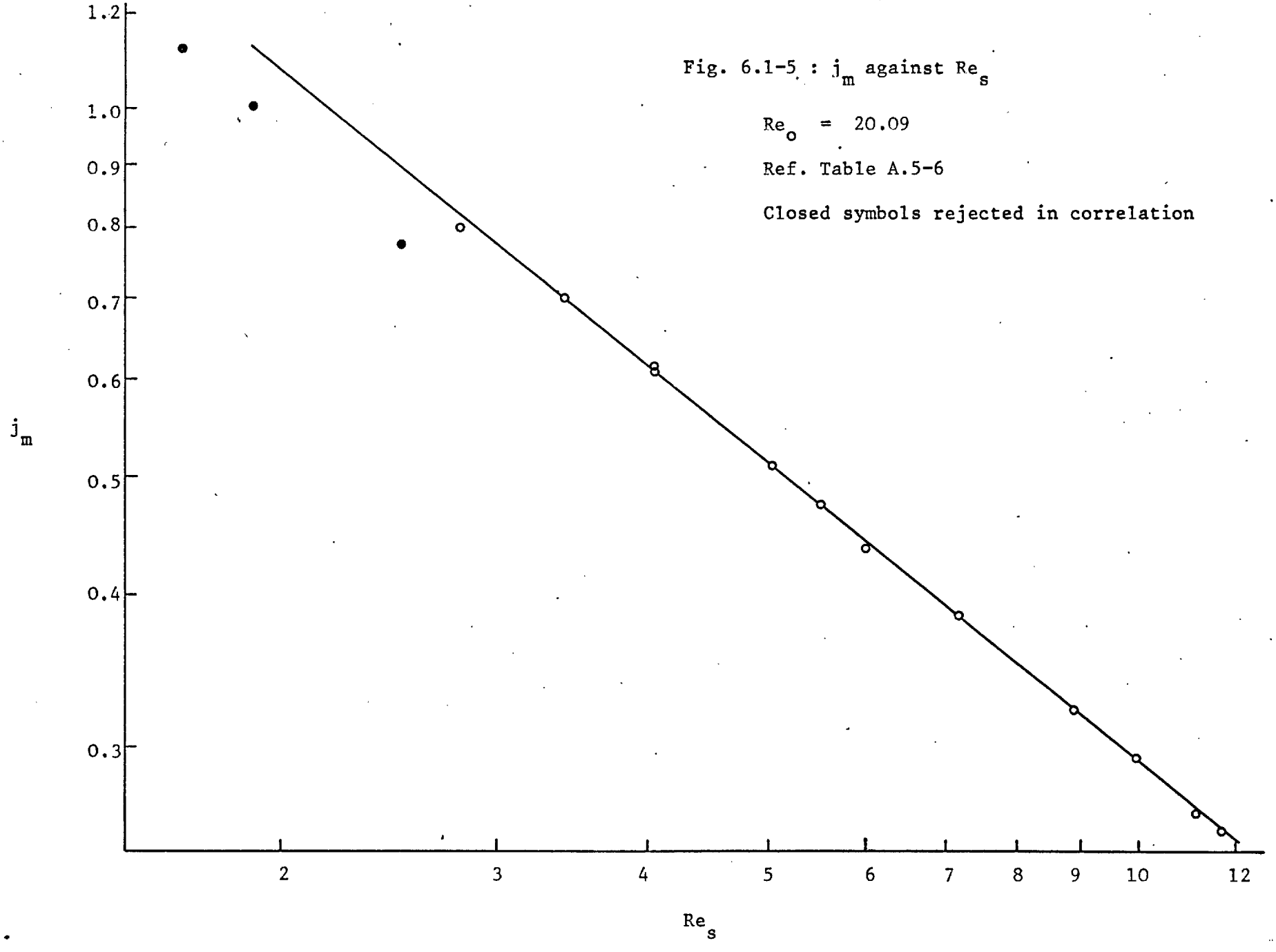

Fig. 6.1-5 : j_m against Re_s

Re_o = 20.09

Ref. Table A.5-6

Closed symbols rejected in correlation

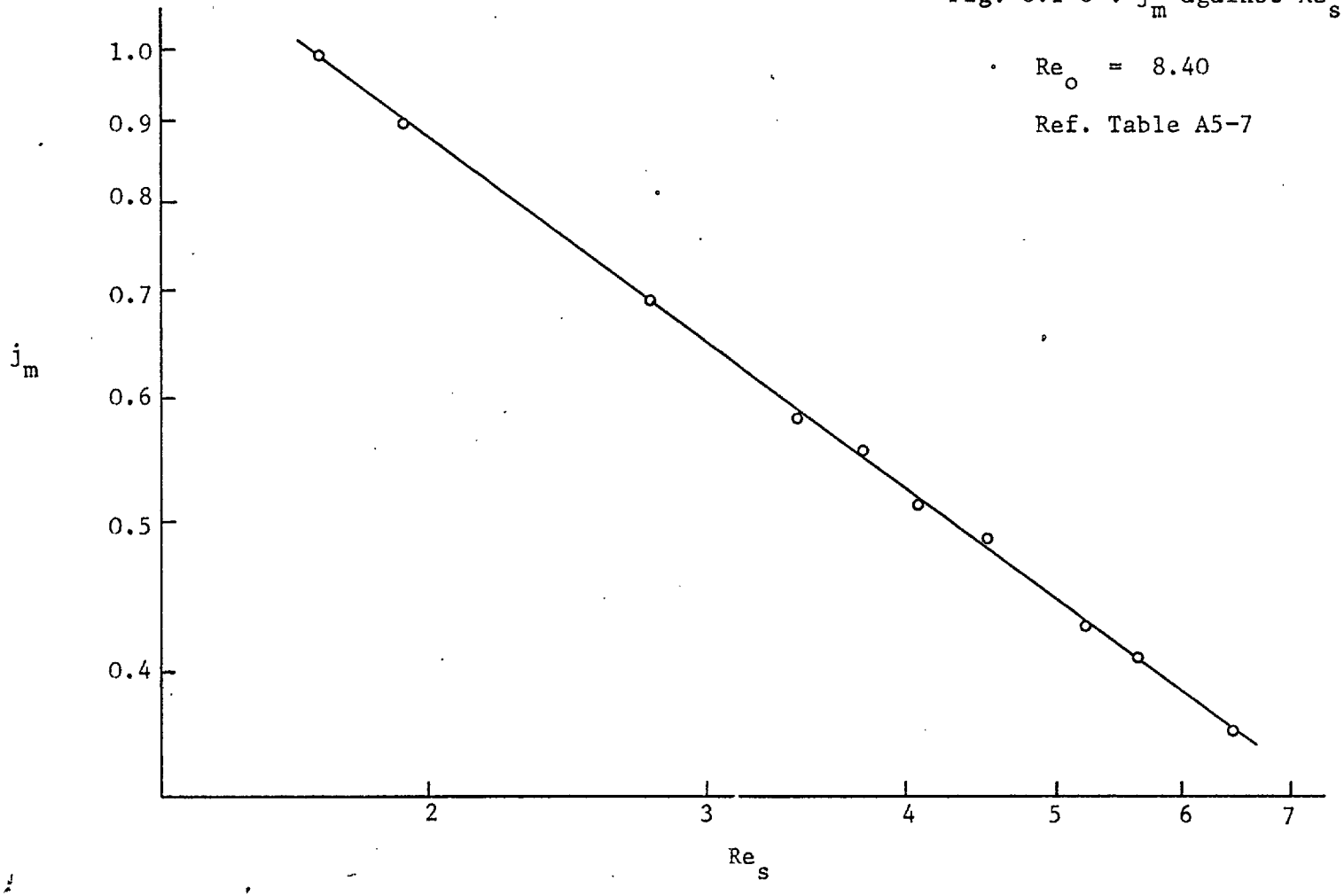

Fig. 6.1-6 : j_m against Re_s

Re_o = 8.40

Ref. Table A5-7

Fig. 6.1-7 : j_m against Re_s

Reproduced from reference (11).

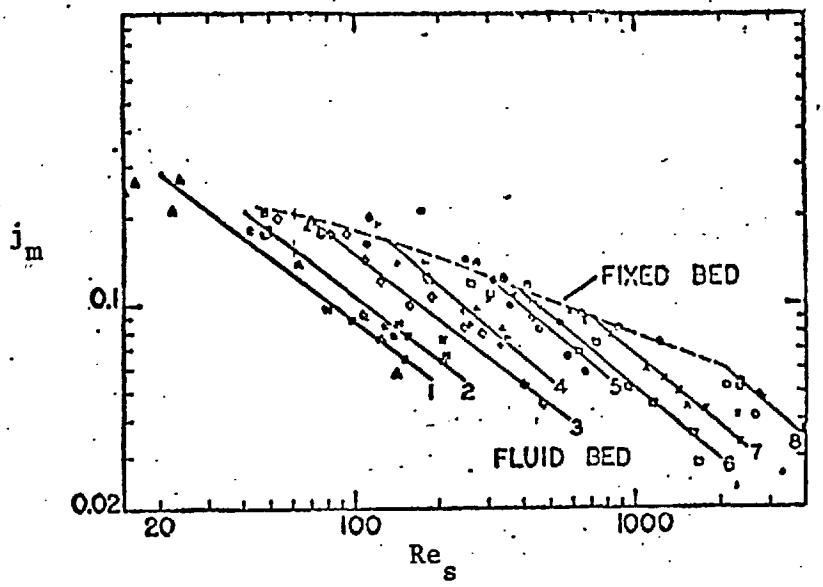

		d (average) in.			d (average) in.
1. Glass beads	△	0.028	5. Large lead shot	⊗	0.078
2. Small lead shot	⊠	0.029	6. Small Celite cylinders	□	0.215
3. Rope seed	◇	0.077	7. Intermediate Celite cylinders	×	0.334
4. Intermediate lead shot	+	0.050	8. Large Celite cylinders	⊙	0.540

Fig. 6.1-8 : $Sh_m\, Sc^{-1/3}$ against ε

Reproduced from reference (14).

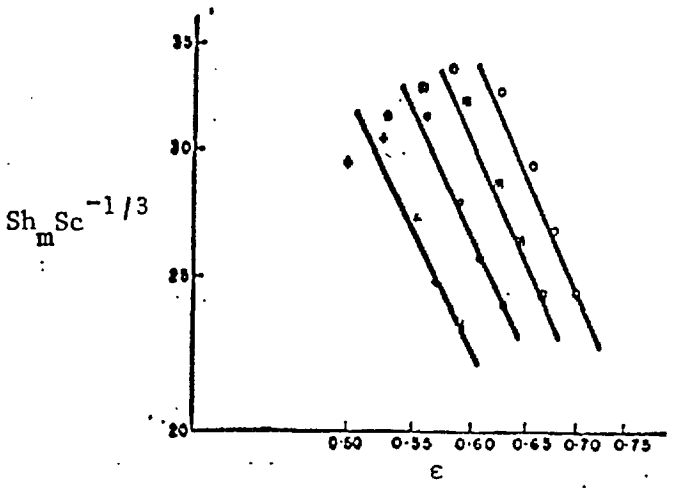

Legend $+Re_s = 150$; $\oplus$ $Re = 175$; $\boxplus Re_s = 200$; $\bigcirc Re_s = 225$.

Re_s	150	175	200	225
Slope	−1.98	−2.04	−2.17	−2.21

Fig. 6.1-9 : q against Re_s

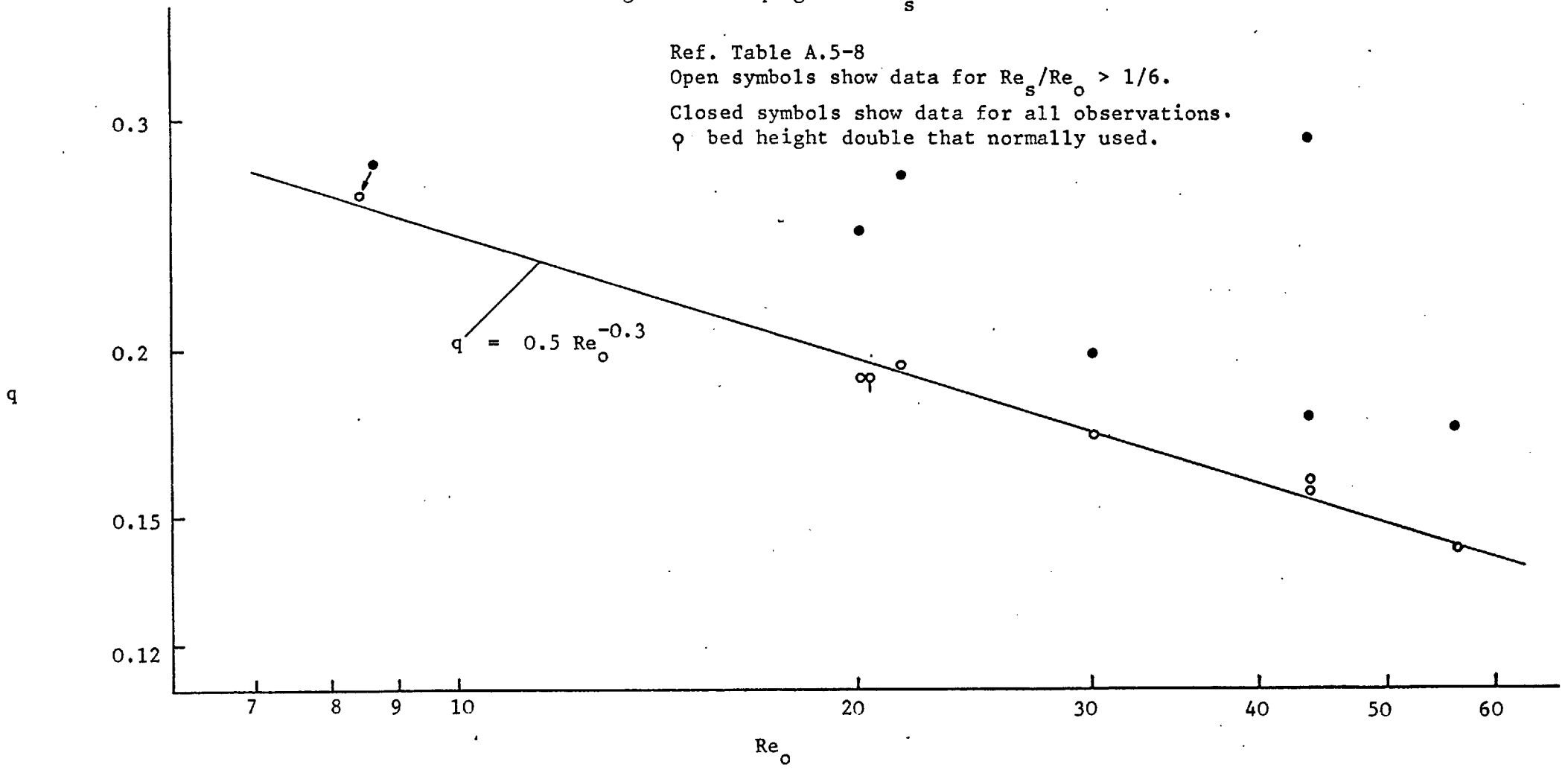

The latter authors' data shows this quite clearly. It is possible that j_m does change smoothly with Re_s over the entire range, i.e. a smooth curve can be drawn in some cases, especially in Figs. 6.1-2a, 2b. However, all the data except in Fig. 6.1-1 have been correlated by a straight line in the range $Re_s/Re_o > 1/6$. In Fig. 6.1-1 data has been correlated for $Re_s/Re_o > 1/7.5$, but as mentioned earlier this choice is somewhat arbitrary and almost the same correlation could be obtained in this case also for data points at $Re_s/Re_o > 1/6$.

The reason for a difference in the mass transfer behaviour at lower voidage, i.e. voidage corresponding to $Re_s/Re_o = 1/6$ which is about 0.55 for the present cases, may be explained by the fact that at low voidage, a fluidized bed tends to maintain an ordered arrangement in which individual particles are arranged in lines parallel to the main flow compared to the random arrangement at higher voidage. This ordered arrangement at low voidage effectively shields part of the particle surface to flow, with the result of a decrease in mass transfer. The existence of an ordered structure in a fluidized bed is known and has been clearly demonstrated by Gunn and Malik (33). These authors measured the drag coefficient for different arrangements of spheres and compared the results with those obtained in a fluidized bed over the entire range of voidage for a large range of flow. They found that at low voidage, the fluidized bed could be closely identified to an ordered arrangement in which the particles were orientated in lines parallel to the main flow. This string-like arrangement would partially shield the particles explaining a lowering of the drag coefficient in a fluidized bed. Classical work of Rowe et al. (66) on drag measurements and that of Peltzman and Pfeffer (59) on mass transfer shows that an axial arrangement would lower drag and mass transfer coefficients. The latter authors referred to this as the "area blockage effect". As the voidage of the bed increases, the corresponding

Reynolds number increases and the ordered structure of the bed tends to disappear. This is due to inherent perturbations originating in the fluid itself. The progression in disorder is probably due to increased inertial forces and increasing turbulence, the strength of which would grow with increase in the Reynolds number. Gunn and Malik (33) concluded that at a Re_s of 0.1 and 10 the corresponding voidages at which a random structure would exist would be above about 0.9 and 0.8. At a Re_s of about 10^3, there would be little trace of any ordered structure in a fluidized bed. In this work, the mass transfer results at a voidage above about 0.55 are well correlated suggesting a uniformity in structure. Since the experimental data fall below the correlating lines for voidages below about 0.55 it could be argued that this reduction is due to an "area blockage" effect because of a string-like arrangement of particles. Above this voidage or $Re_s/Re_o > 1/6$ the particles are randomly oriented and an increase of mass transfer occurs. In this study it is difficult to know exactly where the transition from order to disorder occurs due to a lack of data at sufficiently close intervals. Also, of course, mass transfer rates are less sensitive to geometric arrangements than are drag measurements. For example, in an axial arrangement of two spheres, no observable difference in mass transfer may be noticed when the spheres are 2 to 3 diameters apart. An effect would be observed in drag coefficient measurements even if the spheres were about 9 diameters part. However, the present mass transfer results give an indication that at low voidage there is a tendency to form an ordered arrangement of particles which is being destroyed as the voidage increases due to increased flow perturbations which disturb the fine balance of forces needed to maintain an ordered structure. This possibly justifies the neglect of data in the lower voidage range in obtaining a suitable correlation, since the task would otherwise be difficult. It

therefore appears that voidage effects can be used to account for the effect of other particles at $Re_s/Re_o > 1/6$, thus justifying the use of equation (6.1-1) in a fluidized bed.

The values of B_o for different Re_o obtained from fluidized bed experiments are tabulated in Table A.5-8. It is seen from the table that the value of B_o is almost constant except for $Re_o = 20.09$ and an average value of 0.857 is taken. The one exception when $B_o = 0.742$ is possibly due to an error in the determination of the volume of particles in the bed. This point can be checked if reliable bed expansion data are available. The bed expansion characteristics are shown in Fig. 6.1-10 and compared with the Richardson-Zaki correlation (64) in Fig. 6.1-11. The Richardson-Zaki correlation is

$$\frac{Re}{Re_o} = \varepsilon^N \qquad (6.1\text{-}10)$$

where $N = 4.45\ Re_o^{-0.1}$ for $1 < Re_o < 500$. In Fig. 6.1-11 the value of N is plotted against Re_o or equivalent Ga where $Ga = \frac{d^3\rho(\rho_s-\rho)g}{\mu^2}$ and compared with the experimental values which are obtained by correlating observed voidage data shown in Fig. 6.1-10. Again, in this correlation the lower voidage range data is neglected. Comparison of the predicted and calculated values of N shows that the bed expansion data is not very reliable. This is thought to be due to the small bed volume used in the experiments which makes bed height measurements difficult because of the uneven surface of the fluidized particles. Further, the cathetometer used to determine the bed height did not have good resolving power making focusing of the instrument difficult. Thus the value $B_o = 0.742$ for $Re_o = 20.09$ is not reliable. However, this is not serious, since the value of B_o is reasonably constant for all other Re_o and the volume of the bed does not effect the value of q as this depends on the ratio of inlet to outlet concentration of the fluid stream. Thus the correla-

Fig. 6.1-10 : ε against Re_s.

Legend	Re_o	Ref. Table
○	8.4	A.5-7
○	21.41	A.5-4
○	29.98	A.5-3
○	43.72	A.5-2a
○	56.16	A.5-1

Closed symbols not included in correlation

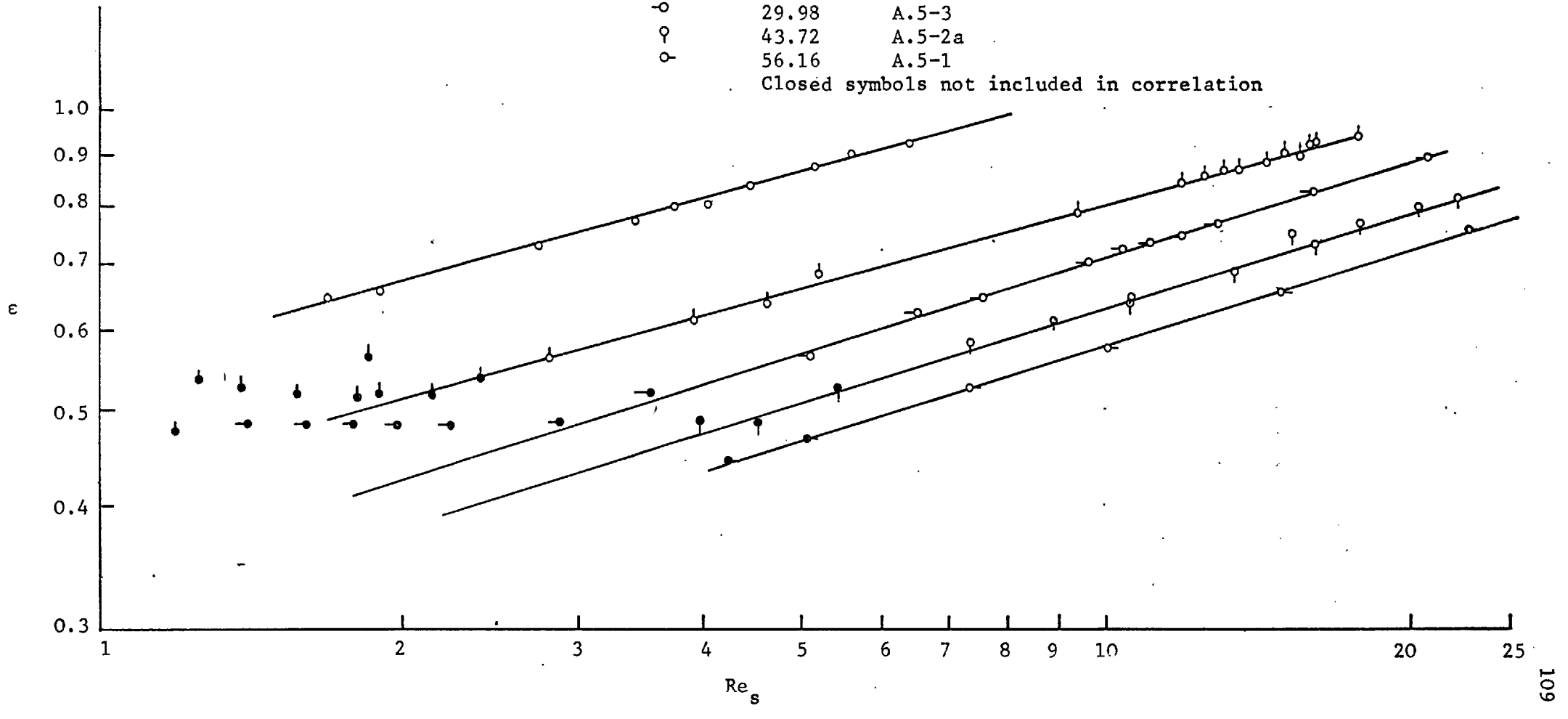

Fig. 6.1-11a : N against Re_o

Ref. Table A.5-8

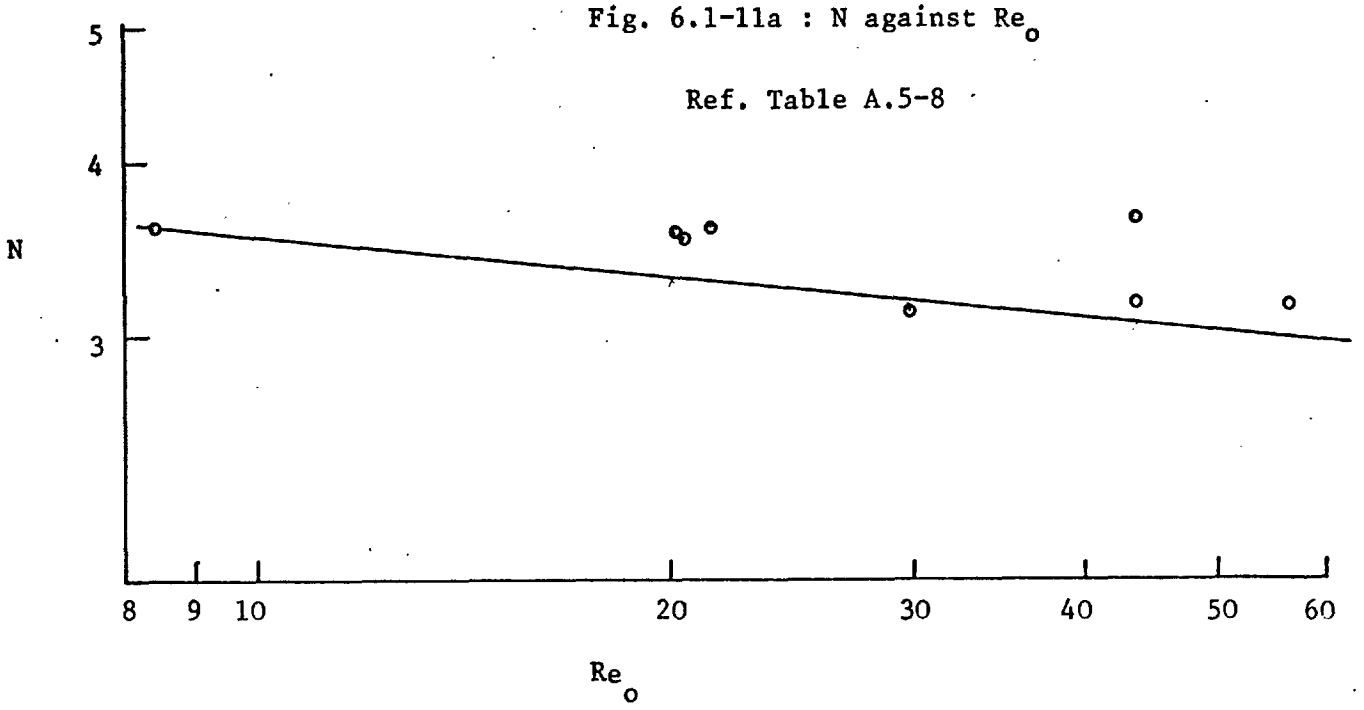

Fig. 6.1-11b : N against Ga

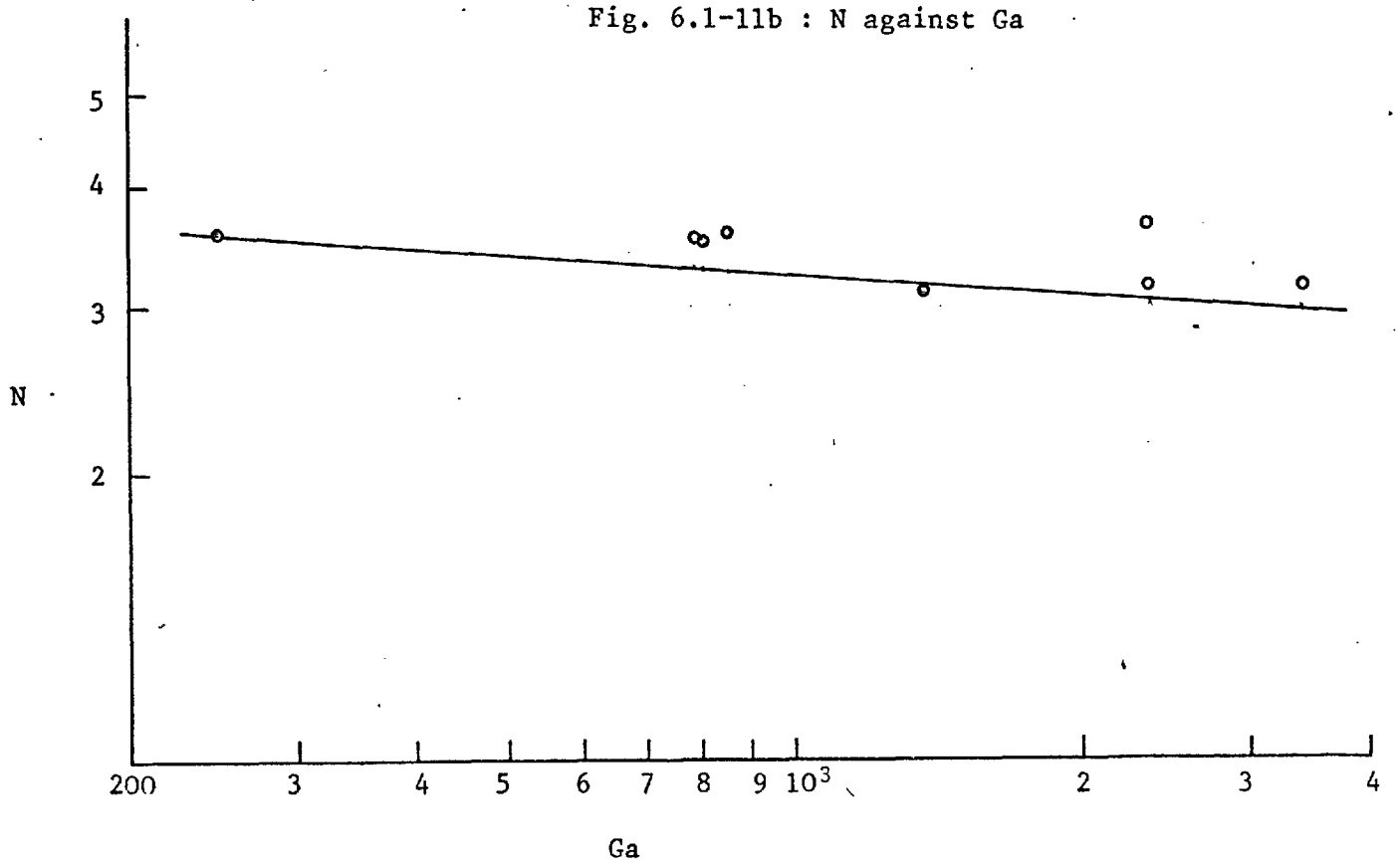

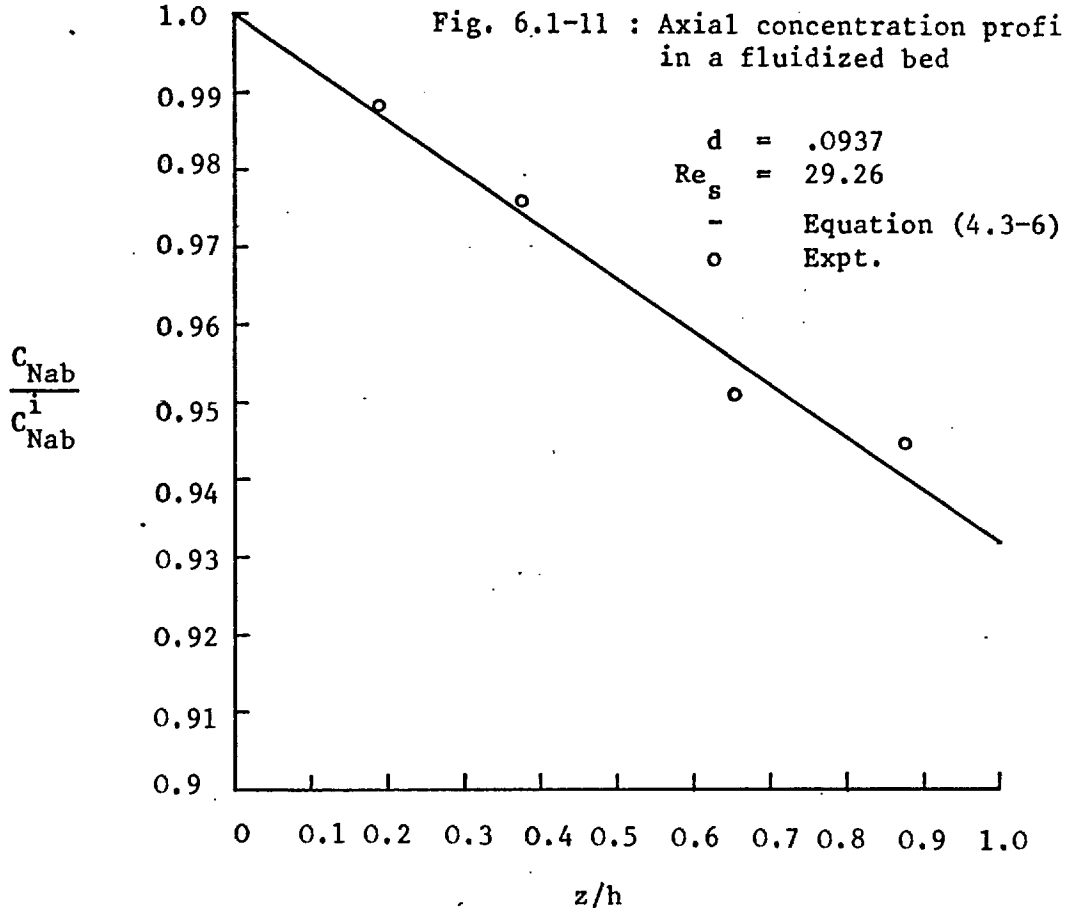

Fig. 6.1-11 : Axial concentration profile in a fluidized bed

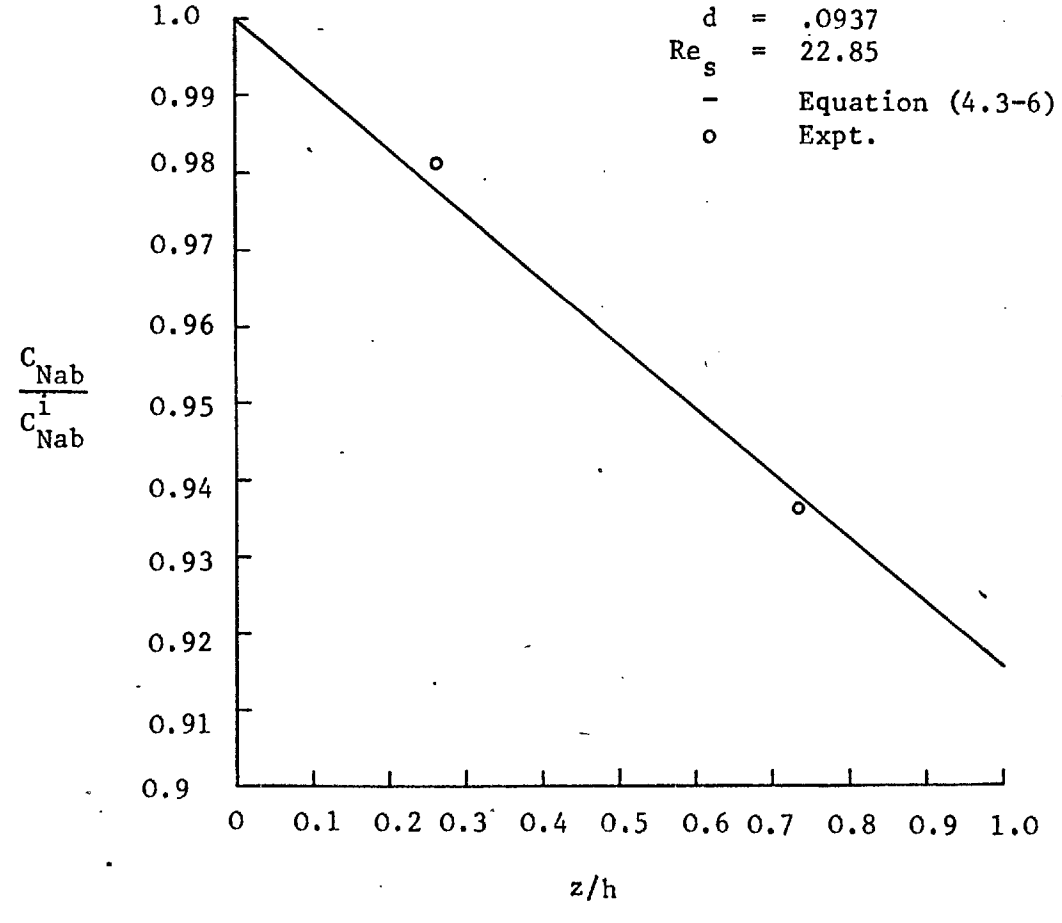

tion suggested for a liquid fluidized bed is;

$$Sh_m = 0.86\ Re_o^{1/2}\left(\frac{Re_s}{Re_o}\right)^q Sc^{1/3} \qquad (6.1\text{-}11a)$$

where $$q = 0.5\ Re_o^{-0.3} \qquad (6.1.11b)$$

The reliability of experimental data may be seen from the j_m against Re_s plots which are plotted on appreciably expanded logarithmic coordinates. Also, the two sets of experiments shown in Fig. 6.1-2a,b are almost identical in every respect except for a slight difference in the volume of particles and were conducted at two different times (more than 3 months apart). The effect of bed height on mass transfer may be seen from Table A.5-5 for which case the experiments were carried out with the bed volume nearly doubled. The value of B_o and q for this case agree well with other data.

Two axial concentration profile measurements are shown in Fig. 6.1-11, which are in agreement with the predicted profile as given by equation (4.3-6). The profiles seem almost linear. This is because the ratio of inlet to outlet concentration is close to unity. However, the data are too few to check the reliability of the measurement.

The value of $B_o = 0.86$ obtained here from fluidized bed data is within the range of values reported for single particle work which has been reviewed in Chapter 2. Note that the symbol B is used in single particle correlations. The theoretical solutions of Ihme et al. (39) and Al-Taha (3) are shown in Fig. 6.1-12. It appears that the former authors predict a value of B about 0.85 whereas the latter author predicts a value of $B = 0.6$ for Re greater than about 50 to 100. The latter study also indicates that for the lower range of Re a correlation of the form suggested in equation (6.1-6) is not suitable, but if

a correlation of this type is sought then B would lie between 0.6 and 0.85. Al-Taha's (3) work is possibly more correct since it predicts a value of about 0.6 for B at a high Reynolds number which is in good agreement with boundary layer theory. Experimentally little data is available in this low range of Re. For $25 < Re < 56$, Chen's (10) benzoic acid solid data and Clinton and Whatley's (12) liquid drop data in the range $5 < Re < 14$ may be corrected using values of B as 0.85 and 0.82 respectively. However Calderbank and Korchinsks' (8) result for heat transfer to mercury drops at $20 < Re < 200$ can be correlated with a value of $B = 0.75$. Also Rowe et al. (67) report a value of $B = 0.74$ for mass and heat transfer studies in the range $20 < Re < 2000$. It is possible that Chen (10) and Clinton and Whatley's (12) values of B are slightly higher. Chen (10) does not report whether he used cast or pressed benzoic acid spheres but it is most likely that he used cast spheres since Chen used the same equipment and methods as reported by Peltzman and Pfeffer (59). The latter authors reported that the use of cast benzoic acid spheres would cause grain dropping and that this apparently increases the physical mass transfer rate due to greater chemical activity of the disordered grain boundaries when compared to the ordered structure of the bulk grain. This random structure of the grain boundaries arises as the crystalline organic material solidifies in a manner quite analogous to metals. Rowe et al. (67), on the other hand, used pressed benzoic acid spheres in their mass transfer experiments which would eliminate any grain dropping phenomenon. The difference in the two liquid drop studies is difficult to explain except to mention that Clinton and Whatley (12), like Calderbank and Korchnisk (8),did not check experimentally if the drops were behaving as true solid spheres, but only assumed so by adding a surfactant, and from the evidence that drops without surfactant had a high initial rate of mass transfer.

Because of the uncertainty as to the correct value of B or B_o for $Re < 100$ some single particle experiments were carried out in this lower range of Re. It was felt that the effect of sphere support and turbulence, could have contributed to the disagreement in other experimental work, though only to a limited degree. To eliminate these effects, the mass transfer experiments were carried out allowing single particles to fall at their terminal settling velocity. The results are shown as j factors against Re_o plotted on a logarithmic coordinate in Fig. 6.1-12. The data lies between the two theoretical predictions but unfortunately, there is some scatter in the data. A mean value of 0.75 for B is suggested. Thus the single particle mass transfer data for $7 < Re_o < 95$ can be expressed by the following equation.

$$Sh_o = 0.75\ Re_o^{1/2}\ Sc^{1/3} \qquad (6.1\text{-}12)$$

The explanation of the scatter in the single particle mass transfer results is probably analytical. It is difficult to obtain uniformity in the preparation of the various sample and standard matrices for the spectro-chemical analysis. In the analysis, it has been assumed that sodium was present in a matrix of $CuSO_4$ which formed the major constituent and that the particle was inert as far as the analysis was concerned. However, this was not so in practice, since in the unknown samples, sodium was present in the particles and in the comparative standards sodium was present as adsorbed Na_2SO_4 in $CuSO_4$ powder and therefore the arcing characteristics of the samples and standards were not necessarily the same. In addition the size of the samples and standards were not the same since the particles were of various sizes and the exact amount of $CuSO_4$ could not always be added for the different determinations due to the error in weighing such small amounts.

Fig. 6.1-12 : single particle results; j against Re

o - Author's experimental values for terminal settling experiments, Ref. Table A.5-9

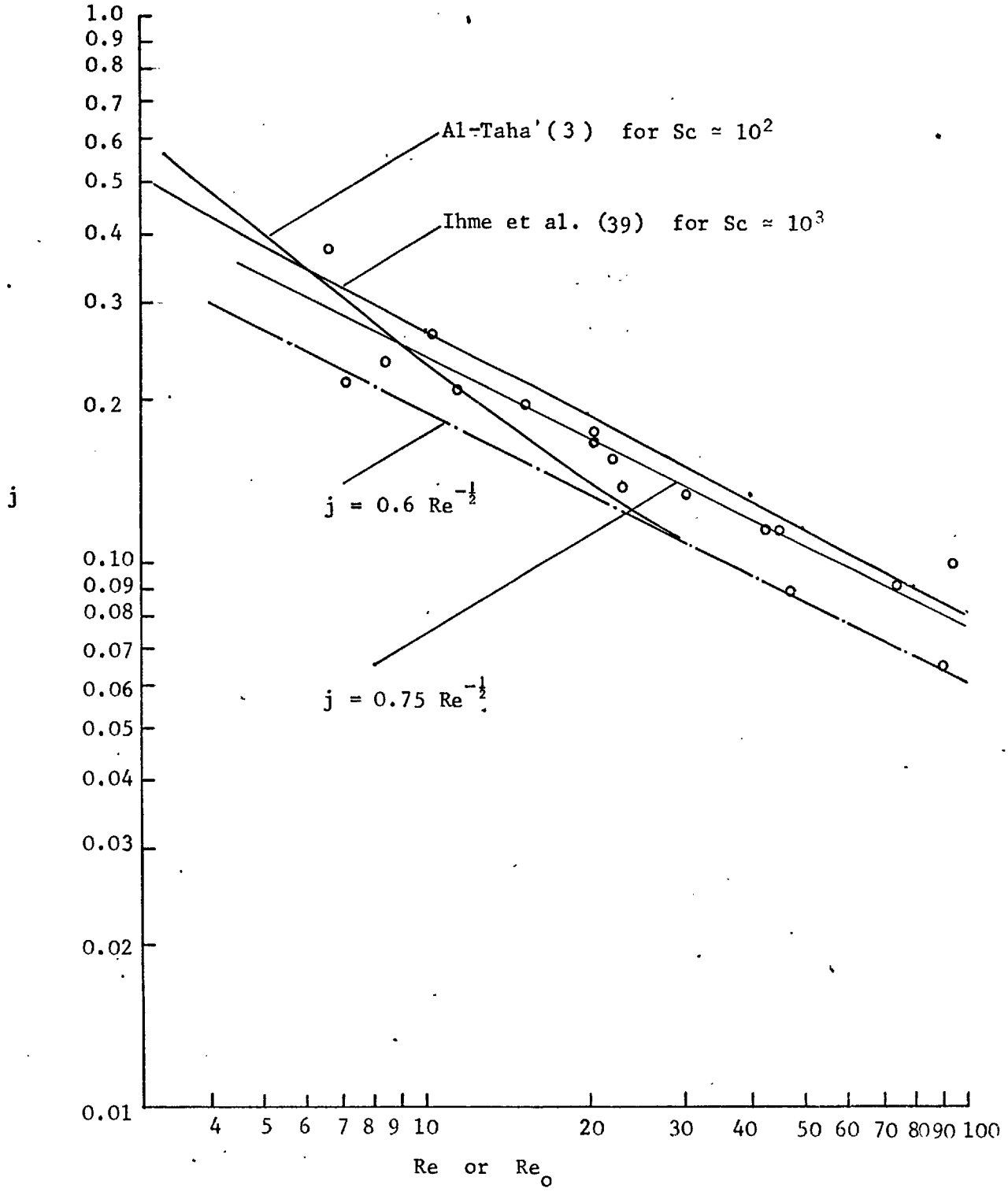

An explanation is now required to account for the difference in the value of B_o (0.86) obtained by extrapolating fluidized bed data and the value (0.75) obtained in single particle work, since intuitively they should be the same. It is possible that the value of B_o obtained from fluidized bed data is increased due to turbulence.

Galloway and Sage (23,24) have reviewed the available information concerning the effect of free stream turbulence on mass and heat transfer rates from single spheres. It is known that the intensity of the free stream turbulence markedly influences the transfer rates in the forward region of a sphere. The above authors found that this effect could be conveniently represented by the use of a Frossling number, defined as

$$Fs = \frac{Sh - 2}{Re^{1/2}\, Sc^{1/3}} \qquad (6.1\text{-}13)$$

Galloway and Sage (23,24) suggested that the local and overall Frossling numbers are linearly related to the square root of the Reynolds number and that the slope increases with increasing turbulence. Based on theoretical considerations and experimental data, they suggested an empirical representation of the Frossling number which would take into account the effect of turbulence in the boundary layer and in the wake and additionally the variation of physical properties through the boundary layer. For negligible variation of physical properties of the fluid through the boundary layer and negligible effect of turbulence on the wake transfer, i.e. for the effect of free stream turbulence on the laminar boundary layer they suggest the following equation for the Frossling number:

$$Fs = E_1 + E_2\alpha' \,(\alpha' + E_3)\, Re^{1/2} Sc^{1/6} \qquad (6.1\text{-}4)$$

where E_1, E_2 and E_3 are constants and α' the intensity of turbulence defined as $\sqrt{\overline{v'^2_z}}/\, U$ where $\overline{v}'_z$ is the time averaged longitudinal fluctuating velocity.

From the analysis of 436 data points for mass transfer these authors recommend the following values:

$$E_1 \simeq 0.55$$

$$E_2 \simeq 0.1$$

$$E_3 \simeq 0.0004$$

Galloway and Sage (24), in the analysis of data covered a range $2 < Re < 483{,}000$ but most of the data was for $Re > 100$. For $\alpha' = 0$, $Fs = E_1 = 0.55$ i.e. the value of B_1 of equation (2.2-1) suggested by Frossling (21). In other words Galloway and Sage recommend equation (2.2-1) for correlating mass transfer data for single spheres. It has been discussed earlier that a more appropriate correlation for single particles would be equation (2.2-17). For Re less than 100 a value of $B_o = B = 0.75$ is recommended for use in equation (2.2-17) as a result of this work. The term B should have the same significance as that of the term E_1 in equation (6.1-14) and therefore the following values of the constants have been chosen:

$$E_1 \simeq 0.75$$

$$E_2 \simeq 0.1$$

$$E_3 \simeq 0.0004$$

This assumes that the magnitude of E_2 and E_3 remains of the same order for $Re < 100$. Recognising that the value of the Frossling number is approximately equal to the value of B_o obtained from fluidized bed work one obtains (equation (6.1-14))

$$0.86 = 0.75 + E_2\alpha' (\alpha + E_3) Re_o^{1/2} Sc^{1/6}$$

$$= 0.75 + 0.1\ \alpha'^2\ Re_o^{1/2}\ Sc^{1/6}$$

since $E_3 \simeq 0.0004 \simeq 0$

Taking a set of values, i.e. $Re_o = 50$, $Sc = 400$ we have

$$\alpha' = \sqrt{\frac{0.11}{0.1 \times 7.1 \times 2.72}} \simeq 0.24$$

The origin of "turbulence" may be attributed to several factors. As flow proceeds in a multiparticle bed, the flow may be divided into several streams which may recombine later depending on the presence of neighbouring particles so that the flow consists of a sequence of "jets" and "wakes". This process of jet division, recombination with associated mixing in the wakes as a result of "side stepping" can give rise to a form of turbulence. The "intensity" of such turbulence is related to the mixing length of the process and is intimately related to the mean flow, particle size, shape and geometry of arrangement. For this reason the turbulence intensity based on this concept has no obvious relationship to the root mean square fluctuating velocity component. The second mode of turbulence may be due to adverse local pressure gradients that can cause boundary layer separation and shedding of vortices. The third may be due to the presence of the distributor.

Galloway and Sage (25) believe that the turbulence due to mixing of fluid streams may interact with the boundary layer flow on the particles in much the same way as free stream turbulence perturbs the laminar boundary layer flows with an enhancement of the transport rate on bluff bodies in a wind tunnel. These authors proposed a model for heat and mass transport in multiparticle systems (25) and evaluated the turbulent intensity using expressions for the Frossling number discussed earlier. In the analysis, the authors assumed the existence of stagnant zones occupied by boundary flow wakes or other relatively stagnant regions and this was taken into account by estimating a pseudo voidage similar to that employed by Kusik and Happel (47). Gaolloway and Sage (25) showed that the turbulent intensities in a fluidized bed gradually increased with

voidage, attained a maximum at voidage about 0.70 and then decreased to the limiting turbulence level of a single particle in an infinite medium. This was expected, since the "stagnant void fraction" showed a maxima with voidage. The average level of the intensity of turbulence as obtained by these authors is about 0.25 for a voidage upto about 0.9. However, their model would not be very suitable at low Reynolds number since the volume of wakes would be quite small. In the present experiments, the effect of "jetting" of streams is also expected to be small since the bed is shallow and in fact the mechanism is more important in fixed beds. It seems that the sintered distributor is possibly responsible for an increased level of turbulence in the present experiments. As the height of the bed was small, it is possible that the turbulence generated by the flow distributor could not decay appreciably. Kricher and Mosberger (44) reported a 30% increase in mass transfer rate in a fluidized bed due to turbulence caused by the distributor plate. Here, an increase of about 11% is thought to occur. Possibly, a convenient method of quantifying this effect would be to measure the pressure drop across the distributor, ~~since this is a measure of the energy dissipation.~~ This factor is also likely to be responsible for the difference in mass transfer measurements of various other authors, since no consideration to the type of distributor is made or reported when comparing data.

Although equations (6.1-11a and b) correlate mass transfer data well in a liquid fluidized bed, they are not useful for fixed and distended beds since the exponent q and Re_o have no meaning in that context. In Chapter 4 a semi-theoretical correlation has been proposed which is sufficiently general to be applicable to any multiparticle assembly. This is expressed by equation (4.2-5) where the coefficient G_4 remains to be determined. The validity of this model lies in the fact that G_4 should

be a constant for any multiparticle assembly and numerically equal to the constant B_o since for a voidage of unity equation (4.2-5) reduces to the case for a single particle. The present fluidized bed mass transfer data are utilised to test this model. Equation (4.2-5) can be written as

$$j'_m = j_m \varepsilon = \frac{Sh_m \, \varepsilon}{Re_s \, Sc^{1/3}} = G_4 \, Re_s^{-\frac{1}{2}} \qquad (6.1\text{-}15)$$

In Fig. 6.1-13 to 6.1-16 j'_m are plotted against Re_s. The solid lines are a least square fit of the data and each line is extrapolated to the corresponding Re_o for easy identification. Fig. 6.1-13 shows the j'_m factor data points for all experimental observations calculated using the measured value of the voidage ε. Fig. 6.1-14 shows the same j'_m factors as smooth correlations for $Re_s/Re_o > 1/6$ i.e. for the case when the different beds are assumed to have a random arrangement of particles. Both these figures show appreciable scatter amongst data for different Re_o cases and no single equation would correlate the different data adequately. It has been mentioned earlier that the voidage measurement in the present experiments is not entirely satisfactory and since $j'_m = j_m \varepsilon$, it is possible that uncertainty in the voidage is responsible for the above failure. Hence, voidage was calculated using the well established Richardson-Zaki correlation (64) and j'_m factors recalculated. This is shown in Fig. 6.1-15 and 16. In Fig. 6.1-15 the data over the entire range of voidage has been correlated and in Fig. 6.1-16 the lower voidage data i.e. for $Re_s/Re_o < 1/6$ has been neglected in the correlations. It may be seen from these two figures that the scatter in the data is greatly reduced when compared to the previous case where measured values of voidages were used to calculate j'_m factors. Minimum scatter occurs in Fig. 6.1-16 except for the spurious case already discussed ($Re_o = 20.09$).

Fig. 6.1-13 : j_m' against Re_s

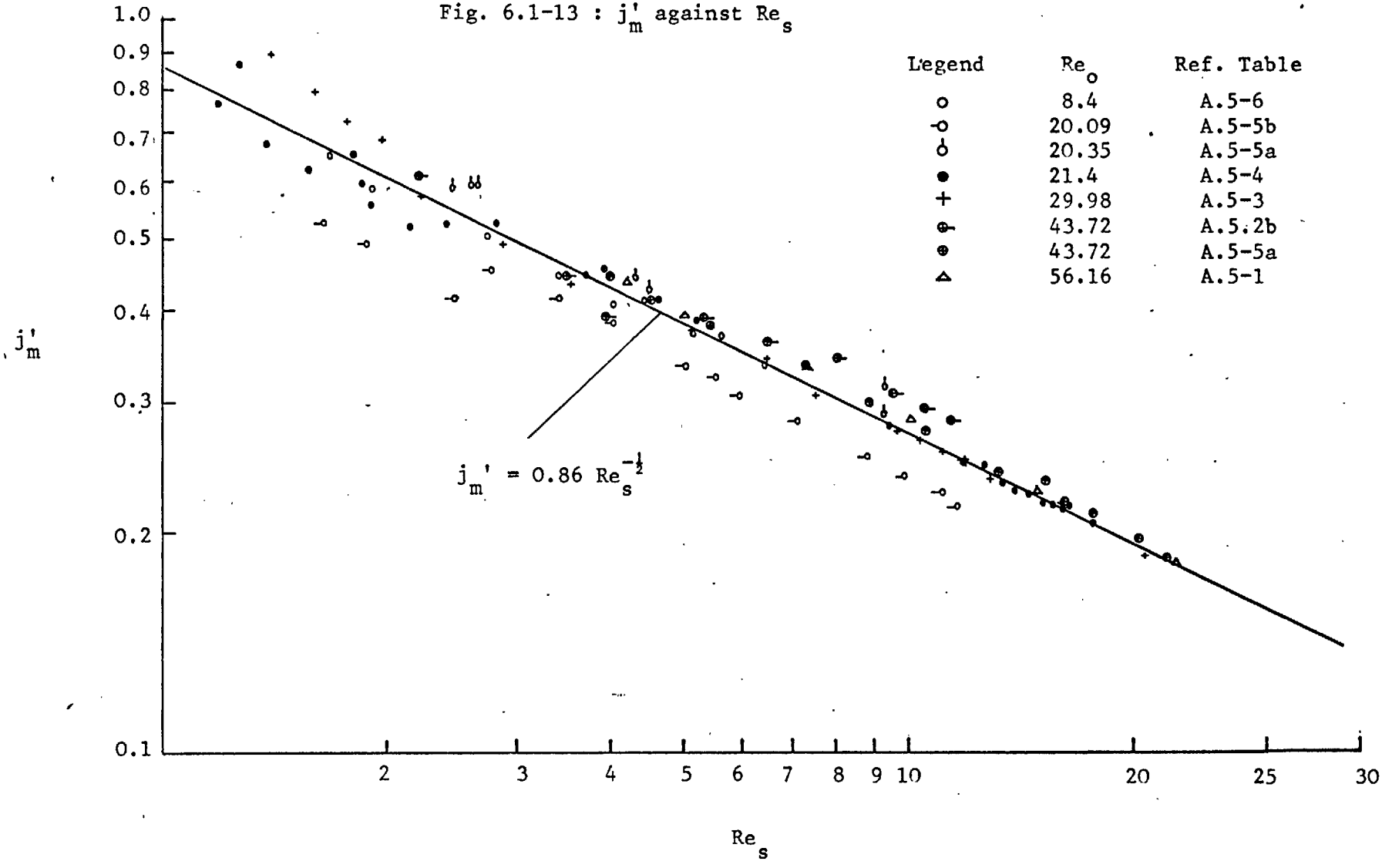

Fig. 6.1-14 : j'_m against Re_s

Correlated lines for data points $Re_s/Re_o > 1/6$ using experimental voidage

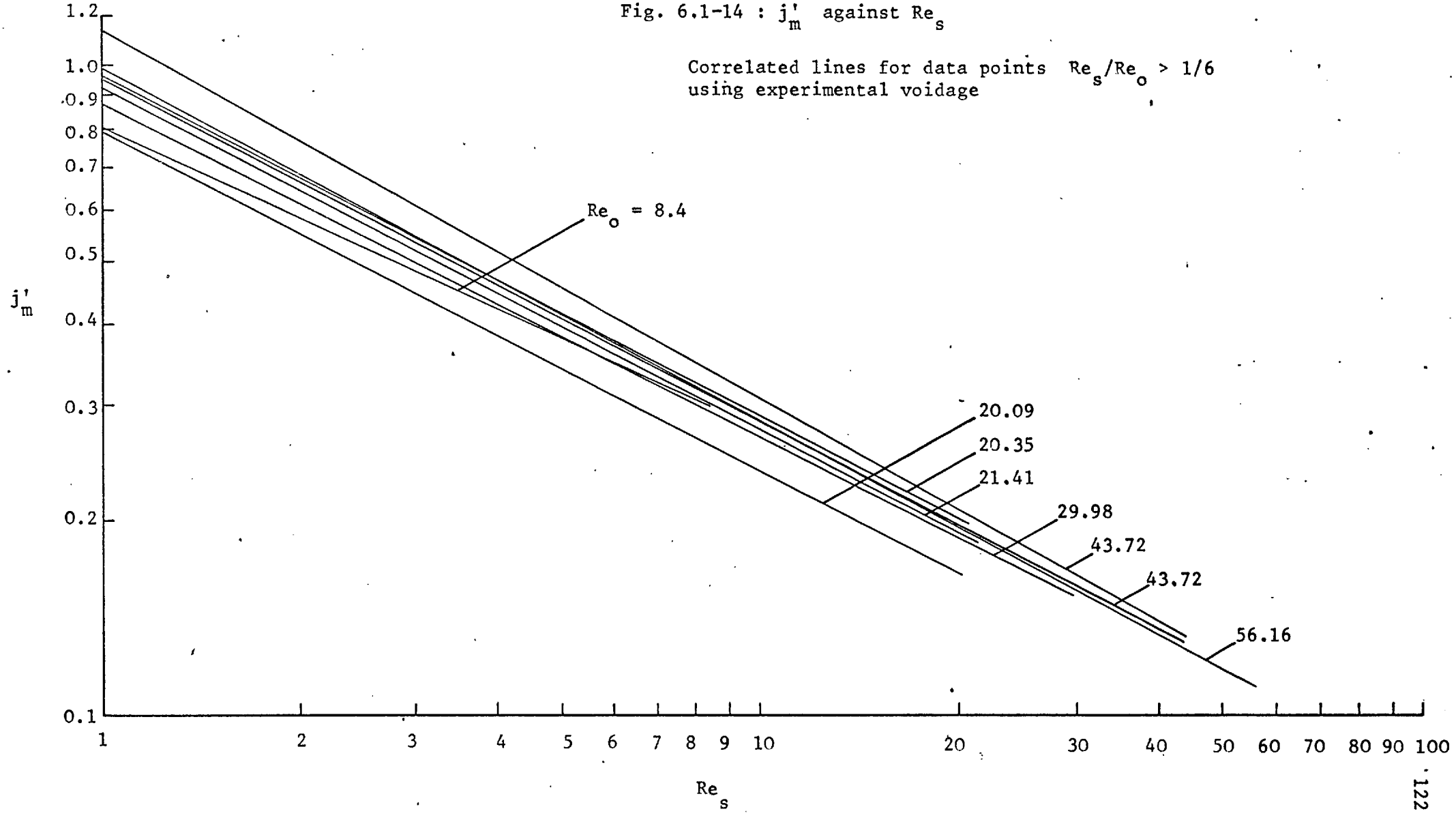

Fig. 6.1-15 : j_m' against Re_s

Correlated lines for data points using predicted value of voidage from Richardson-Zaki equation.

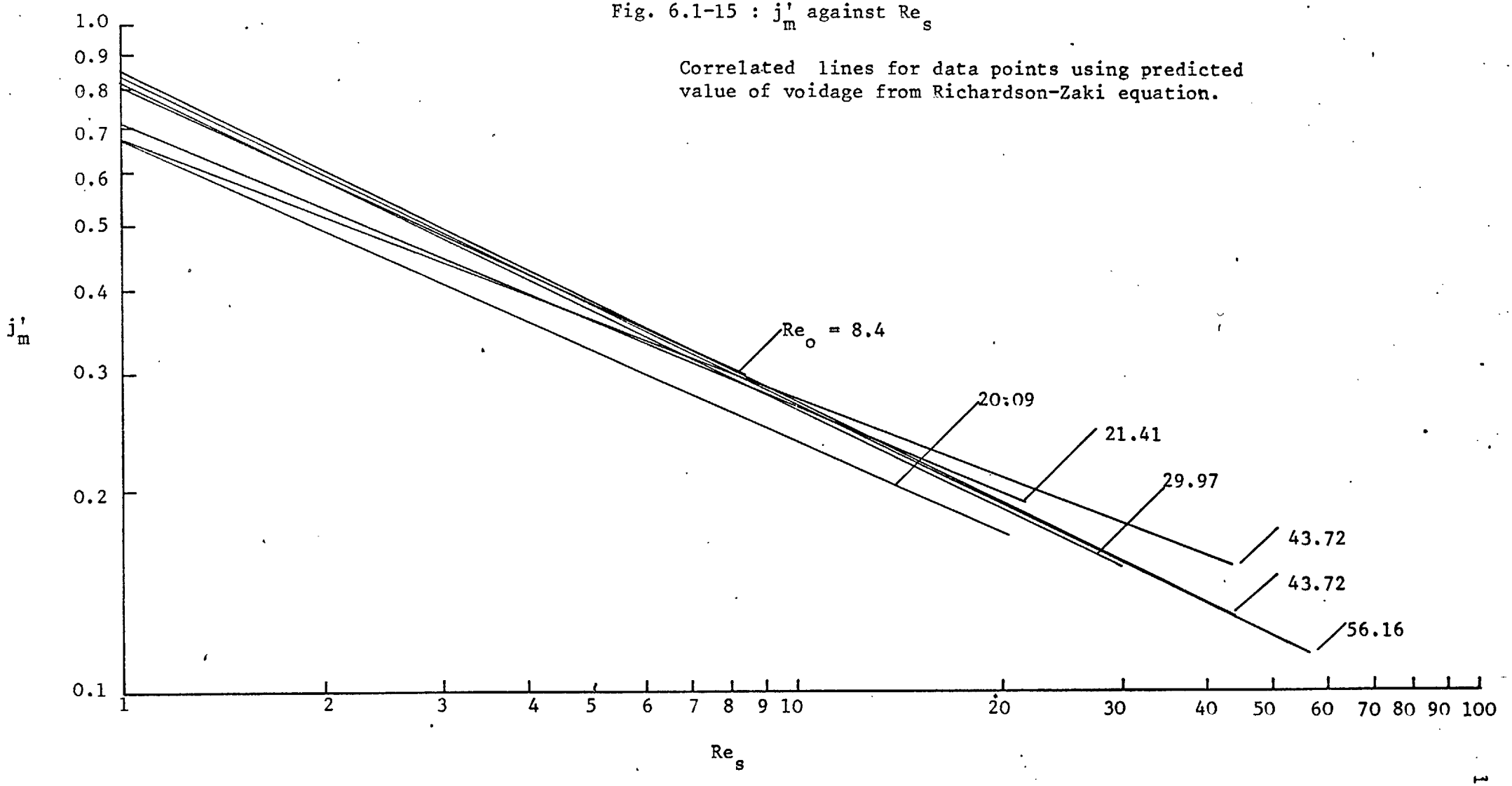

Fig. 6-16 : j'_m against Re_s

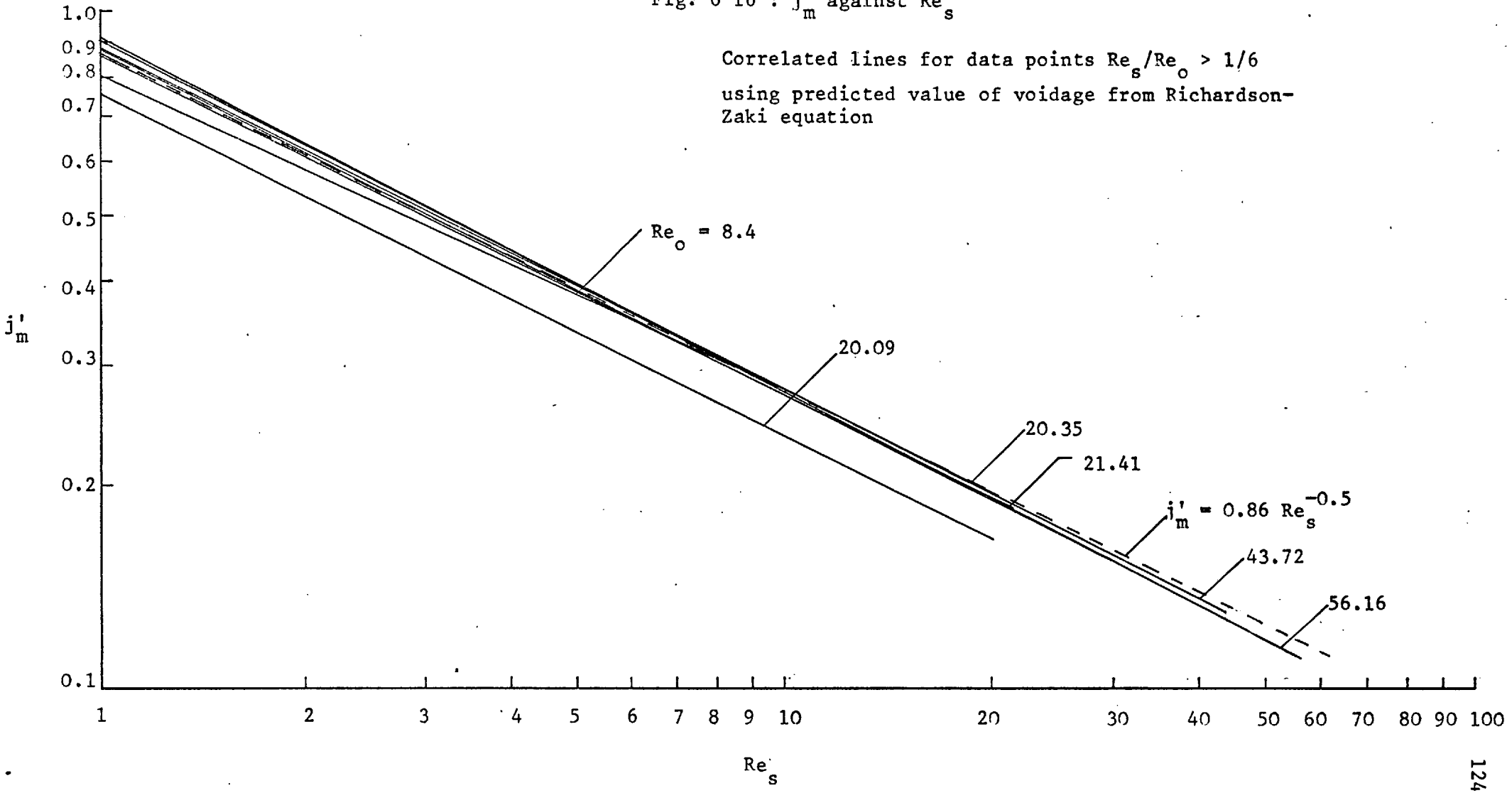

In Fig. 6.1-16 equation (6.1-15) with G_4 taken equal to $B_o = 0.86$ is shown as a dotted line and this may be considered as an adequate expression for mass transfer in multiparticle system. The expression is

$$Sh_m = \frac{0.86}{\epsilon} Re_s^{1/2} Sc^{1/3} \qquad (6.1\text{-}16)$$

This equation is in close agreement with that of Snowdon and Turner (72) who report a value of 0.81 for the constant in the equation.

Equation (6.1-11a) may be directly compared with the above equation by eliminating Re_o from the former using the Richardson-Zaki correlation which takes the form

$$Sh_m = 0.86\ \epsilon^{N(q-0.5)} Re_s^{1/2} Sc^{1/3} \qquad (6.1\text{-}17)$$

Thus when $N(q-0.5) = -1$ the above equation agrees with equation (6.1-16). From Table A.5-8 or using the appropriate correlation the following values may be written:

Re_o	N	q	N(q-0.5)
8.4	3.6	0.26	-1.008
56.16	3.29	0.19	-1.02
500	2.39	0.07	-1.03

The value of $N(q-0.5)$ may be taken as -1.0 so that both equations (6.1-11) and (6.1-16) are equivalent in a fluidized bed and that $Sh_m \propto \epsilon^{-1}$. The latter conclusion is directly reached from boundary layer theory.

A comparison of equation (6.1-16) with the data available in the literature is shown in Fig. 6.1-17 taken from Beek's paper (6). The present correlation is possibly a slight improvement on the correlation proposed by Snowdon and Turner (72). A further comparison is shown in Fig. 6.1-18. Also shown in this Figure is the result for free surface model for $\epsilon = 0.85$ obtained by Leclair and Hamielec (49) and given by

Fig. 6.1-17 : j'_m against Re_s

Reproduced from reference (6)

Legend	Reference
■□	Chu, Kalil and Wetteroth (11)
+	McCune and Wilhelm (53)
▼▽	Snowdon and Turner (72)
×	Thodos, Hongen and Gamson (79)
◇	Thodos and Recetti (80)
o	Thodos and Petrovic (81)

Closed symbols, + and x : packed beds
Open symbols : fluidized beds

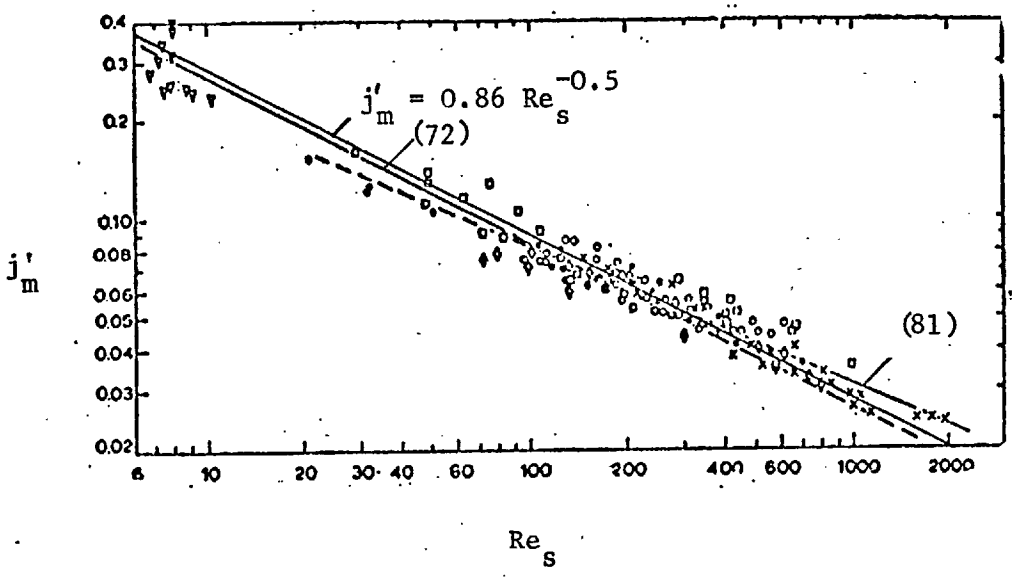

Fig. 6.1-18 : j'_m against Re_s

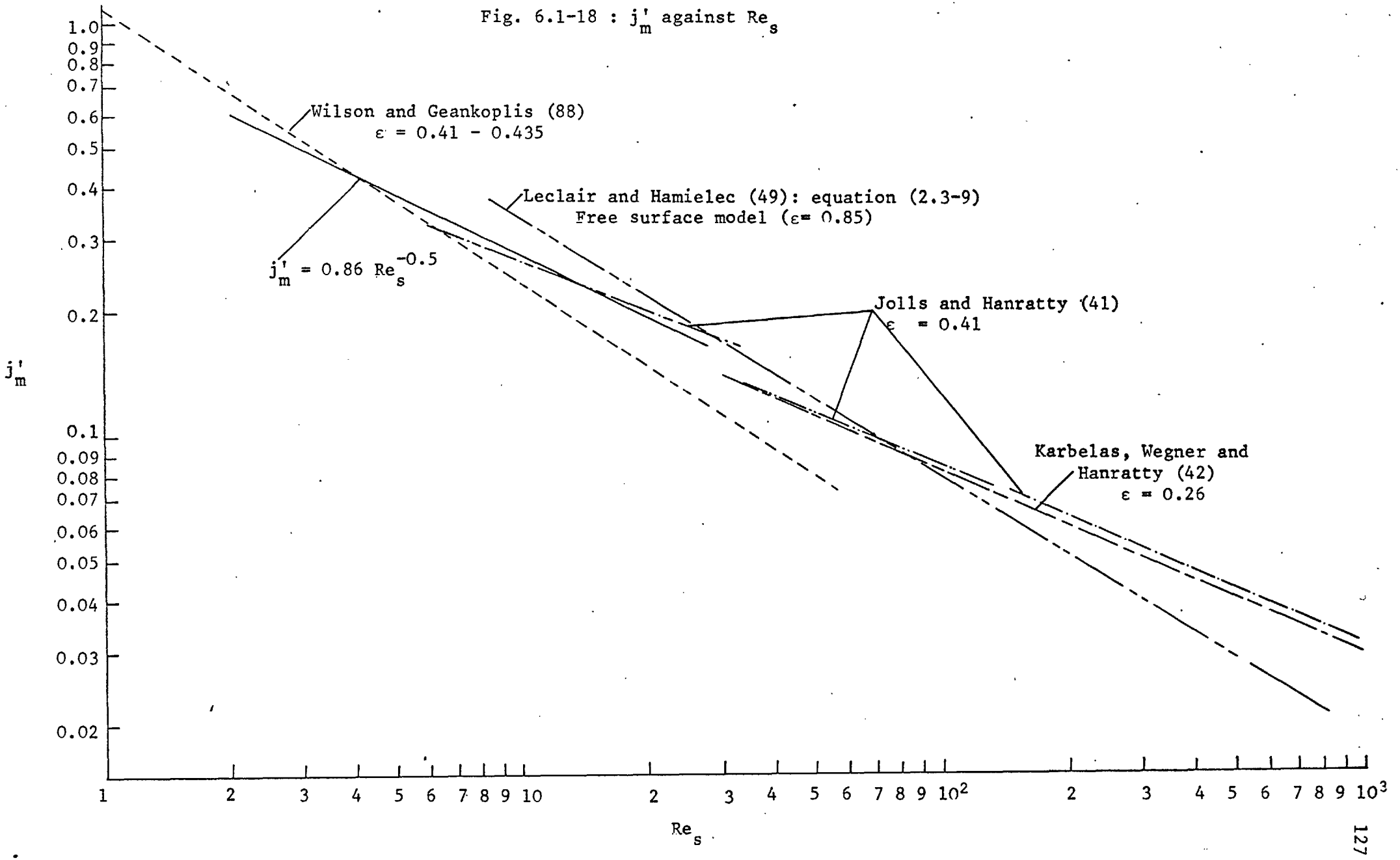

equation (2.3-9). As expected the free surface model shows a positive deviation at low Re_s and a negative deviation at high Re_s. This trend in the deviation of the free surface model from experimental data is similar to that observed by Leclair and Hamielec (48) in the drag comparison. The fluidized bed data of Couderc et al. (14) are not available in tabular form for comparison. Their proposed correlation predicts $Sh_m \propto \varepsilon^{-2} Re_s$; however their bed expansion data possibly may be represented by $\varepsilon \propto Re_s^{0.5}$ so that Couderc et al.'s (14) correlation could also be expressed as $Sh_m \propto \varepsilon^{-1} Re_s^{0.5}$.

It would be interesting to find out why the data in a fixed, distended and fluidized bed may be represented by a single equation although the physical character of the fluidized bed is quite different from the former types of bed. In a fluidized bed, the voidage may fluctuate and the particles are moving. The boundary layer model that describes the flow in any multiparticle assembly does not take into account any such affects; it only considers that the length of the boundary layer is proportional to the product of voidage and diameter and thus one would expect that the form of the correlation may be the same but that the coefficient G_4 of equation (4.2-5) would be different for fixed or distended and fluidized beds.

Assume that equation (4.2-5) is valid for fixed or distended beds with no variation of the filtration velocity with respect to the particle and no local variation of voidage, then $\overline{K}_c$ may be written as

$$\overline{K}_c \propto \frac{U_s^{0.5}}{\varepsilon} \qquad (6.1\text{-}18)$$

where U_S is the superficial or the filtration velocity and this is the same whether with respect to the particles in the bed or an observer fixed in space.

In a fluidized bed, the particles are moving up and down in the bed, so that the settling velocity of a particle at any instant could be expressed as an average velocity which is the superficial velocity and a small upward or downward velocity of the particles. Also the voidage of the bed may similarly be represented by an average voidage and a small deviation from the mean. Thus in a fluidized bed

$$U_s = \overline{U}_s + \Delta U_s$$
$$\varepsilon = \overline{\varepsilon} + \Delta\varepsilon$$

where U_s is the settling velocity of a particle and ε is a local voidage and ΔU_s and $\Delta\varepsilon$ are small deviations from the mean value and bar denotes an average value.

Now let equation (6.1-18) which is assumed to be valid for a fixed or distended bed be perturbed by a small amount in the variables U_s and ε so that the deviations are small compared to the mean value. It is assumed that these deviations are of the same order in a fluidized bed. Then one can expand the variables around the mean values approximately as follows:

$$U_s^{0.5} = \overline{U}_s^{0.5} + \frac{0.5}{\overline{U}_s^{.5}} \Delta U_s - \frac{0.25}{2} \frac{(\Delta U_s)^2}{\overline{U}_s^{1.5}} + \text{smaller terms}$$

$$\therefore \overline{U_s^{0.5}} = \overline{U}_s^{0.5} - \frac{0.25}{2} \frac{\overline{(\Delta U_s)^2}}{\overline{U}_s^{1.5}} \quad \text{since } \overline{\Delta U_s} = 0$$

$$\text{or} \quad \overline{U_s^{0.5}} = \overline{U}_s^{0.5} \left[1 - \frac{0.25}{2} \overline{\left(\frac{\Delta U_s}{\overline{U}_s} \right)^2} \right] \qquad (6.1\text{-}19)$$

Similarly

$$\varepsilon^{-1} = \overline{\varepsilon}^{-1} - \overline{\varepsilon}^{-2} \Delta\varepsilon + \overline{\varepsilon}^{-3} (\Delta\varepsilon)^2 + \text{smaller terms}$$

$$\therefore \overline{\varepsilon^{-1}} = \overline{\varepsilon}^{-1} + \overline{\varepsilon}^{-3} \overline{(\Delta\varepsilon)^2} \quad \text{since } \overline{\Delta\varepsilon} = 0$$

$$\text{or} \quad \overline{\varepsilon^{-1}} = \bar{\varepsilon}^{-1}\left[1 + \overline{\left(\frac{\Delta\varepsilon}{\bar{\varepsilon}}\right)^2}\right] \tag{6.1-20}$$

Then the average value of the mass transfer coefficient can be written from equation (6.1-19) and (6.1-20) as

$$\overline{K_c} = \frac{\bar{U}_s^{0.5}}{\bar{\varepsilon}}\left[1 - \frac{0.25}{2}\overline{\left(\frac{\Delta U_s}{\bar{U}_s}\right)^2}\right]\left[1 + \overline{\left(\frac{\Delta\varepsilon}{\bar{\varepsilon}}\right)^2}\right] \tag{6.1-21}$$

The first term in the brackets is less than unity and the second term more than unity, i.e. the particle motion tends to lower the mass transfer coefficient and this is offset by a fluctuation in voidage and assuming that the order of these fluctuations are the same, then they would cancel each other out. This means that the combined effect of movement of particles and voidage fluctuations does not effect equation (6.1-18). This may explain why the same equation applies in fixed, distended and fluidized beds.

6.2. Solution of the forced convective diffusion equation

Equation (4.1-14) shows $\bar{K}_v$ varies with flow rate in a manner similar to other solid-fluid systems having constant diffusivity except for the appearance of the term F. For example, for creeping flow (equation (2.2-8))

$$\psi = -\frac{1}{2} U \sin^2\theta \left[r^2 - \frac{3}{2} Rr + \frac{R^3}{2r}\right]$$

$$\therefore \quad \psi_o'' = -\frac{3}{2} U \sin^2\theta$$

and substitution of this value in the integral in equation (4.1-14) yields

$$\int_o^{\pi} \sqrt{\frac{3}{2} U \sin^2\theta}\, d\theta = \sqrt{\frac{3}{2} U}\,\frac{\pi}{2}$$

and the expression for $\overline{K}_v$ is

$$\overline{K}_v = 1.31 \left(\frac{3}{2}\right)^{1/3} \left(\frac{\pi}{2}\right)^{2/3} F \left(\frac{D_{AS}}{d}\right)^{2/3} U^{1/3}$$

$$= 2.03 \, F \left(\frac{D_{AS}}{d}\right)^{2/3} U^{1/3}$$

When $y_{AR} \to y_{Ab} \to 0$, from equation (4.1-13) $F \to (1/12)^{1/3}$ and

$$\overline{K}_v = 0.89 \left(\frac{D_{AS}}{d}\right)^{2/3} U^{1/3}$$

In the limit when $y_{AR} \to y_{Ab} \to 0$, the controlling diffusivity is D_{AS}, i.e. as if only species 'A' is present. This limiting value is comparable with a constant diffusivity case. Friedlander (18) has also reported a value of 0.89 for the above coefficient for a constant diffusivity case using a somewhat similar concentration profile and this possibly gives added confidence to the solution obtained. Equation (4.1-14) would also predict the square root dependence of mass transfer on velocity at high flow rate.

It is difficult to say whether this solution predicts the correct dependence of the mass transfer coefficient on concentration. Snowdon and Turner (73) showed that for the limiting cases

$$y_{AR} \to y_{Ab} \to 0 \qquad \text{and} \qquad y_{AR} \to y_{Ab} \to 1,$$

the mass transfer coefficient would vary by a factor of $(\alpha+1)^{2/3}$. Though their (73) solution is based on a "stagnant film" type analysis their prediction seems reasonable. This may follow from the following argument.

The diffusional flux may be written using equation (A.3-29) as follows:

For $y_{AR} \to y_{Ab} \to 0$

$$J_A^*\Big|_{x=0} = - C_{Cb} D_{AS} \left(\frac{dy_A}{dx}\right)_{\substack{x=0 \\ y_{AR} \to y_{Ab} \to 0}} = K_v(\theta)\, C_{Cb}(y_{AR} - y_{Ab})$$

and $y_{AR} \to y_{Ab} \to 1$

$$J_A^*\Big|_{x=0} = - C_{Cb} D_{\theta s} \left(\frac{dy_A}{dx}\right)_{\substack{x=0 \\ y_{AR} \to y_{Ab} \to 1}} = K_v(\theta)\, C_{Cb}(y_{AR} - y_{Ab})$$

Now drawing an analogy with single particle mass transfer studies at constant diffusivity, it is probable that the mass transfer coefficient would differ by a factor $(\frac{D_{AS}}{D_{BS}})^{2/3} = (\alpha+1)^{2/3}$ for the two limiting cases. In the present analysis this ratio is $\frac{2^{1/3}(\alpha+1)}{(\alpha+2)^{1/3}}$. The former conclusion is rather intuitive and until an exact solution is available any further comment would be premature.

BIBLIOGRAPHY

1. Acrivos, A., and Taylor, T.D., Phys. Fluids. 5, 387, 1962.
2. Anderson, T.B., and Jackson, R., Ind. Eng. Chem. Fundamentals 6, 527, 1967.
3. Al-Taha, Taha Rasool, Ph.D. Thesis, 1970, London University, London.
4. Baird, M.H.I., and Hamielec, A.E., Can. J. Chem. Eng. 40, 119, 1962.
5. Barker, J.J., Ind. Eng. Chem. (a) 57, no.4, 43, 1965. (b) 57, no.5, 33, 1965.
6. Beek, W.J., Proc. Int. Symp. Fluidization, June 6-9, 1967, p 507, Eindhoven, Ed. Drinkenburg, A.A.H., Netherlands University Press, Amsterdam, 1967.
7. Bird, R.B., Stewart, W.E., and Lightfoot, E.S., Transport Phenomena, (a) p 554, (b) p (702), (c) (563), John Wiley and Sons Inc. London, 1965.
8. Calderbank, P.H., and Korchinsk, I.J.O., Chem. Eng. Sci. 6, 65, 1956.
9. Carberry, J.J., A.I.Ch.E.J. 6, 460, 1960.
10. Chen, Wu-Chi, Ph.D. Thesis, City University of New York, U.S.A., 1969.
11. Chu, J.C., Kalil, J., and Wetteroth, W.A., Chem. Eng. Prog. 49, 141, 1953.
12. Clinton, S.D., and Whatley, M.E., A.I.Ch.E.J. 18, 486, 1972.
13. Cornish, A.R.H., Trans. Inst. Chem. Engrs. 43, T332, 1965.
14. Couderc, J.P., Gibert, H., and Angelino, H., Chem. Eng. Sci. 27, 11, 1972.
15. Couderc, J.P., Gibert, H., and Angelino, H., ibid, 27, 45, 1972.
16. Duncan, A.M., The Principles of Electrochemistry, Reinhold Publishing Corporation N.Y. , 1939, Third Print 1950.

17. Evans, G.C., and Gerald, C.F., Chem. Eng. Prog. 49, 135, 1953.

18. Friedlander, S.K., A.I.Ch.E.J. 3, 43, 1957.

19. Friedlander, S.K., ibid 7, 347, 1961.

20. Frossling, N., NACA, T.M. 1432, 1958.

21. Frossling, N., Ferlands Beiträge zur Geophysik, 52, 170, 1938, English Translation: Fforde, K., U.K.A.E.A. Research Group, Harwell, 1963.

22. Gaffney, B.W., and Drew, T.B., Ind. Eng. Chem. 42, 1120, 1950.

23. Galloway, T.R., and Sage, B.H., Int. J. Heat Mass Transfer, 10, 1195, 1967.

24. Galloway, T.R., and Sage, B.H., ibid, 11, 539, 1968.

25. Galloway, T.R., and Sage, B.H., Chem. Eng. Sci. 25, 495, 1970.

26. Garner, F.H., and Grafton, R.W., Proc. Roy. Soc. A224, 64, 1954.

27. Garner, F.H., and Keey, R.B., Chem. Eng. Sci. 9, 119, 1958.

28. Garner, F.H., and Suckling, R.D., A.I.Ch.E.J. 4, 114, 1958.

29. Gillespie, B.M., Crandall, E.D., and Carberry, J.J., A.I.Ch.E.J. 14, 483, 1968.

30. Gelperin, N.I., and Einstein, V.G., Fluidization, p 471 Ed. Davidson, J.F., and Harrison, D., Academic Press, London, 1971.

31. Godard, K., and Richardson, J.F., Chem. Eng. Sci. 24, 363, 1969.

32. Grafton, R.W., Chem. Eng. Sci. 18, 457, 1963.

33. Gunn, D.J., Malik, A.A., Trans. Instn. Chem. Engrs. 44, T371, 1966.

34. Happel, J., A.I.Ch.J. 4, 197, 1958.

35. Happel, J., and Brenner, H., Low Reynolds Number Hydrodynamics, Prentice-Hall Inc., Englewood Cliffs, N.J., 1965.

36. Hasimoto, H., J.F. Mech. 5, 317, 1959.

37. Helfferich, F., Ion Exchange, (a) p 274, (b) p 267, (c) p (134), McGraw-Hill, London 1962.

38. Hughmark, G.A., A.I.Ch.E.J. 18, 1020, 1972.

39. Ihme, F., Schmidt-Traub, H., and Brauer, H., Chemie-Ing-Techn. 44, 306, 1972.

40. Jolls, K.R., and Hanratty, T.J., Chem. Eng. Sci. 21, 1185, 1966.

41. Jolls, K.R., and Hanratty, T.J., A.I.Ch.E.J. 15, 199, 1969.

42. Karabelas, A.J., Wegner, T.H., and Hanratty, T.T., Chem. Eng. Sci. 26, 1581, 1971.

43. Kataoka, T., Yoshida, H., and Ueyama, K., J. Chem. Eng. Japan, 5, 132, 1972.

44. Krischer, O., Mosberger, E., Proc. 2nd All-Soviet Conf. on Heat Mass Transfer, Ed. Gazley Jr. C., Hartnett, J.P., and Eckert, E.R.G. Rand report R-451-Pr. University Microfilms Library Services, 1967, vol V, p 97.

45. Kronig, R., and Bruijsten, J., Appl. Sci. Res. Sect A, 2, 439, 1951.

46. Kuni, D., and Suzuki, M., Int. J. Heat Mass Transfer, 10, 845, 1967.

47. Kusik, C.L.,and Happel, J., Ind. Eng. Chem. Fundamentals, 1, 163, 1962.

48. Leclair, B.P., and Hamielec, A.E., Ind. Eng. Chem. Fundamentals, 7, 542, 1968.

49. Leclair, B.P., Hamielec, A.E., I. Chem. E. Symp. Series No 30, p 197, 1968 (Instn. Chem. Engrs. London).

50. Levich, V.G., Physicochemical Hydrodynamics, p 80, Prentice-Hall Inc., Englewood Cliffs, N.J. 1962.

51. Linton, M., and Sutherland, K.L., Chem. Eng. Sci. 12, 214, 1960.

52. Lochiel, A.C., and Calderbank, P.H., Chem. Eng. Sci. 19, 471, 1964.

53. McCune, L.K., and Wilhelm, L.K., Ind. Eng. Chem. 41, 1124, 1949.

54. Mixon, F.O., and Carberry, J.J., Chem. Eng. Sci. 13, 30, 1960.

55. Miyauchi, T., J. Chem. Eng. Japan 4, 238, 1971.

56. Miyauchi, T., and Nomura, T., Int. Chem. Eng. 12, 360, 1972.

57. Mullin, J.W., and Treleaven, C.R., Symp. Interaction between fluids and particles (London: Instn. Chem. Engrs.), p 203, 1962.

58. Panton, R., J.Fl. Mech. 31, 273, 1968.

59. Peltzman, A., and Pfeffer, R., Chem. Eng. Prog. Symp. Series 63, 49, 1967.

60. Pfeffer, R., and Happel, J., A.I.Ch.E.J. 10, 605, 1964.

61. Pfeffer, R., Ind. Eng. Chem. Fundamentals, 3, 380, 1964.

62. Rahman, K., M.Sc. Thesis, 1969, London University, London.

63. Ranz, M.W., and Marshall, W.R., Chem. Eng. Prog. 48, 141, 1952.

64. Richardson, J.F., and Zaki, W.N., Trans. Instn. Chem. Engrs. 32, 35, 1954.

65. Rowe, P.N., Int. J. Heat Mass Transfer 6, 989, 1963.

66. Rowe, P.N., and Henwood, G.A., Trans. Instn. Chem. Engrs. 39, 43, 1961.

67. Rowe, P.N., Claxton, K.T., and Lewis, J.B., ibid, 43, T14, 1965.

68. Rowe, P.N., and Claxton, K.T., ibid 43, T321, 1965.

69. Scribner, B.F., and Margoshes, M., Treatise on Analytical Chemistry, Ed. Kolthoff, I.M., and Elving, P.J., John Wiley and Sons, Inc., London 1965, vol 6, Chapter 64, p 3347.

70. Sih, P.H., and Newman, J., Int. J. Heat Mass Transfer 10, 1749, 1967.

71. Slater, M.J., Conf. Ion Exchange in the Process Industries (July 16-18, 1969, London), p 127, The Society of Chemical Industries, 1970.

72. Snowdon, C.B., and Turner, J.C.R., Proc. Int. Symp. Fluidization (June 6-9, 1967, Eindhoven), Ed. Drinkenburg, A.A.H., Netherlands University Press, Amsterdam, 1967, p 599.

73. Snowdon, C.B., and Turner, J.C.R., Chem. Eng. Sci. 23, 221, 1968.

74. Stevenson, P.G., Conf. Ion Exchange in the Process Industries (July 16-18, 1969, London), p 115, The Society of Chemical Industries, 1970.

75. Taganov, I.N., and Romankov, P.G., Theo. Found. Chem. Eng. 2, 659, 1967.

76. Taylor, T.D., Basic Developments in Fluid Mechanics, vol II, Ed. Holt, E., Academic Press, 1968.

77. Thoenes, D., and Kramers, H., Chem. Eng. Sci. 8, 271, 1958.

78. Thodos, G., and Hobson, M., Chem. Eng. Prog. 47, 370, 1951.

79. Thodos, G., Hougen, O.A., and Gamson, B.W., Trans. Am. Inst. Chem. Engrs. 39, 1, 1953.

80. Thodos, G., and Riccetti, R.E., A.J.Ch.E.J., 7, 443, 1961.

81. Thodos, G., and Petrorvic, L.J., Proc. Int. Symp. Fluidization (June 6-9, 1967, Eindhoven), Ed. Drinkenburg, A.A.H., Netherlands University Press, Amsterdam, 1967, p 586.

82. Thodos, G., and Wilkins, A.I.Ch.E.J., 15, 47, 1969.

83. Thodos, G., and Yoon, P., ibid, 27, 1549, 1972.

84. Voskanyan, A.B., Golovin, A.M., and Tolmachev, V.V., J. Appl. Mech. and Tech. Phy. 7, 94, 1966.

85. Watts, R.G., J. Heat Transfer, Trans. A.S.M.E. 94, 1, Feb 1972.

86. Weber, W.J., and Keinath, T.M., Water Pollution Control Federation, 40, 741, 1968.

87. Whitaker, S., Chem. Eng. Sci. 28, 139, 1973.

88. Wilson, E.J., and Geankoplis, C.J., ibid, 5, 9, 1966.

89. Yaron, I., and Gal-Orb, B., Int. J. Heat Mass Transfer 14, 727, 1971.

90. Yuge, T., Rept. Inst. High Speed Mechanics of Tohoku University, 6, 143, 1956.

91. Zabrodsky, S.S., Int. J. Heat Mass Transfer 6, 23, 1963.

92. Zabrodsky, S.S., ibid, 10, 1793, 1967.

APPENDICES

A.1. Diffusion under concentration gradient and an external force

The simplest case of diffusion is concentration diffusion in a binary system and this is usually expressed by Fick's law of diffusion. Consider liquid phase diffusion in a binary ion exchange system under conditions of constant temperature and pressure and where ions are present in low concentration. A binary ion exchange system consists of two phases, namely the exchanger phase which is normally a solid and a liquid phase. The liquid phase contains the ions designated as 'A' and 'B' which are the exchanging ions often called counter ions, mobile non exchanging ions 'C' called the coions which are oppositely charged to that of counter ions and the solvent. The solid phase contains an inert matrix with fixed coionic groups and the mobile counter ions. Thus the liquid phase has four components, namely two counter ions, one coion and the solvent.

Another characteristic of an ion exchange system is the presence of an electric field which must be taken into account in the driving force for the diffusion flux. This electric field arises due to a tendency for the creation of a disturbance of the electroneutrality which is caused when the mobilities of the counter ions are different. If the mobilities of the diffusion ions are different, the faster ion tends to diffuse at a higher rate and any excess flux produces an electric field which slows down the faster ions and accelerates the slower ions. The result is a diffusion potential restoring electroneutrality. The deviations from electroneutrality remain negligible except in the electric double layer at the ion exchanger-solution interface which is only a few angstrom units thick (37b).

Since binary ion exchange is strictly a multicomponent system, it will be treated in that way rather than by starting with the usual

Nernst-Planck equations. There is some ambiguity as to the identification of the diffusion coefficient in the Nernst-Planck equation. Most authors use the term self-diffusion coefficient but actually mean binary diffusion coefficient of ion-solvent pair. It will be seen that when ions are present at low concentration, then they may be assumed to diffuse independently of each other and each ion-solvent pair may be treated as a binary pair and the Nernst-Planck equation applied. Also the identification of diffusion coefficient will be clear.

The theory of diffusion is complex and not complete. Diffusion in dilute gases has been treated quite satisfactorily by kinetic theory. It has also been observed that many dense gases and fluids may be treated by kinetic theory quite adequately. The following definitions and terms will be useful in recognising various terms of the kinetic theory result. For a mixture having n components

$$v = \frac{\sum_{i=1}^{n} \rho_i v_i}{\sum_{i=1}^{n} \rho_i}$$ and $n_i = \rho_i v_i$ are the mass average velocity of the mixture and mass flux of species i with respect to stationary coordinates respectively.

$$v^* = \frac{\sum_{i=1}^{n} C_i v_i}{\sum_{i=1}^{n} C_i}$$ and $N_i = C_i v_i$ are the corresponding molar quantities as above. (A.1-1)

$j_i = \rho_i (v_i - v)$ is the mass flux of species i with respect to mass average velocity and is called diffusion mass flux.

$J_i^* = C_i(v_i - v^*)$ is the corresponding molar diffusion flux as above

$$\sum_{i=1}^{n} \rho_i = \rho, \quad \sum_{i=1}^{n} C_i = C, \quad w_i = \frac{\rho_i}{\rho}, \quad x_i = \frac{C_i}{C}$$

where ρ_i, C_i, w_i and x_i are the density, molar concentration, mass fraction and mole fraction of species i and ρ and C are the density and molar concentration of the mixture

The kinetic theory result (7C) for mass flux with respect to mass average velocity due to a concentration gradient and an external force (neglecting pressure and thermal diffusion) in ideal solution, is given by

$$j_i = \frac{C^2}{\rho} \sum_{j=1}^{n} M_i M_j \mathcal{D}_{ij} \left[\nabla x_j + \frac{M_j X_j}{RT} \left(-g_j + \sum_{k=1}^{n} \frac{\rho_k}{\rho} g_k \right) \right] \quad (A.1\text{-}2)$$

Here $\mathcal{D}_{ij}$ is the diffusivity of the pair i-j in a multicomponent mixture. Here g is the external force and M the molecular weight. Because $\mathcal{D}_{ij}$ is concentration dependent equation (A.1-2) is inconvenient to use. However, for some calculations an effective binary diffusion coefficient D_{im} may be defined for species i in a mixture. This is seen below.

The molar flux for species 'A' in a binary mixture of species 'A' and 'B' may be written after manipulating equations (A.1-1) and (A.1-2) as

$$N_A = -CD_{AB} \left[\nabla x_A + \frac{M_A X_A}{RT} \left\{ -g_A + (g_A w_A + g_B w_B) \right\} \right] + x_A(N_A + N_B) \quad (A.1\text{-}3)$$

The special notation D_{AB} is used for $Đ_{AB}$ in a binary mixture. In an analogous way, the molar flux of species i in a mixture of n components can be written in terms of a diffusion coefficient D_{im} called the effective binary diffusion coefficient for the species i as

$$N_i = -C D_{im}\left[\nabla x_i + \frac{M_i X_i}{RT}\left(-g_i + \sum_{j=1}^{n} w_j g_j\right)\right] + x_i \sum_{j=1}^{n} N_j \qquad (A.1\text{-}4)$$

Here an expression for D_{im} will be sought in terms of appropriate binary diffusion coefficients for trace concentrations of species 2, 3, 4..in nearly pure species 1.

The Stefan-Maxwell equation for this case is given as (7C)

$$\nabla x_i + \frac{M_i X_i}{RT}\left[-g_i + \sum_{j=1}^{n} w_j g_j\right] = \sum_{j=1}^{n} \frac{1}{C D_{ij}} (x_i N_j - x_j N_i) \qquad (A.1\text{-}5)$$

It may be mentioned here that equation (A.1-5) is derived from (A.1-2) and contains the D_{ij} rather than the $Đ_{ij}$. Equation (A.1-4) may now be written as

$$\nabla x_i + \frac{M_i X_i}{RT}\left[-g_i + \sum_{j=1}^{n} w_j g_j\right] = \frac{-N_i + x_i \sum_{j=1}^{n} N_j}{C D_{im}} \qquad (A.1\text{-}6)$$

Comparing equations (A.1-5) and (A.1-6) we have

$$\frac{-N_i + x_i \sum_{j=1}^{n} N_j}{C D_{im}} = \sum_{j=1}^{n} \frac{1}{C D_{ij}} (x_i N_j - x_j N_i) \qquad (A.1\text{-}7)$$

If component 1 is present as nearly a pure species, i.e. $x_1 \simeq 1$ and $x_i \simeq 0$ $(i \neq 1)$ equation (A.1-7) reduces to

$$\frac{N_i}{C D_{im}} = \frac{N_i}{C D_{i1}}$$

i.e. $$D_{im} = D_{il} \qquad \text{(A.1-8)}$$

Thus diffusion coefficient of the trace species i in a mixture is equal to the binary diffusion coefficient of the species i and the nearly pure component. This is not the self diffusion coefficient. Self diffusion means diffusion of species i in itself.

It is possible to write the diffusion flux for the ionic species in a mixture where the ion may be subjected to an external electric force due to its ionic nature. Also a body force B acts on each species. The total force g_i may then be written as

$$g_i = B + \frac{N_{AV}}{M_i} Z_i \underline{q} E$$

$$= B - \frac{Z_i}{M_i} F \nabla \phi \qquad \text{(A.1-9)}$$

where $\underline{q}$ is the electric charge, E is the electric field, ϕ is the potential and its gradient taken as negative, N_{AV} the Avogadro number, F the Faraday constant, Z the valency of the ion, and B the gravity force. Using equation (A.1-9) one can write

$$g_i - \sum_{j=1}^{n} w_j g_j$$

$$= B - \frac{Z_i}{M_i} F \nabla \phi - \sum_{j=1}^{n} w_j \left(B - \frac{Z_j}{M_j} F \nabla \phi \right)$$

$$= B - \frac{Z_i}{M_i} F \nabla \phi - B \sum_{j=1}^{n} w_j + \sum_{j=1}^{n} \frac{\rho_j}{\rho} \frac{Z_j}{M_j} F \nabla \phi$$

$$= - \left(\frac{Z_i}{M_i} - \frac{1}{\rho} \sum_{j=1}^{n} C_j Z_j \right) F \nabla \phi$$

$$= - \frac{Z_i}{M_i} F \nabla \phi \qquad \text{(A.1-10)}$$

Since $\sum_{j=1}^{n} C_j Z_j = 0$ for the condition of electroneutrality.

Using equation (A.1-10) equation (A.1-4) may be written as

$$N_i = C\, D_{im} \left[\nabla x_i + \frac{x_i Z_i}{RT} F \nabla \phi \right] + x_i \sum_{j=1}^{n} N_j \qquad \text{(A.1-11)}$$

From equation (A.1-1)

$$N_i = J_i^* + x_i \sum_{j=1}^{n} N_j$$

and hence the expression for the diffusion flux J_i^* can be written from equation (A.1-11) as

$$J_i^* = - D_{im} \left[\nabla C_i + \frac{C_i Z_i}{RT} F \nabla \phi \right] \qquad \text{(A.1-12)}$$

Equation (A.1-12) is the Nernst-Planck equation.

A.2. Diffusional flux in terms of concentration gradient for a binary ion exchange system

In general, the liquid phase of a binary ion exchange system contains four components, namely the two counter-ions 'A' and 'B', the co-ion 'C' and the solvent 'S'. The co-ions in the solution phase are not held fixed as are the counterparts in the resin phase. This mobility of the co-ions creates a non zero concentration gradient for the co-ions, though no net transfer of co-ions can occur across the solid liquid interface due to the existence of a Donnan potential which prevents co-ion transfer (37C).

The diffusion flux of the ionic species may be expressed by equation (A.1-12) when ions are present in low concentration. This is given in terms of an effective binary diffusion coefficient for the diffusing species and the solvent and two gradients, viz., the concentration and electric for the driving force of the diffusion flux. However, it is possible to express the diffusion flux in terms of the concentration gradient alone, but with a complicated form of the diffusion coefficient which in general is dependent on concentration.

From equation (A.1-12), the liquid phase diffusion flux equations for the individual ionic species for a binary ion exchange case are;

$$J_A^* = - D_{AS} \left[\nabla C_A + \frac{Z_A C_A}{RT} F \nabla \phi \right] \qquad \text{(A.2-1.1)}$$

$$J_B^* = - D_{BS} \left[\nabla C_B + \frac{Z_B C_B}{RT} F \nabla \phi \right] \qquad \text{(A.2-1.2)}$$

$$J_C^* = - D_{CS} \left[\nabla C_C - \frac{Z_C C_C}{RT} F \nabla \phi \right] \qquad \text{(A.2-1.3)}$$

It may be seen that in equation (A.2-1.3) the electric potential gradient is taken as opposite, in this case positive for the co-ion 'C' since

the charge is opposite to that of the counter ions.

The following relations apply to the condition of electroneutrality and no net current, i.e.

$$\sum_{i=A,B,C} Z_i C_i = 0 \qquad \text{condition of electroneutrality}$$

i.e. $$Z_A C_A + Z_B C_B = Z_c C_C \tag{A.2-2}$$

and $$F \sum_{i=A,B,C} Z_i N_i = 0 \qquad \text{condition of no net current}$$

i.e. $$Z_A N_A + Z_B N_B = Z_C N_C$$

From equation (A.1-1), $N_A = J_A^* + C_A v^*$ and hence

$$Z_A J_A^* + Z_B J_B^* + (Z_A C_A + Z_B C_B) v^* = Z_C J_C^* + Z_C C_C v^*$$

Using equation (A.2-2)

$$Z_A J_A^* + Z_B J_B^* = Z_C J_C^* \tag{A.2-3}$$

Equations (A.1-1) may now be manipulated with the conditions (A.2-2) and (A.2-3) to yield the following relationship without the appearance of the electric potential gradient and in terms of the concentration gradient of only one of the species.

$$- \frac{J_A^*}{D_{AS}} + \frac{Z_A Z_B C_A}{Z_C C_C (Z_B + Z_C)} \left[\frac{J_A^*}{D_{AS}} + \frac{J_B^*}{D_{BS}} - \frac{Z_C}{Z_B} \frac{J_C^*}{D_{CS}} \right]$$

$$= \frac{Z_C C_C (Z_B + Z_C) - Z_A C_A (Z_B - Z_A)}{Z_C C_C (Z_B + Z_C)} \nabla C_A \tag{A.2-4}$$

A.3. Solution of the forced convective diffusion equation (4.1-10)

Equation (4.1-10) represents the continuity equation for the species 'A' in a binary homovalent ion exchange system. In spherical coordinates it is given as

$$v_r \frac{\partial C_A}{\partial r} + \frac{v_\theta}{r} \frac{\partial C_A}{\partial \theta} = \frac{1}{r^2} \frac{\partial}{\partial r} \left(\frac{2D_{AS}}{\alpha \frac{C_A}{C_C} + 2} r^2 \frac{\partial C_A}{\partial r} \right) \qquad \text{(A.3-1) and (4.1-10)}$$

In writing equation (A.3-1) it is assumed that the Peclet number is high so that diffusion in the angular direction θ, may be neglected; also the problem is considered symmetrical in the ϕ direction. The coordinates are shown in Fig A.3-1.

Fig A.3-1. Coordinate system used in describing equation (A.3-1).

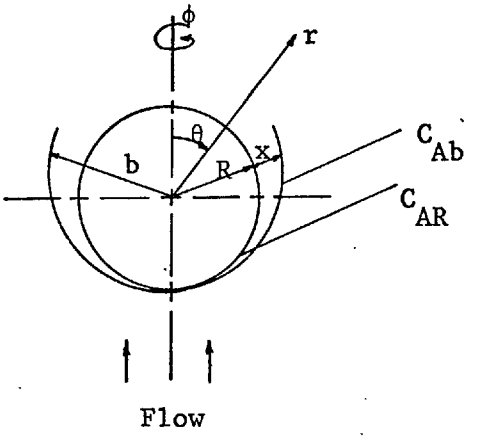

Let v_r and v_θ be expressed in terms of the stream function ψ. In spherical coordinates, they are

$$v_r = -\frac{1}{r^2 \sin\theta} \frac{\partial \psi}{\partial \theta}$$

$$v_\theta = +\frac{1}{r \sin\theta} \frac{\partial \psi}{\partial r} \qquad \text{(A.3-2)}$$

Define a new radial coordinate x as

$$x = r - R \tag{A.3-3}$$

The boundary conditions are

$$\begin{aligned} r &= R, \quad x = 0, \quad C_A = C_{AR} \\ r &= R + b, \quad x = b, \quad C_A = C_{Ab} \end{aligned} \tag{A.3-4}$$

where b is the thickness of the concentration boundary layer. Using these new variables equation (A.3-1) becomes

$$-\frac{\partial\psi}{\partial\theta}\frac{\partial C_A}{\partial x} + \frac{\partial\psi}{\partial r}\frac{\partial C_A}{\partial\theta} = \sin\theta\,\frac{\partial}{\partial x}\left(\frac{2D_{AS}}{\alpha\,\frac{C_A}{C_C} + 2}\,R^2\,\frac{\partial C_A}{\partial x}\right) \tag{A.3-5}$$

Here $R + x \simeq R$ since $x << R$ due to the assumption of large Peclet number.

Since the problem is non linear, an exact solution is difficult and therefore, an approximate solution will be attempted. An integral method of analysis will be used for this purpose.

Equation (A.3-5) may be rewritten as follows

$$-\frac{\partial\psi}{\partial\theta}\frac{\partial}{\partial x}(C_A - C_{Ab}) - (C_A - C_{Ab})\frac{\partial^2\psi}{\partial x\partial\theta} + (C_A - C_{Ab})\frac{\partial^2\psi}{\partial x\partial\theta} + \frac{\partial\psi}{\partial x}\frac{\partial}{\partial\theta}(C_A - C_{Ab})$$

$$= \sin\theta\,\frac{\partial}{\partial x}\left[\frac{2D_{AS}}{\alpha\,C_A/C_C + 2}\,R^2\,\frac{\partial C_A}{\partial x}\right]$$

or

$$-\frac{\partial}{\partial x}\left[(C_A - C_{Ab})\frac{\partial\psi}{\partial\theta}\right] + \frac{\partial}{\partial\theta}\left[(C_A - C_{Ab})\frac{\partial\psi}{\partial x}\right]$$

$$= \sin\theta\,\frac{\partial}{\partial x}\left[\frac{2D_{AS}}{\alpha\,C_A/C_C + 2}\,R^2\,\frac{\partial C_A}{\partial x}\right] \tag{A.3-6}$$

Integrating equation (A.3-6) between the limits $x = 0$ and $x = b$ i.e. across the concentration boundary layer gives

$$- \left[(C_A - C_{Ab}) \frac{\partial \psi}{\partial x} \right]_{x=0}^{x=b} + \int_{x=0}^{x=b} \frac{\partial}{\partial \theta} (C_A - C_{Ab}) \frac{\partial \psi}{\partial x} \cdot dx$$

$$= \sin\theta \left[\frac{2D_{AS}}{\alpha C_A/C_C + 2} R^2 \frac{\partial C_A}{\partial x} \right]_{x=0}^{x=b}$$

or

$$\int_{x=0}^{x=b} \frac{\partial}{\partial \theta} (C_A - C_{Ab}) \frac{\partial \psi}{\partial x} dx = - \left[\frac{2D_{AS} R^2 \sin\theta}{\alpha C_A/C_C + 2} \frac{\partial C_A}{\partial x} \right]_{x=0} \qquad (A.3\text{-}7)$$

The following facts have been used to obtain equation (A.3-7);

$$\left[(C_A - C_{Ab}) \frac{\partial \psi}{\partial \theta} \right]_{x=0} = 0 \qquad \text{since} \quad \frac{\partial \psi}{\partial \theta} = 0$$

$$\left[(C_A - C_{Ab}) \frac{\partial \psi}{\partial \theta} \right]_{x=b} = 0 \qquad \text{since} \quad (C_A - C_{Ab})_{x=b} = 0$$

$$\left[\frac{2D_{AS} R^2 \sin\theta}{\alpha C_{A/} C_C + 2} \frac{\partial C_A}{\partial x} \right]_{x=b} = 0 \qquad \text{since} \left(\frac{\partial C_A}{\partial x} \right)_{x=b} = 0 \quad \text{at the edge}$$

of the concentration boundary layer which is located at $x = b$, any gradient of concentration would vanish. Using the Leibnitz formula the left-hand side of equation (A.3-7) becomes

$$\int_{x=0}^{x=b} \frac{\partial}{\partial \theta} (C_A - C_{Ab}) \frac{\partial \psi}{\partial x} dx =$$

$$= \frac{d}{d\theta} \int_{x=0}^{x=b} (C_A - C_{Ab}) \frac{\partial \psi}{\partial x} \cdot dx - \left[\frac{db}{d\theta} (C_A - C_{Ab}) \frac{\partial \psi}{\partial x} \right]_{x=b} + \left[\frac{dx}{d\theta} (C_A - C_{Ab}) \frac{\partial \psi}{\partial x} \right]_{x=0}$$

The last two terms on the right-hand side are zero and equation (A.3-7) can be written as

$$\frac{d}{d\theta} \int_{x=0}^{x=b} (C_A - C_{Ab}) \frac{\partial \psi}{\partial x} dx = -\left[\frac{2D_{AS} R^2 \sin\theta}{\alpha C_A/C_C + 2} \frac{\partial C_A}{\partial x}\right]_{x=0} \quad (A.3\text{-}8)$$

The integral quantity of the above equation is related to the total amount of mass diffused which can be seen from the following relationship.

$$2\pi M' = \int_0^{2\pi} \int_0^{\pi} \underbrace{-\left(\frac{2D_{AS}}{\alpha C_A/C_C + 2}\right)_{x=0}}_{\text{diffusion coefficient}} \underbrace{\left(\frac{\partial C_A}{\partial x}\right)_{x=0}}_{\text{concentration gradient}} \underbrace{R^2 \sin\theta \, d\theta \, d\phi}_{\text{area}}$$

Thus equation (A.3-8) may be written as

$$\frac{dM'}{d\theta} = \frac{d}{d\theta} \int_{x=0}^{x=b} (C_A - C_{Ab}) \frac{\partial \psi}{\partial x} dx = -\left[\frac{2D_{AS} R^2 \sin\theta}{\alpha C_A/C_C + 2} \frac{\partial A}{\partial x}\right]_{x=0}$$

Also $$\int (C_A - C_{Ab}) \, d\psi = \int_{x=0}^{x=b} d\{(C_A - C_{Ab})\psi\} - \int_{x=0}^{x=b} \psi \, d C_A$$

Hence $$\frac{dM'}{d\theta} = -\frac{d}{d\theta} \int_{x=0}^{x=b} \psi \, d C_A = -\left[\frac{2D_{AS} R^2 \sin\theta}{\alpha C_A/C_C + 2} \frac{\partial C_A}{\partial x}\right]_{x=0} \quad (A.3\text{-}9)$$

$$\text{where} \quad M' = -\int_{x=0}^{x=b} \psi \, d C_A \quad (A.3\text{-}10)$$

Since the above equations have two dependent variables C_A and C_C, it is convenient to define a single variable called the equivalent fraction as

$$y_A = \frac{C_A}{C_C} \quad (A.3\text{-}11)$$

Now $dC_A - y_A dC_C = C_C\, dy_A$

From equation (4.1-6) we have

$$dC_C = -\frac{\alpha}{\alpha\, y_A + 2}\, dC_A \qquad \text{(A.3-12)}$$

Then using equation (4.1-8)

$$dC_A = \frac{C_{Cb}\,(\alpha\, y_{Ab} + 1)^{\frac{1}{2}}\,(\alpha\, y_A + 2)}{2(\alpha\, y_A + 1)^{3/2}}\, d\, y_A \qquad \text{(A.3-13)}$$

Replacing this new variable in equation (A.3-9) and using a new symbol M

$$-\frac{dM}{d\theta} = \frac{d}{d\theta} \int_{x=0}^{x=b} \psi\, \frac{(\alpha y_A+2)}{(\alpha y_A+1)^{3/2}}\, \frac{\partial y_A}{\partial x}\, dx =$$

$$= \frac{2D_{AS}\, R^2 \sin\theta}{(\alpha y_{AR}+1)^{3/2}} \left(\frac{\partial y_A}{\partial x}\right)_{x=0} \qquad \text{(A.3-14)}$$

The corresponding boundary conditions are

$$\begin{aligned} x &= 0, \qquad y_A = y_{AR} \\ x &= b, \qquad y_A = y_{Ab} \end{aligned} \qquad \text{(A.3-15)}$$

A concentration profile is now assumed which satisfies as many boundary conditions as possible and yet is quite simple to manipulate. The following concentration profile is chosen:

$$y_A = \frac{1}{\alpha} \left[\frac{1}{(f_1 - f_3 \frac{x}{b})^2} - 1\right] \qquad \text{(A.3-16)}$$

where
$$f_1 = \frac{1}{(1 + \alpha y_{AR})^{\frac{1}{2}}}$$
$$f_2 = \frac{1}{(1 + \alpha y_{Ab})^{\frac{1}{2}}} \qquad \text{(A.3-17)}$$
and $f_3 = f_1 - f_2$

The above profile satisfies the boundary conditions (A.3-15). In addition it satisfies the condition

$$\frac{\partial}{\partial x}\left[\frac{R^2}{(\alpha y_A + 1)^{3/2}}\frac{\partial y}{\partial x}\right] = 0 \quad \text{both at} \quad x = 0 \quad \text{and} \quad x = b$$

which follows from equation (A.3-5). This is true only when the concentration boundary layer is thin, i.e. $R + x \simeq R$. However the concentration profile does not satisfy the condition $\frac{\partial y_A}{\partial x} = 0$ at $x = b$ and this is a common limitation met by other workers when a relatively simple concentration profile is used.

As this is a thin concentration boundary layer problem, it is sufficient to use the velocity field near the surface of the particle. Hence ψ is expanded around the surface as follows

$$\psi = \psi_R + \psi_R' x + \psi_R'' \frac{x^2}{2} + \ldots$$

$$\simeq \psi_R'' \frac{x^2}{2} \qquad \text{(A.3-18)}$$

Since ψ_R and $\psi_R' = 0$ where the primes indicate the first and second derivative and the subscript R indicates the surface of the particle.

$$\text{Let} \quad p = \frac{1}{(f_1 - f_3 \frac{x}{b})} \qquad \text{(A.3-19)}$$

Then

$$\left.\begin{aligned}
(\alpha y_A + 2) &= \frac{1}{(f_1 - f_3 \frac{x}{b})^2} + 1 = p^2 + 1 \\
(\alpha y_A + 1)^{3/2} &= \frac{1}{(f_1 - f_3 \frac{x}{b})^3} = p^3 \\
\frac{\partial y}{\partial x} &= \frac{2f_3}{\alpha b(f_1 - f_3 \frac{x}{b})^3} = \frac{2f_3}{\alpha b} p^3
\end{aligned}\right\} \qquad \text{(A.3-20)}$$

$$dx = \frac{b}{f_3}\frac{dp}{p^2}$$

$$\psi_R'' \frac{x^2}{2} = \psi_R'' \frac{b^2}{2f_3^2}\left(f_1 - \frac{1}{p}\right)^2$$

The boundary conditions are

$$\begin{aligned} x &= 0, \qquad p = \frac{1}{f_1} \\ x &= b, \qquad p = \frac{1}{f_1 - f_3} = \frac{1}{f_2} \end{aligned} \tag{A.3-21}$$

Substituting the quantities in equations (A.3-20) and (A.3 21) and using equation (A.3-14) one can write

$$M = -\frac{b^2\psi_R''}{f_3{}^2\alpha}\int_{1/f_1}^{1/f_2}\frac{(p^2+1)}{p^2}\left(f_1 - \frac{1}{p}\right)^2 dp$$

$$= -\frac{b^2\psi_R''}{f_3{}^2\alpha}\left[-f_1 \ln\left(\frac{f_1}{f_2}\right)^2 + \frac{(f_1 - f_2)^3}{3} + \frac{f_1{}^2 - f_2{}^2}{f_2}\right]$$

$$= -\frac{b^2\psi_R''A}{f_3{}^2\alpha}$$

$$\text{or,} \quad b = \sqrt{\frac{Mf_3{}^2\alpha}{-\psi_R''A}} \tag{A.3-22}$$

$$\text{where} \quad A = -f_1 \ln\left(\frac{f_1}{f_2}\right)^2 + \frac{(f_1 - f_2)^3}{3} + \frac{f_1{}^2 - f_2{}^2}{f_2} \tag{A.3-23}$$

Also from equations (A.3-14) and (A.3-17)

$$\frac{dM}{d\theta} = -\frac{2D_{AS}R^2 \sin\theta}{(\alpha y_{AR}+1)^{3/2}}\left(\frac{\partial y_A}{\partial x}\right)_{x=0}$$

$$= - 2D_{AS} R^2 \sin\theta f_1^3 \left(\frac{\partial y}{\partial x}\right)_{x=0} \qquad \text{(A.3-24)}$$

$$= - \frac{4D_{AS} R^2 \sin\theta f_3}{\alpha b} \qquad \text{(A.3-25)}$$

Since from equation (A.3-20)

$$\left(\frac{\partial y}{\partial x}\right)_{x=0} = \frac{2f_3}{\alpha b f_1^3}$$

Also from equation (A.3-24)

$$\left(\frac{\partial y}{\partial x}\right)_{x=0} = - \frac{1}{2D_{AS} R^2 \sin\theta f_1^3} \frac{dM}{d\theta} \qquad \text{(A.3-26)}$$

Replacing equation (A.3-22) in equation (A.3-24)

$$\int_0^M \sqrt{M}\, dM = - \int_\pi^0 \sqrt{\frac{-\psi_R'' A}{\alpha}} \frac{4D_{AS} R^2 \sin\theta\, d\theta}{\alpha}$$

The lower limit on the left hand side shows that at $\theta = \pi$ nothing has diffused. On integration

$$M = (6D_{AS}R^2)^{2/3} \frac{A^{1/3}}{\alpha} \left[\int_0^\pi \sqrt{-\psi_R''} \sin\theta\, d\theta\right]^{2/3} \qquad \text{(A.3-27)}$$

The flux $J_A^*\Big|_{x=0}$ may be written from equation (4.1-7) as

$$J_A^*\Big|_{x=0} = - \frac{2D_{AS}}{\alpha \frac{C_A}{C_C} + 2} \left(\frac{dC_A}{dx}\right)_{x=0}$$

or in terms of y_A from equations (A.3-11) and (A.3-13) as

$$J_A^*\Big|_{x=0} = - \frac{D_{AS}\, C_{Cb}\, (\alpha y_{Ab}+1)^{1/2}}{(\alpha y_{AR}+1)^{3/2}} \left(\frac{dy_A}{dx}\right)_{x=0} \qquad \text{(A.3-28)}$$

A local mass transfer coefficient $K_V(\theta)$ is now defined as

$$J_A^*\Big|_{x=0} = - \frac{D_{AS}\, C_{Cb}\, (\alpha y_{Ab}+1)^{1/2}}{(\alpha y_{AR}+1)^{3/2}} \left(\frac{dy_A}{dx}\right)_{x=0}$$

$$= K_V(\theta)\, C_{Cb}\, (y_{AR} - y_{Ab}) \qquad \text{(A.3-29)}$$

The subscript V in K_V serves to remind that the diffusion coefficient is not constant in this system.

Using equations (A.3-17) and (A.3-26)

$$K_V(\theta) = \frac{1}{2f_2\, R^2 \sin\theta\, (y_{AR} - y_{Ab})} \frac{dM}{d\theta}$$

and the average mass transfer coefficient $\overline{K}_V$ is

$$\overline{K}_V = \frac{1}{4\pi R^2} \int_o^{2\pi} \int_o^{\pi} \frac{R^2 \sin\theta\, d\theta\, d\phi}{2f_2\, R^2 \sin\theta\, (y_{AR} - y_{Ab})} \frac{dM}{d\theta}$$

$$= - \frac{1}{4f_2\, R^2\, (y_{AR} - y_{Ab})} \int_{\pi}^{o} dM$$

$$= - \frac{M}{4f_2\, R^2\, (y_{AR} - y_{Ab})} \qquad \text{(A.3-30)}$$

and from equation (A.3-27)

$$\overline{K}_V = - \frac{(6D_{AS}R^2)^{2/3} A^{1/3}}{4f_2\, \alpha\, R^2 (y_{AR} - y_{Ab})} \left[\int_o^{\pi} \sqrt{-\psi_R''} \sin\theta\, d\theta \right]^{2/3}$$

or on substitution the value of A from equation (A.3-23) and using $R = d/2$ we have

$$\bar{K}_V = \frac{(12)^{2/3} D_{AS}^{2/3}}{4 d^{2/3} f_2 \alpha (y_{AR} - y_{Ab})} \left[f_1 \ln \left(\frac{f_1}{f_2}\right)^2 - \frac{(f_1 - f_2)^3}{3} - \frac{f_1^2 - f_2^2}{f_2} \right]^{1/3}$$

$$\times \left[\int_o^\pi \sqrt{-\psi_R''} \sin\theta \, d\theta \right]^{2/3}$$

$$= 1.31 \left(\frac{D_{AS}}{d}\right)^{2/3} F \left[\int_o^\pi \sqrt{-\psi_R''} \sin\theta \, d\theta \right]^{2/3} \qquad \text{(A.3-31)}$$

where F may be written after substituting the values of f_1 and f_2 from equations (A.3-17) as

$$F = (1 + \alpha y_{Ab})^{\frac{1}{2}} \left[\frac{\frac{1}{(\alpha y_{AR}+1)^{\frac{1}{2}}} \ln \frac{1 + \alpha y_{Ab}}{1 + \alpha y_{AR}} - (1+\alpha y_{Ab})^{\frac{1}{2}} \left(\frac{1}{\alpha y_{AR}+1} - \frac{1}{\alpha y_{Ab}+1} \right)}{\alpha^3 (y_{AR} - y_{Ab})^3} \right.$$

$$\left. - \frac{1}{3} \frac{\left\{ \frac{1}{(1 + \alpha y_{AR})^{\frac{1}{2}}} - \frac{1}{(1 + \alpha y_{Ab})^{\frac{1}{2}}} \right\}^3}{\alpha^3 (y_{AR} - y_{Ab})^3} \right]^{1/3} \qquad \text{(A.3-32)}$$

It would be interesting to find the limiting value of the quantity F when $y_{AR} \to y_{Ab}$, but this is cumbersome, since when $y_{AR} \to y_{Ab}$, the limit of the first term in the bracket of equation (A.3-32) on straightforward substitution becomes indefinite. However differentiating the numerator and the denominator three times with respect to y_{AR} the limit of the first term is obtained as

$$\frac{1}{24(\alpha y_{Ab} + 1)^{7/2}}$$

The second term in the bracket of equation (A.3-32) may be written as

$$-\frac{1}{3}\left[\frac{1}{(1+\alpha y_{AR})^{\frac{1}{2}}(1+\alpha y_{Ab}) + (1+\alpha y_{AR})(1+\alpha y_{Ab})^{\frac{1}{2}}}\right]^3$$

In the limit

$$\left.\begin{aligned} y_{AR} \to y_{Ab} \to 0 \qquad & F \to \left(\frac{1}{12}\right)^{1/3} \\ \text{and when} \qquad y_{AR} \to y_{Ab} \to 1 \qquad & \\ F \to (1+\alpha)^{\frac{1}{2}} & \left[\frac{1}{24(1+\alpha)^{7/2}} + \frac{1}{24(1+\alpha)^{9/2}}\right]^{1/3} \\ = \frac{1}{24^{1/3}} & \frac{(\alpha+2)^{1/3}}{(1+\alpha)} \end{aligned}\right\} \qquad \text{(A.3-33)}$$

A.4. Spectrochemical analysis for the Na^+ content in a polystyrene resin bead

Spectrochemical analysis uses the characteristic radiation emitted by atoms and molecules for their identification and quantitative determination. Most atoms and molecules can be exicted by a light source such that some electrons are raised to a higher energy orbital and subsequently decay emitting characteristic radiation.

In analytical spectroscopy, the intensity of the emitted radiation and concentration of an element is usually determined empirically by means of standard samples having known concentrations. In addition, relative intensities are usually measured avoiding the considerable difficulty that would be encountered in the measurement of absolute intensities. For the present case the Na^{5889} line was chosen for the quantitative estimation of sodium in an ion exchange resin particle using an arc as the excitation source.

Because the line intensities can be afffected by several factors due to variation in excitation, optical alignment exposure etc. the straightforward comparative method does not provide a sufficiently precise estimate of concentration. The internal standard method provides an effective means of improving the precision of spectrographic analysis. The internal standard is an element that is present in each sample and standardised as a major constituent preferably at a fixed concentration. The reason why the internal standard should be present as a major constituent can be understood by studying the following hypothetical intensity vs. concentration curve shown in Fig. A.4-1. Above a certain value of the concentration of an element, the intensity of a line attains a constant value. Thus, a major constituent in a sample would exhibit this characteristic. In the internal standard method, it is assumed that all the variables, other

Fig. A.4-1. A hypothetical intensity vs. concentration curve.

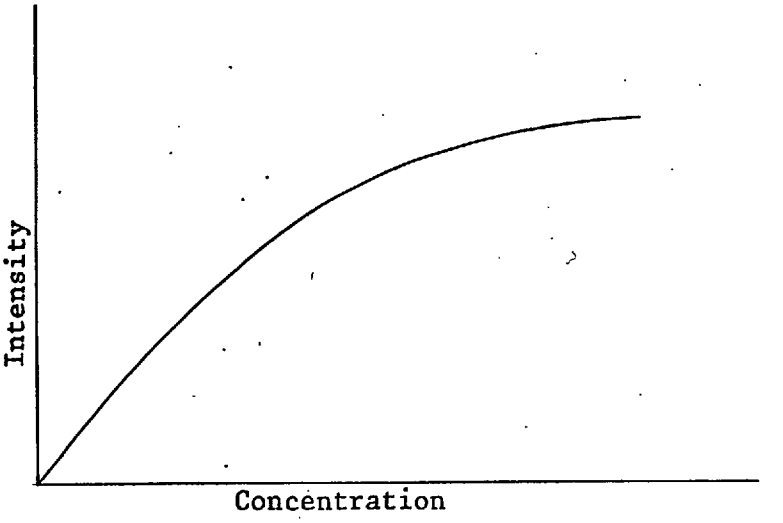

than concentration, affect the measured intensities of the analysis line and the internal standard line to the same degree so that the intensity ratio of the samples and standards to the internal standard would be a better measure of the amount of material present. The internal standard method is expected to provide an automatic correction for the factors mentioned above. Unfortunately the case may not be so simple, since a difference in ionization and excitation potentials, boiling points, stability of compounds and self-reversal affects would effect the intensity ratio, limiting the choice of internal standards. Thus in all applications, the validity of the fundamental assumption of the internal standard method and the reliability of results depends upon reproducibility of excitation optics and photography and must be checked out experimentally.

The basic assumption of the internal standard method is then

$$C_A = f(I_A/I_S)$$

where C_A is the concentration and I_A and I_S are the relative inten-

sities of the analyte and internal standard line. For many cases, the experimental data indicates that concentration may be expressed as

$$\log C_A = K_1 \log I_A/I_S + K_2$$

where K_1 and K_2 may be assumed constants. In the present case Cu^{5782} is used as the internal standard line.

To calculate the intensity ratios, it is necessary to convert the microphotometer readings to relative intensities. In order to do so the film or the plate referred to as the emulsion in which the spectrum is recorded, must be calibrated so that its response to light is known quantitatively. The calibration is simplified greatly by the use of relative intensities, so that it is not necessary to calibrate the emulsion in an absolute sense. Of the various methods of emulsion calibration the "two line" method has been chosen.

In the two line method of emulsion calibration, two suitable lines bearing a fixed intensity ratio are selected and several spectrograms are recorded by varying the intensity. Thus a datum is provided, by the two readings, one representing an intensity weaker or stronger by some fixed ratio. The line pair should have the characteristics that the intensity ratio remains constant and be independent of composition which can be accomplished using two lines of the same element which have similar excitation characteristics and that they should be sharply defined and free from the interfering effects of other elements. Also it has been found advantageous experimentally that the intensity of the two lines should be between 1.2 and 2 and that the wave length of the lines should differ by no more than 100 Å. In the present experiments the two lines selected are Na^{5889} and Na^{5895}, the former being the line used for quantitative estimation. To produce a series of spectrograms a seven step sector has been used. The procedure for calculation is as follows.

Both members of the line pair, i.e. Na^{5889} and Na^{5895} are measured in all spectrograms by a microphotometer, setting the full scale deflection of the microphotometer reading 100 for an unexposed emulsion and a reading of zero on an image of infinite density. Using the pair of points a curve known as the preliminary curve is plotted, usually in logarithmic coordinates. Such a plot is shown in Fig. A.4-2.

Next the emulsion calibration curve is plotted using the preliminary curve and the intensity ratio of the two lines. As the initial point on the emulsion curve, a deflection say 92 which is higher than any to be used in the analysis, is selected. Now using this value as the ordinate in the preliminary curve a value of 90 is read from the abscissa. Now if the deflection 92 is given an intensity of 1.0, then the relative intensity for the reading 90 would differ by a factor r_1 which is the ratio of the intensity of the two lines. Now the value of 90 is used as the ordinate in the preliminary curve to obtain a second value of 88 from the abscissa which corresponds to a relative intensity of r_1^2 compared to that of 1.0 for a microphotometer deflection of 92. This process is repeated, until deflections take a value smaller than any used in the routine analysis. Using the readings of the ordinate and the corresponding relative intensity an emulsion calibration curve can now be plotted. The sole purpose of this curve is to provide a means of determining the value of the relative intensity factor for any microphotometer deflection from a given datum (in this case a value of microphotometer deflection 92 is given a value 1.0 for the intensity factor). Hence, the actual intensity ratio of the two lines are not required except very roughly. The ratio of the microphotometer reading may serve as a measure of the ratio of intensity of the two lines. Since, the response of the emulsion is not linear over the entire range of exposure, an average value of the ratio for the two line pair has been used as the intensity ratio

Fig. A.4-2 : Preliminary curve

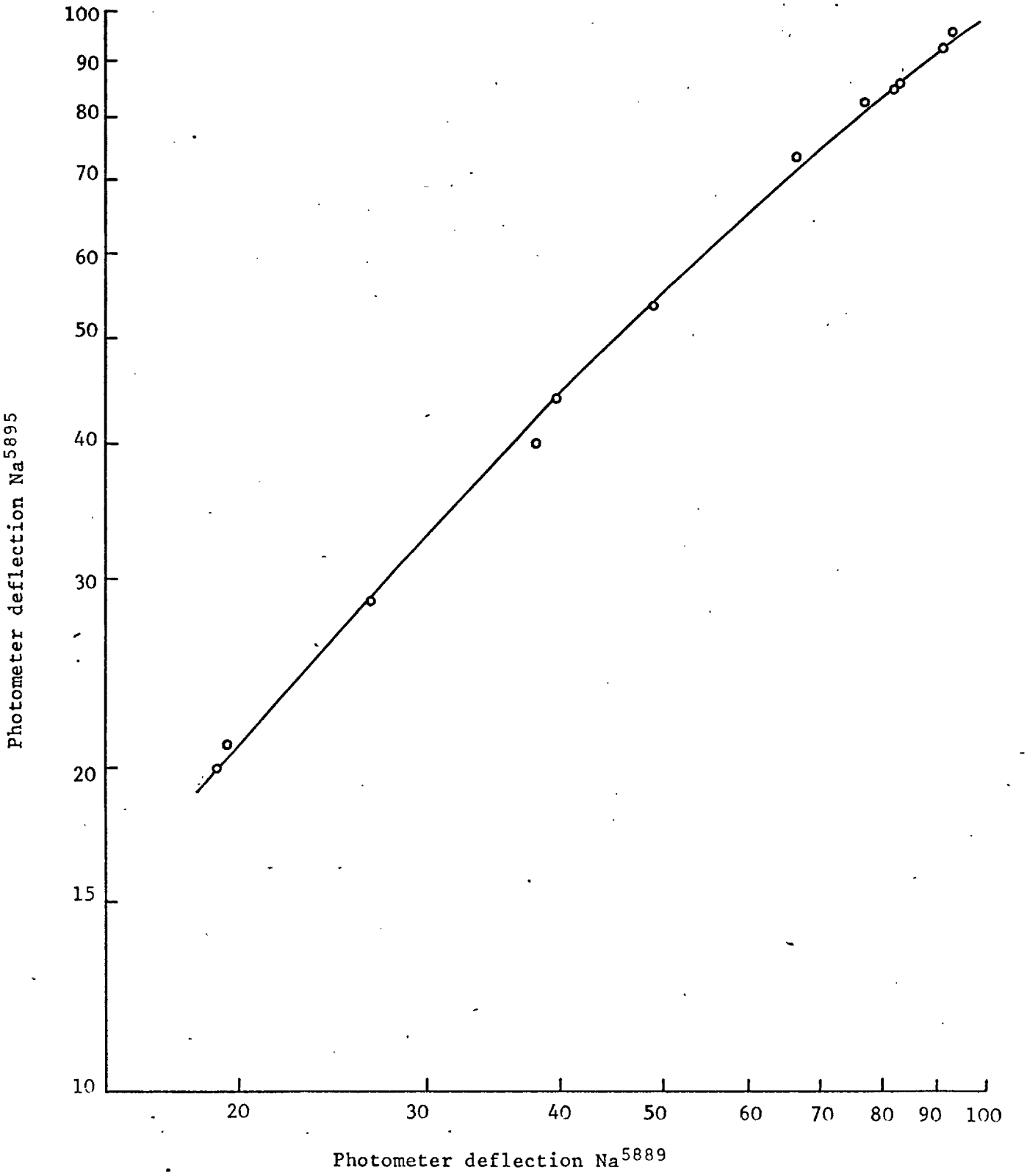

Fig A.4-3 : Emulsion calibration curve

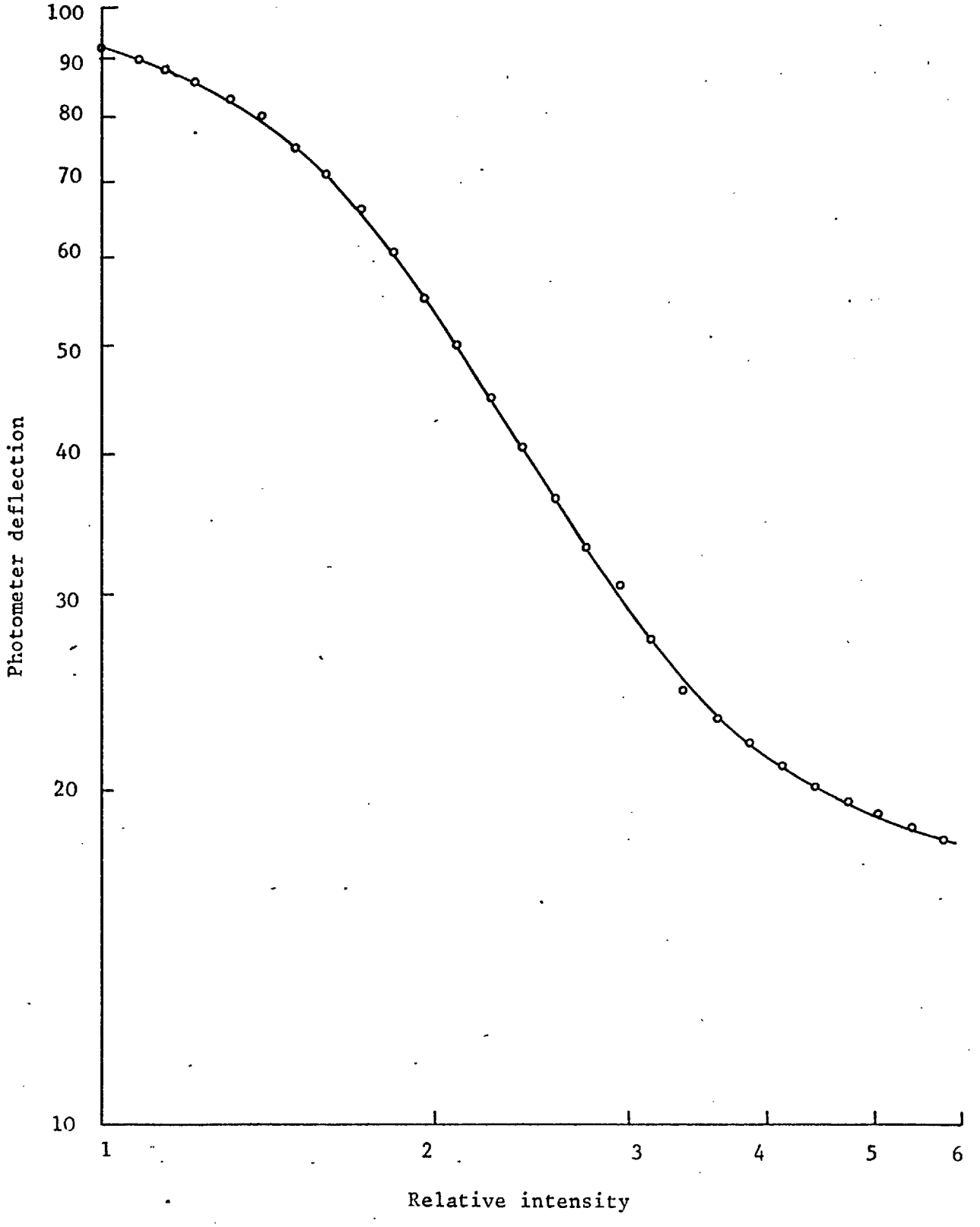

Fig. A.4-8 : Relative intensity ratio against concentration in ppm

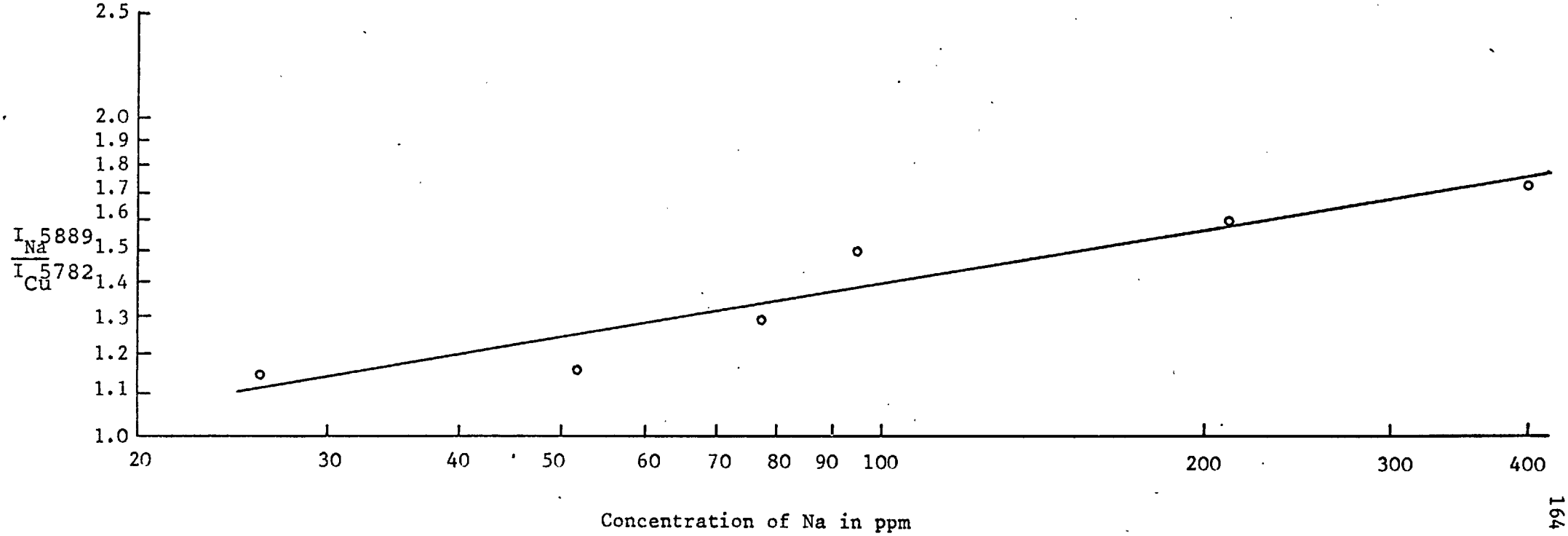

factor. Fig. A.4-3 shows such a curve where an intensity ratio factor of 1.07 has been used.

The next step is the calculation of the relative intensities of the analyte and internal standard line for the unknowns and standards. Using the ratio of the relative intensities of the standards and internal standards a curve is plotted. Such a curve is shown in Fig. A.4-4 and knowing the relative intensity ratios of the unknowns, their concentration can be determined.

The analysis was performed by carefully transferring an ion exchange particle to a small polythene container after the mass transfer experiments. The water adhering to the particles was soaked with a clean tissue, and transferred to a weighted graphite electrode, which had a 3 mm crater at one of its ends for the containment of samples. The particles and the electrode were then weighed to determine the weight of the particle. Then about 2 to 3 mg of spectrographically pure $CuSO_4$ was added to the electrode and weighed to determine the weight of $CuSO_4$ added. The comparative standards were prepared by injecting a known amount of Na_2SO_4 solution on the $CuSO_4$. For reproducible results grinding of the $CuSO_4$ granules to fine powder was necessary. The standards were then dried and weighed. The electrodes were then mounted on an E 492 quartz Hilger and Watts spectrograph one after another and arced. The electrode containing the samples formed the bottom electrode and a 60° coned graphite electrode formed the top electrode with a 2mm gap between them. A 4.5 amp DC arc with 10 sec exposure time was used in arcing. The preliminary curves were obtained by touching the electrodes with bare hand which had sufficient sodium and a step sector used to obtain a series of suitable spectrograms. An Ilford R-40 plate in the visible range was used. A 3 minute developing time in caustic-hydroquinone at $18^{\circ}C$, 15 minutes fixing time using Kodafix rapid-

fixer and 15 minutes washing time in tap water was found suitable for the purpose.

A general reference to spectrochemical analysis may be found in reference (69).

A.5. Calculated experimental data

Fluidized bed data Table A.5-1 to A.5-8.

Table A.5-1

Re_o = 56.16

d = 0.106 cm

V_B = 4.71 cm^3

ρ_s = 1.23 gm/cm^3

Re_s	ε	$\bar{K}_C$	Sh	Sc	j_m	j'_m
4.23	0.443	0.00616	31.04	424.26	0.976	0.433
5.09	0.469	0.00634	31.92	424.29	0.834	0.391
* 7.35	0.525	0.00702	35.36	424.04	0.640	0.336
10.09	0.575	0.00735	36.99	424.08	0.488	0.281
14.97	0.655	0.00776	39.07	424.11	0.347	0.228
22.96	0.751	0.00825	41.56	424.14	0.241	0.181

$$j_m = 3.55\ Re_s^{-0.859}$$

* Data above the asterisk symbol were not used for correlation.

Table A.5-2a

Re_o = 43.72

d = 0.0938 cm

V_B = 5.65 cm^3

ρ_s = 1.23 gm/cm^3

Re_s	ε	$\bar{K}_C$	Sh	Sc	j_m	j'_m
4.00	0.488	0.00613	27.36	424.71	0.910	0.444
4.54	0.486	0.00653	29.12	424.50	0.854	0.415
5.50	0.526	0.00671	29.93	424.77	0.724	0.381
7.39	0.581	0.00724	32.26	424.60	0.581	0.338
* 8.92	0.613	0.00735	32.78	424.86	0.489	0.300
10.62	0.637	0.00757	33.76	424.88	0.423	0.269
10.62	0.647	0.00757	33.75	424.66	0.423	0.274
13.32	0.687	0.00785	35.02	424.68	0.350	0.240
15.22	0.748	0.00803	35.82	424.93	0.313	0.234
16.04	0.729	0.00814	36.30	424.70	0.301	0.219
17.81	0.766	0.00827	36.87	424.71	0.275	0.211
20.35	0.799	0.00835	37.27	424.95	0.244	0.195
22.22	0.810	0.00855	38.11	424.73	0.228	0.185

$$j_m = 3.118\ Re_s^{-0.844}$$

* Data above asterisk symbol were not used for correlation.

Table A.5-2b

Re_o = 43.72

d = 0.0938 cm

V_B = 5.62 cm^3

ρ_s = 1.23 gm/cm^3

Re_s	ε	$\overline{K}_C$	Sh	Sc	j_m	j'_m
2.22	0.452	0.00505	22.52	424.24	1.350	0.610
3.54	0.491	0.00546	24.31	424.37	0.914	0.449
3.94	0.465	0.00563	25.09	424.39	0.847	0.394
5.43	0.544	0.00659	29.37	424.43	0.719	0.391
6.52	0.574	0.00692	30.83	424.46	0.630	0.362
7.38	0.588	0.00714	31.81	424.48	0.574	0.338
8.14	0.644	0.00736	32.83	424.68	0.537	0.346
* 8.86	0.656	0.00746	33.27	424.69	0.500	0.328
9.59	0.671	0.00747	33.32	424.71	0.462	0.310
10.59	0.686	0.00770	34.35	424.72	0.432	0.296
11.42	0.708	0.00775	34.57	424.73	0.403	0.285

$$j_m = 3.118\ Re_s^{-0.840}$$

* Data above asterisk symbol were not used for correlation.

Table A.5-3

Re_o = 29.98

d = 0.0650 cm

V_B = 4.64 cm^3

ρ_s = 1.32 gm/cm^3

Re_s	ε	$\overline{K}_C$	Sh	Sc	j_m	j'_m
1.40	0.481	0.00665	18.15	336.31	1.861	0.896
1.62	0.481	0.00683	18.65	336.36	1.656	0.797
1.78	0.481	0.00687	18.75	336.39	1.515	0.729
1.99	0.481	0.00718	19.59	336.42	1.419	0.683
2.24	0.481	0.00680	18.57	336.48	1.919	0.573
2.89	0.486	0.00748	20.42	336.53	1.015	0.493
3.54	0.519	0.00753	20.52	335.70	0.833	0.433
* 5.13	0.569	0.00868	23.65	335.75	0.664	0.378
6.51	0.624	0.00915	24.93	335.77	0.551	0.344
7.58	0.645	0.00922	25.12	335.79	0.477	0.308
9.64	0.702	0.00958	26.12	335.81	0.390	0.274
10.45	0.726	0.00981	26.75	336.02	0.368	0.267
11.15	0.734	0.00989	26.98	336.02	0.348	0.256
11.89	0.747	0.01010	27.54	336.03	0.333	0.249
12.90	0.770	0.01004	27.39	336.04	0.305	0.235
16.07	0.821	0.01083	29.50	335.57	0.264	0.217
20.80	0.892	0.01095	29.84	335.58	0.206	0.184

$$j_m = 2.567\ Re_s^{-0.827}$$

* Data above asterisk symbol were not used for correlation.

Table A.5-4

Re_o = 21.41
d = 0.0669 cm
V_B = 5.26 cm^3
ρ_s = 1.23 gm/cm^3

Re_s	ε	$\overline{K}_C$	Sh	Sc	j_m	j'_m
1.19	0.475	0.00450	14.30	424.59	1.601	0.761
1.26	0.534	0.00481	15.27	423.49	1.611	0.860
1.37	0.526	0.00415	13.21	424.52	1.283	0.675
1.58	0.518	0.00447	14.21	424.55	1.197	0.620
1.81	0.511	0.00546	17.36	424.71	1.275	0.652
1.86	0.561	0.00466	14.78	423.61	1.060	0.595
1.90	0.518	0.00479	15.24	424.61	1.066	0.552
2.17	0.515	0.00516	16.42	424.63	1.008	0.519
2.43	0.534	0.00565	17.96	424.83	0.985	0.526
* 2.82	0.562	0.00624	19.82	423.70	0.937	0.526
3.92	0.614	0.00690	21.89	423.76	0.744	0.457
4.65	0.638	0.00715	22.69	423.80	0.649	0.414
5.22	0.682	0.00704	22.34	423.78	0.570	0.389
9.42	0.786	0.00788	25.03	423.86	0.354	0.278
11.83	0.841	0.00828	26.28	423.75	0.296	0.249
12.67	0.858	0.00862	27.36	423.76	0.288	0.247
13.38	0.862	0.00855	27.15	423.76	0.270	0.233
13.80	0.864	0.00859	27.25	423.48	0.263	0.227
14.50	0.887	0.00866	27.47	423.49	0.252	0.224
15.15	0.903	0.00869	27.56	423.49	0.242	0.219
15.63	0.894	0.00902	28.59	422.97	0.244	0.218
16.15	0.920	0.00888	28.15	423.50	0.232	0.214
16.30	0.923	0.00899	28.48	423.03	0.233	0.215
17.74	0.939	0.00922	29.20	423.04	0.219	0.206

$$j_m = 2.188\ Re_s^{-0.805}$$

* Data above asterisk symbol were not used for correlation.

Table A.5-5

Re_o = 20.35

d = 0.0669 cm

V_B = 9.07 cm^3

ρ_s = 1.2 gm/cm^3

Re_s	ϵ	$\bar{K}_C$	Sh	Sc	j_m	j'_m
2.47	0.565	0.00599	19.60	451.66	1.032	0.584
2.61	0.573	0.00633	20.68	451.66	1.031	0.591
2.67	0.577	0.00642	20.98	451.66	1.026	0.591
4.34	0.662	0.00678	22.17	451.66	0.666	0.441
4.53	0.669	0.00672	21.97	451.66	0.633	0.423
9.21	0.824	0.00755	24.70	451.66	0.349	0.288
9.39	0.824	0.00839	27.42	451.66	0.381	0.314

$$j_m = 2.204\ Re_s^{-0.809}$$

Table A.5-6

Re_o = 20.09

d = 0.0581 cm

V_B = 4.23 cm^3

ρ_s = 1.32 gm/cm^3

Re_s	ε	$\overline{K}_C$	Sh	Sc	j_m	j'_m
1.65	0.473	0.00503	13.88	423.88	1.119	0.530
1.90	0.493	0.00520	14.35	423.92	1.008	0.497
2.50	0.542	0.00525	14.49	424.00	0.773	0.419
* 2.80	0.567	0.00605	16.71	424.69	0.795	0.450
3.42	0.594	0.00651	17.97	424.02	0.701	0.416
4.03	0.630	0.00671	18.50	424.77	0.612	0.386
4.05	0.632	0.00675	18.66	424.73	0.614	0.388
5.02	0.662	0.00697	19.27	424.77	0.511	0.338
5.53	0.681	0.00712	19.69	424.83	0.474	0.323
5.99	0.703	0.00708	19.56	424.12	0.435	0.306
7.11	0.734	0.00740	20.46	424.83	0.383	0.281
8.81	0.786	0.00767	21.22	424.86	0.321	0.252
9.95	0.808	0.00797	22.00	424.18	0.294	0.238
11.04	0.829	0.00807	22.32	424.64	0.269	0.223
11.64	0.845	0.00808	22.34	424.89	0.255	0.216

$$j_m = 1.874\ Re_s^{-0.809}$$

* Data above asterisk symbol were not used for correlation.

Table A.5-7

Re_o = 8.40

d = 0.0396 cm

V_B = 4.46 cm^3

ρ_s = 1.32 gm/cm^3

Re_s	ε	$\overline{K}_C$	Sh	Sc	j_m	j'_m
1.68	0.645	0.00671	12.62	424.22	0.998	0.644
1.91	0.654	0.00680	12.82	425.22	0.895	0.585
2.75	0.728	0.00763	14.36	424.38	0.695	0.507
3.44	0.768	0.00794	14.98	425.43	0.580	0.445
3.77	0.799	0.00835	15.73	424.46	0.556	0.444
4.07	0.800	0.00824	15.55	425.48	0.509	0.407
4.49	0.839	0.00877	16.51	424.50	0.490	0.411
5.20	0.872	0.00879	16.60	425.54	0.425	0.370
5.63	0.901	0.00921	17.35	424.56	0.410	0.370
6.43	0.923	0.00940	17.75	425.59	0.367	0.339

$$j_m = 1.457\ Re_s^{-0.739}$$

Table A.5-8

Ref.	Table	Re_o	q-1	B_o	$N_{predicted}$	$N_{expt.}$
	A.5-1	56.16	-0.859	0.837	2.97	3.16
	A.5-2a	43.72	-0.844	0.850	3.05	3.16
	A.5-2b	43.72	-0.840	0.862	3.05	3.67
	A.5-3	29.98	-0.827	0.843	3.17	3.15
	A.5-4	21.41	-0.805	0.860	3.28	3.59
	A.5-5	20.35	-0.809	0.868	3.29	3.50
	A.5-6	20.09	-0.809	0.742	3.30	3.56
	A.5-7	8.4	-0.739	0.877	3.60	3.60

Table A.5-9

Single particle results

d cm	T °C	ρ_s gm/cm^3	Re_o	$\overline{K}_C \times 10^3$ cm/sec	Sh	Sc	j
0.0402	24.1	1.28	7.18	6.04	11.75	440.83	0.215
0.0626	23.8	1.28	20.53	8.63	26.28	447.09	0.167
0.0735	24.0	1.28	30.35	8.61	30.67	443.47	0.133
0.1443	23.8	1.20	94.66	10.26	72.00	447.09	0.100
0.0418	23.7	1.28	8.41	7.43	15.11	448.00	0.235
0.0619	24.7	1.28	20.67	9.18	27.18	430.40	0.174
0.0489	24.3	1.28	11.63	7.83	18.46	437.33	0.209
0.0980	24.7	1.20	42.60	7.94	37.23	430.40	0.116
0.0646	24.3	1.28	22.12	8.38	26.08	437.33	0.155
0.0377	24.6	1.28	6.67	10.57	19.12	432.08	0.379
0.1405	24.7	1.20	90.61	6.68	44.88	429.54	0.066
0.6634	24.7	1.28	23.19	7.57	24.05	430.40	0.137
0.1023	25.0	1.20	47.07	6.53	31.53	426.12	0.089
0.0544	24.9	1.28	15.36	8.97	22.69	426.97	0.196
0.1270	24.9	1.20	15.24	8.34	51.82	426.97	0.092
0.0448	24.9	1.28	10.32	9.34	20.40	427.82	0.262
0.0991	24.8	1.20	45.23	8.11	39.22	428.68	0.115

A.6. Sample of particle properties

A typical particle size distribution is shown in Fig. A.6-1. The surface averaged mean diameter of this sample is 0.0950 cm and the standard deviation is ±0.0044. Since the average of the population is not known a 't' test was made to estimate the deviation of the population mean from the sample mean. For 95% confidence limit the population mean is within 1.8% of the sample mean.

Fig. A.6-2 shows the variation of resin diameter with loading. In the figure Q denotes resin loading, i.e. the ratio of the amount of Na^+ in the particle to the total capacity of the particle and d_Q denotes the ratio of diameter of particle in H^+ form to that of mixed i.e. (H^+, Na^+) form. The density of particles were calculated determining particle terminal Reynolds number Re_o and using the correlation (64)

$$Ga = 18\ Re_o + 2.7\ Re_o^{1.687} \quad \text{for} \quad 3.6 < Ga < 10^5$$

where

$$Ga = \frac{d^3\ \rho(\rho_s - \rho)\ g}{\mu^2}$$ and is known as the Galileo number.

Here ρ_s is the density of the particle.

Fig. A.6-1 : A typical histogram of particle diameter:
4.75 to 6.25 microscope intervals
= 0.0254 cm
Mean diameter of sample 0.0950 cm

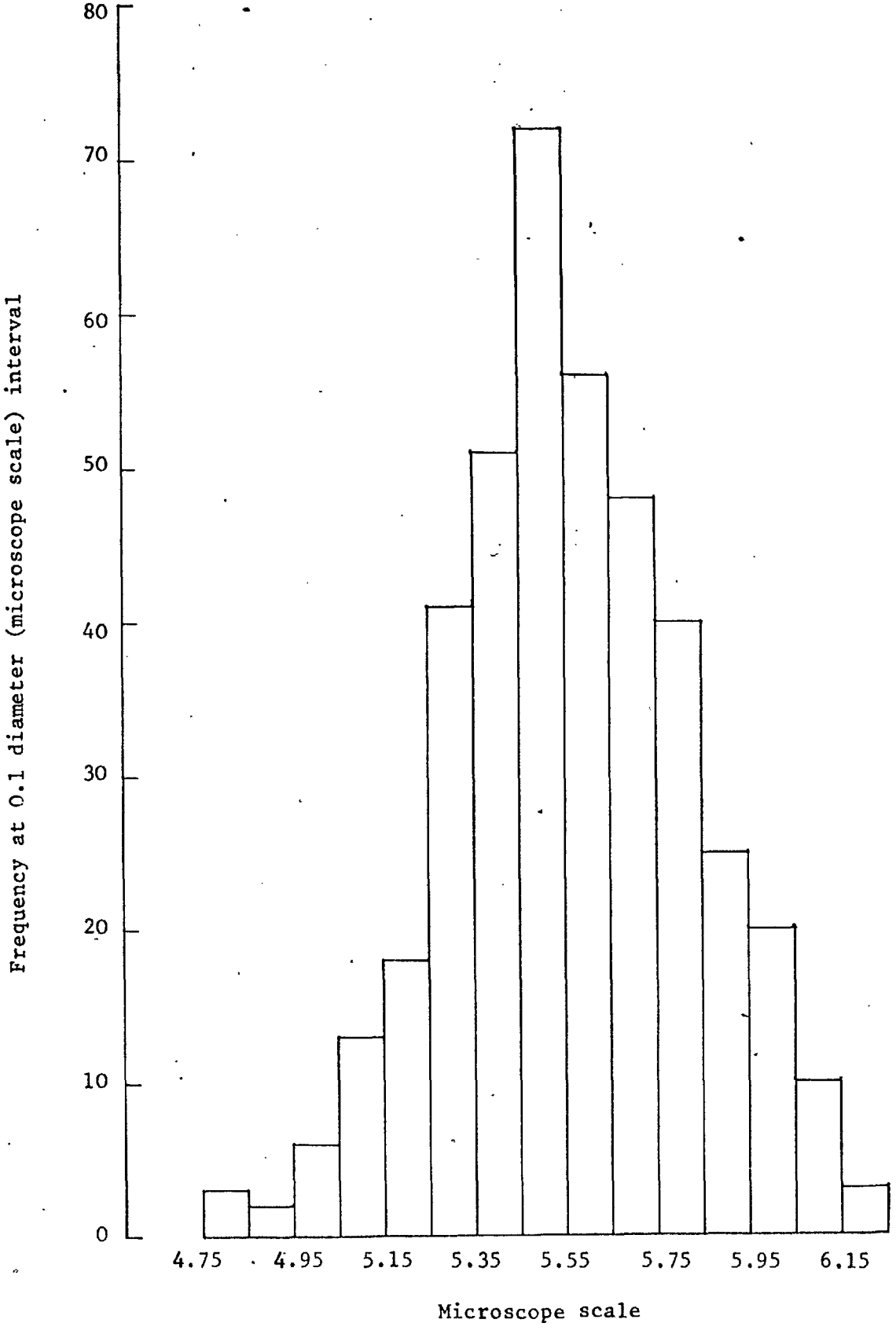

Fig. A.6-2 : variation of resin diameter with loading in about 10^{-2} (N) NaOH solution.